General Disclaimer

One or more of the Following Statements may affect this Document

- This document has been reproduced from the best copy furnished by the organizational source. It is being released in the interest of making available as much information as possible.

- This document may contain data, which exceeds the sheet parameters. It was furnished in this condition by the organizational source and is the best copy available.

- This document may contain tone-on-tone or color graphs, charts and/or pictures, which have been reproduced in black and white.

- This document is paginated as submitted by the original source.

- Portions of this document are not fully legible due to the historical nature of some of the material. However, it is the best reproduction available from the original submission.

STUDY OF MULTIPLE RESERVE ELECTROCHEMICAL POWER SOURCE

Final Report

by

George Ciprios

January 1969

National Aeronautics and Space Administration
Washington, D.C.

Contract No. NAS 7-673

ESSO RESEARCH AND ENGINEERING COMPANY

Government Research Laboratory
Linden, New Jersey 07036

CAT- 03

GR-1-MPS-69

STUDY OF MULTIPLE RESERVE ELECTROCHEMICAL POWER SOURCE

FINAL TECHNICAL REPORT
JANUARY, 1969

CONTRACT NO. NAS 7-673
11 JUNE 1968 TO 15 DECEMBER 1968

PREPARED BY

GEORGE CIPRIOS

ESSO RESEARCH AND ENGINEERING COMPANY
GOVERNMENT RESEARCH LABORATORY
LINDEN, NEW JERSEY

FOR

NATIONAL AERONAUTICS AND SPACE ADMINISTRATION
WASHINGTON, D.C.

FOREWORD

This final technical report describes the results of feasibility studies on a fuel cell multiple-reserve electrochemical power source conducted by Esso Research and Engineering Company for the National Aeronautics and Space Administration, Washington, D. C. The experimental and analytical studies were performed under Contract No. NAS 7-673, administered under the direction of NASA Headquarters, Washington, D. C. Mr. Ernst Cohn was the Technical Manager for this program.

The contribution of Mr. E. H. Okrent, who initiated these studies, is acknowledged with thanks.

TABLE OF CONTENTS

APPENDICES

ILLUSTRATIONS

TABLES

APPENDIX ILLUSTRATIONS

APPENDIX TABLES

ABSTRACT

A study was conducted to define the feasibility of a fuel cell multiple-reserve electrochemical power source for projected space missions. Neat hydrazine and 98 wt. % hydrogen peroxide are used as storable reactants. Appropriate high temperature reactors, containing propellent decomposition catalysts, are used to generate hydrogen and oxygen feed gases for the fuel cell.

Allis-Chalmers fuel cell modules were selected for the center-line design on the basis of low specific weight and demonstrated boot-strap start-up capability. Catalysts with adequate activity are available to permit instantaneous reactor start-up with either reactant at +5°C, the design dead-storage temperature. Only small amounts of catalyst were needed for complete reactant decomposition, but added amounts of ammonia decomposition catalyst are required to increase hydrogen yield. A palladium diffuser is used to recover ultrapure hydrogen, permitting efficient fuel cell operation. Overall system thermal control in near-sun and deep-space environments is a critical problem requiring further study.

Integrated power plant specific energies ranged from 122 to 292 WH/lb for mission on-load times of 100 or 1000 hrs and power levels of 200 to 5000 watts. A capsule sheath and insulation were included in the weight analysis, but projected system temperature excursions for flights extending to 9 A.U. were still excessive. Doubling the weight of the system capsule sheath and thermal control insulation would decrease specific energy by about 10%. Projected fuel cell/gas generator system costs were low, ranging from 600 to about 10,000 $/KWH, making this an attractive space power approach.

SUMMARY AND CONCLUSIONS

This final technical report describes the results of feasibility studies on a fuel cell multiple-reserve electrochemical power source conducted by Esso Research and Engineering Company for the National Aeronautics and Space Administration, Washington, D. C. The experimental and analytical studies were performed under Contract No. NAS 7-673.

Storable reactants are used to extend the scope of potential fuel cell power applications in space missions. The center-line system design consists of reactant storage and conditioning sections coupled to a fuel cell energy conversion device. Appropriate decomposition reactors are used to convert the neat hydrazine and concentrated, 98 wt. % hydrogen peroxide reactants into hydrogen and oxygen feeds for the fuel cell.

Fuel Cell Subsystem

To minimize prospective development costs, only state-of-the-art fuel cell systems were considered for the multiple-restart power pack. Allis-Chalmers' fuel cell modules were selected on the basis of low specific weight, demonstrated boot-strap start-up capability and good storage characteristics. Preliminary trade-off studies were conducted to select the number and types of modules resulting in minimum reactant storage and fuel cell weight for assumed missions requiring 100 or 1000 hrs operation at power levels ranging from 200 to 5000 watts. A typical Jovian mission dead-storage time of 3 years was assumed. Allis-Chalmers radiation-cooled and liquid-cooled modules gave minimum projected system weights. Conservative, 50-60 day performance data, were used in the analysis.

Fuel cell operation with impure reactants was reviewed because the nominal decomposition products will contain large amounts of inert diluents. In particular, the direct use of the hydrogen-nitrogen product from the hydrazine decomposition reactor will result in substantial performance debits when operating at a high hydrogen utilization factor. Fortunately, a palladium-silver diffuser can be used to provide high yields of ultrapure hydrogen for the fuel cell. Similarly, pure oxygen is obtained by adjusting the operating conditions of the condenser used to separate by-product water from the hydrogen peroxide decomposition products. Substantial reductions in reactant storage requirements were obtained by operating the fuel cell with pure feed gases. The minimum fuel cell storage temperature is -40°C, fixed by the freeze point of the caustic electrolyte.

Hydrogen Generator Subsystem

The hydrogen generator subsystem contains the hydrazine storage tank, a decomposition reactor and hydrogen purifier, and associated hardware. Bladder expulsion and advanced capillary-action tankage were found suitable. The capillary tanks were selected to minimize potential reactant decomposition during prolonged storage in contact with bladder materials.

Experimental studies showed that only small amounts of available propellent catalysts are required to decompose hydrazine completely at high temperature. Instantaneous start-up was obtained at design ambient temperatures of about +5°C. The decomposition products contained substantial amounts of by-product ammonia. Additional studies showed that suitable ammonia decomposition catalysts are available to increase the overall yield of hydrogen. These catalysts operate effectively at temperatures above 500°C. Integrated reactor designs were prepared to maintain the ammonia catalyst bed at these temperatures. A palladium diffuser was designed to permit the high yield recovery of pure hydrogen. The hydrogen product is stored in an accumulation tank.

The use of neat hydrazine requires minimum in-flight storage temperatures of +2°C, the freeze point of hydrazine. An alternative approach, using dilute hydrazine in auxiliary tankage for start-up was rejected on the basis of increased complexity and low reliability. Also, a low-temperature hydrazine decomposition reactor, using potassium hydroxide moderator, was rejected on the basis of poor hydrogen selectivity.

Oxygen Generator Subsystem

An analogous system was defined to generate oxygen from hydrogen peroxide using small amounts of decomposition catalysts developed in propellent studies. Experimental studies showed that stoichiometric oxygen yields can be obtained at ambient temperatures of +5°C. These studies also showed that 98 wt. % hydrogen peroxide is a suitable reactant, provided intensive cleaning and passivation procedures are used to minimize auto-decomposition in the storage section hardware.

A radiator/condenser and induced-vortex cyclone are used to separate by-product water and to recover a 99.3 volume % oxygen feed gas. The oxygen is stored in an accumulator tank, sized to provide the 15-minute supply required for fuel cell start-up from +5°C.

Systems Integration and Final Design Studies

The power system components, including the fuel cell module, hydrogen generator and oxygen generator, were integrated, using an in-line packaging concept. A capsule sheath and structural elements were included. Thermal control problems were studied briefly. The capsule interior can be maintained at +5°C in deep space (AU = 9) by combined use of plutonium 238 radioisotope heating elements and cryogenic insulation. However, severe near-sun temperature excursions limit the attractiveness of this simple, passive control scheme. Time limitations prevented further analysis of this problem, but a solution must be found to ensure the operability of the proposed multiple-restart power plant and the on-board electronic payload.

The integrated power plants had specific energies ranging from 122 to 292 WH/lb, depending on mission operating time and power level. These values include the weight of the thermal control system consisting of the capsule sheath and insulation. However, projected system temperature excursions for missions extending to 9 A.U. from the run were still excessive. The weight of the thermal control system remains the major area of uncertainty. Doubling the weight of the thermal control system would decrease specific energy by about 10%. A literature search for spacecraft thermal control techniques was performed (NASA Literature Search Number 8203), but time was not available for an evaluation of the 462 references uncovered. Reactant decomposition during high temperature sterilization for lander missions may be high. Fly-by missions may be a more appropriate application for the storable reactant, fuel cell power system.

These systems look attractive for missions having on-load times of 50 to 600 hours, compared with radioisotope thermoelectric generators, down-rated solar cells and advanced multiple-restart batteries. In addition, projected power system costs, ranging from 600 to about 10,000 $/KWH, indicate that the fuel cell/gas generator approach may be the cheapest solution.

These studies have shown that attractive fuel cell power plants, having multiple-restart capability, can be designed for missions requiring long dead-storage times. The use of storable reactants, coupled with appropriate feed gas generator facilities, will extend the opportunities for effective application of fuel cell technology. Maximum spin-off use was made of available space propellent technology and experience. The use of state-of-the-art components and concepts will reduce future power plant development costs sharply. Further study of the fuel cell system approach is clearly justified.

Feasible solutions appear available for the technical problems uncovered, with the possible exception of a low weight, low power requirement thermal control system for maintaining capsule temperatures at about 5°C throughout the mission. This is an area requiring further analysis prior to commitment of development funds. The problem is common to all proposed deep space missions that use temperature-sensitive electronic sensing instrumentation or power generation equipment that must be operated at about -60°C or higher.

Further studies should be directed toward solving the problem areas listed below. Critical factors are asterisked for emphasis.

- Mission Requirements

  * Specific mission objectives must be defined, including time in transit and end-goal location in the solar system.

  - Power requirements, in the form of specific load profiles and number of start-ups, must be defined.

- Fuel Cell Subsystem

  * The effect of repeated boot-strap startup from 5°C on fuel cell life must be determined.

  - Startup capability after prolonged dead storage at 5±°C must be demonstrated.

  - Permissible purge cycles for the oxygen cavity must be defined to fix the effect of water vapor diluent on oxygen utilization. Also, the interaction between added water vapor and the static moisture removal mechanism must be analyzed.

  - Design techniques are required to ensure that fuel cell glycol coolant will not freeze during startup of the space radiator system.

  - The effect of reliability requirements and module redundancy on overall weight must be defined.

- Hydrogen Generator Subsystem

  * The integrated reactor concept for maintaining acceptable temperatures within the ammonia catalyst bed must be demonstrated to ensure high hydrogen yields.

  - Adequate materials of construction must be found, capable of withstanding exposure to hydrogen and oxygen at temperatures of at least 600°C at 500 psi.

  - The effect of high pressure operation on the kinetics of ammonia decomposition must be evaluated to define catalyst requirements.

- Potential fabrication problems with the palladium diffuser must be assessed.

- The operability of capillary-action tankage must be verified so that a final choice of tankage type can be made. These studies are also required for the oxygen generator subsystem.

- The operating characteristics of suitable feed pumps must be defined to permit an accurate estimate of system parasitic power requirements. These studies should include the oxygen generator feed pump.

- Trade-off studies are required to evaluate potential weight savings for storage of compressed pure hydrogen product.

- Oxygen Generator Subsystem

  * The fluid mechanical design and operation of the induced-vortex cyclone device for separating by-product water must be verified. Purge hardware must selectively bleed water, not oxygen, to maintain high system yields and efficiency.

  - Optimization studies are needed to define the best geometry for the water condenser.

- Integrated System

  * A thermal management concept must be devised to ensure limited excursions of capsule temperature during deep-space flights.

  - Optimization studies are needed to define minimum capsule sheath and internal structural weights.

  - Overall system dynamic response must be evaluated, including performance transients during start-up.

  - Control systems requirements must be defined.

  - The effect on reactant storage requirements of short exposures to high temperature must be defined, if heat sterilization capability is required for lander missions.

SECTION 1

INTRODUCTION

This report describes the results of feasibility studies on a fuel cell multiple-reserve electrochemical power source conducted by Esso Research and Engineering Company for the National Aeronautics and Space Administration, Washington, D.C. The experimental and analytical studies were performed under Contract No. NAS 7-673.

At present, a broad range of potential space missions are under intensive review and discussion. In addition to post-Apollo lunar missions, interplanetary explorations are now feasible. Thus, the Space Science Board has described the desirability of several unmanned Venus and Mars fly-by and lander missions for the 1970-1975 period (1). Recommendations were made to extend these missions to include a Jupiter fly-by. Recently, Murray proposed a national space strategy that would concentrate on demanding, remote-sensing missions (2). These include a 1972-1973 Jupiter fly-by and, eventually, a 1976-1979 grand tour to Neptune with a 1000 lb spacecraft. This would be launched with the Titan III/Centaur booster, although the Saturn booster is also available.

The availability of large payload, Saturn-class rockets does not mean that the search for light weight, high efficiency power sources will end. With the prospect of continued funding restrictions, total mission costs will play an increasingly severe role in the selection among system options. Limitations imposed by booster capability and cost will define the launch weight of future spacecraft. In turn, this means that the development and construction costs of potentially long-lived or restartable spacecraft power sources also must be reasonable. In addition to solar cells (3) and radioisotope thermoelectric generators (RTG). batteries and fuel cells should be considered as potential power systems for these missions.

Batteries may provide a suitable electrochemical power source, but current batteries have poor storage characteristics in the activated state. Advanced, multiple-reserve batteries are conceivable, but none are operational at present.

On the other hand, fuel cells may offer a cheaper and potentially attractive power source. Traditional trade-off studies have usually defined a limited role for the fuel cell. A typical analysis presented by Szego and Cohn (4), is shown in Figure 1. For short duration missions, the intrinsic energy storage characteristics of chemical fuels limit the maximum attractive mission time of hydrogen-oxygen fuel cells. In addition, the adverse effect of boil-off losses precludes the use of cryogenic reactant storage for missions requiring long dead-storage times.

Figure 1

TRADITIONAL TRADE-OFF ANALYSIS
FOR SPACE POWER SYSTEMS

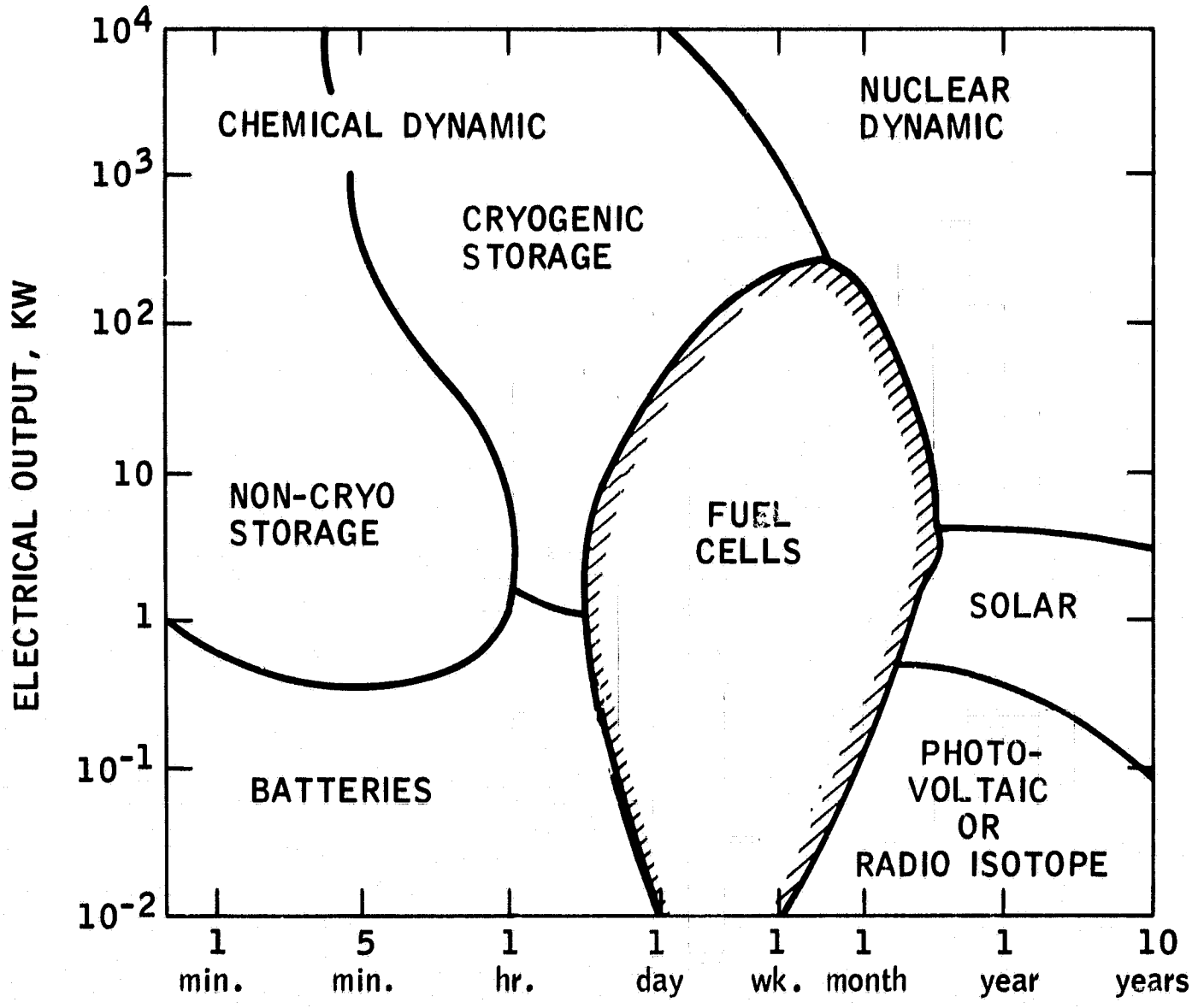

However, storable reactant sources exist. Thus, hydrazine and hydrogen peroxide may be substituted as sources of hydrogen and oxygen as fuel for missions where repeated service is required every few months during long-duration flights. The major problem is to provide a suitably packaged system using proven fuel cell components. This approach makes maximum use of previously developed electrochemical systems and couples this with the technology available from government-financed studies on storable propellants. This coupling should sharply reduce prospective development costs for a new, multiple-restart power source.

The remainder of this report discusses the critical aspects of the multiple-reserve fuel cell system, including the associated fuel gas generation subsections.

SECTION 2

ANALYTICAL AND EXPERIMENTAL STUDIES

The use of storable reactants should extend the scope of attractive fuel cell power applications to include multiple restart missions after prolonged storage. Therefore, a study was made to define the feasibility of adapting available hydrazine and hydrogen peroxide propellant technology to permit coupled operation with existing and proven fuel cell systems. The analytical studies connected with this program relied heavily on published data to define critical problem areas and to provide a basis for selection of a system approach where several options existed. A brief, supplementary experimental program was carried out to fill in gaps in current knowledge, particularly in the area of decomposition catalyst activity.

Separate phases of this section will describe the center-line power system design and discuss the selection and design of the fuel cell, hydrogen generator and oxygen generator components, and the integration of these systems.

Phase 1 - General Power System Description

A preliminary description of the overall power system will clarify the interrelation of key subsystems. In addition, an alternative approach is discussed.

Part a - Center-Line Design

The center-line design or base case for this feasibility study consists of a reactant storage and conditioning section coupled to a fuel cell energy conversion device. A schematic flow diagram of the system is shown in Figure 2.

Neat hydrazine and concentrated, 98 wt.% hydrogen peroxide are stored in appropriate pressurized tankage at about 50-100 psi. The tank valves are opened and feed pump start-up occurs upon reception of a command signal from earth or a demand signal from the fuel cell. Reactants are pumped at design flow rates and about 500 psi to an integrated reactor. This reactor contains hydrazine and hydrogen peroxide decomposition catalysts that generate hydrogen and oxygen, respectively. Additional quantities of ammonia decomposition catalyst are used to increase the yield of hydrogen from hydrazine decomposition. A pure hydrogen fuel cell feed at about 30 psi is produced by passing the hydrogen generator effluent through a palladium-silver diffuser. After cooling in a space radiator, this hydrogen is stored in an accumulation tank for subsequent use in the fuel cell. The nitrogen-rich diffuser bleed gas is also cooled and used to provide hydrazine feed tank pressurant. Excess nitrogen is vented overboard.

Figure 2

SCHEMATIC FLOW DIAGRAM OF MULTIPLE RESTART FUEL CELL POWER SOURCE

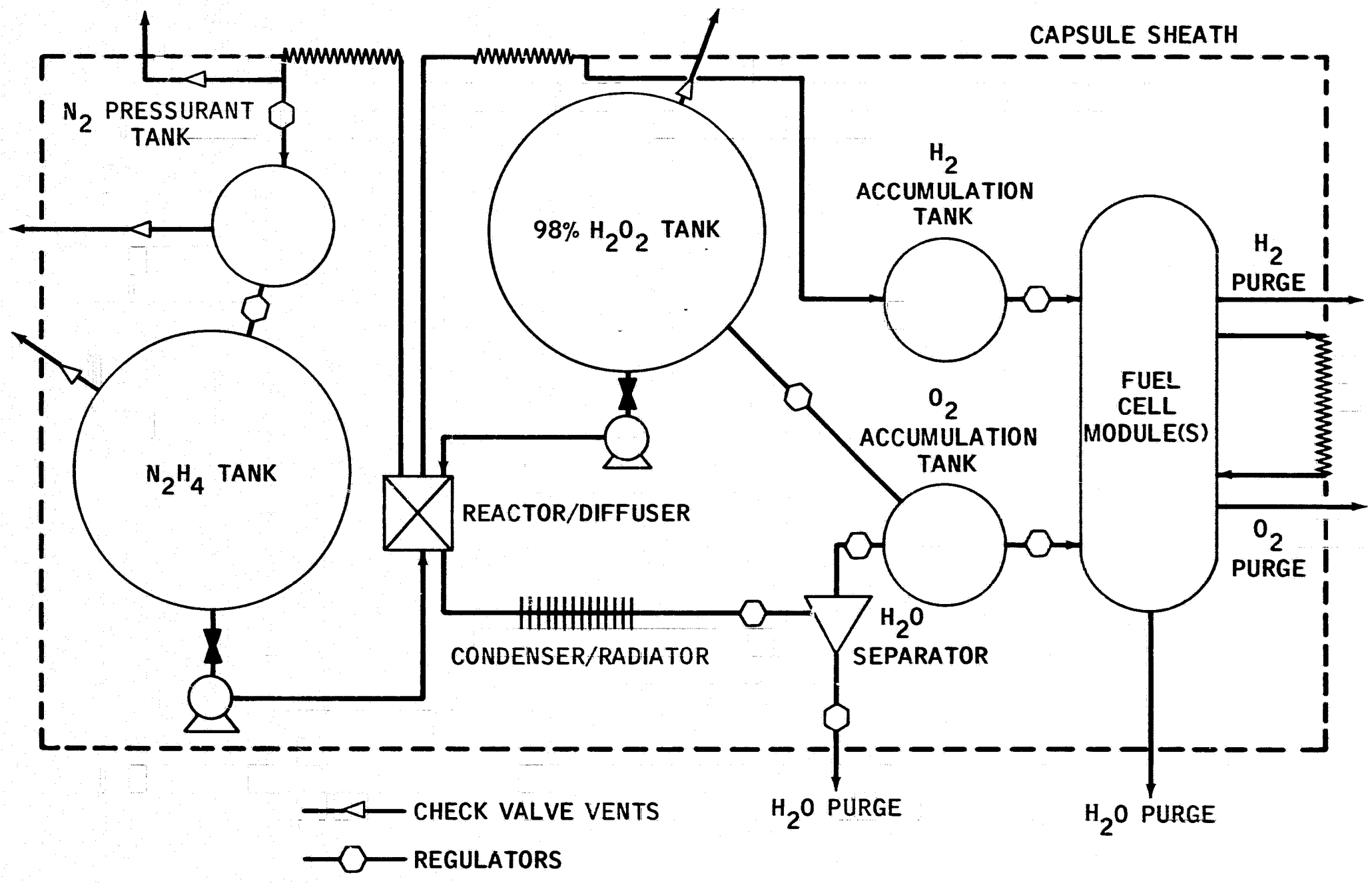

The hydrogen peroxide decomposition product, containing oxygen and water vapor, is cooled under pressure in a radiator condenser and passed to an induced-vortex cyclone separator to remove condensed water. This water is purged overboard. Essentially "dry" oxygen is stored in a high pressure accumulation tank for use in the fuel cell and as a pressurant for the peroxide storage tank.

Standard Allis-Chalmers fuel cell module(s) are used as energy conversion devices. Upon demand, the modules receive gaseous reactants from the generator system accumulation tanks. An open-cycle operational mode is used. Thus, product water is vented overboard, as are the fuel cell hydrogen and oxygen purge streams. Where required, a space radiator is provided to chill the fuel cell module coolant.

The entire system is enclosed in an insulated variable-emittance sheath to provide a reasonably constant storage temperature during deep space missions ranging from 1 to 9 A.U. from the sun. Small plutonium 238 radioisotope heating elements are provided to maintain temperatures above 2°C, the freezing point of neat hydrazine.

Designs were evaluated for typical Jovian planetary exploration missions. In the absence of specific mission requirements and load profiles, net power outputs ranging from 200 to 5000 watts for 100 to 1000 hrs. were selected. Dead storage times for these missions would be about 3 years. Multiple restart capability is required throughout the mission.

Part b - Alternative, Low Temperature System

An alternative gas generator system, capable of start-up from temperatures as low as -40°C, was also considered. This approach requires intermediate tankage to store diluted, low freeze point, reactant feeds for start-up. Active decomposition catalysts are available for this system variant. However, extra tankage is required, and complex operational modes and fluid handling procedures are needed. In addition, most of the stored reactants will be solid at -40°C, and must be remelted, under zero G conditions, using the decomposition reactor product gases as heat exchange fluids. This alternative was considered more complex and unreliable than the centerline design and was dropped. A description and analysis of the modified system is presented in Appendix 1.

Phase 2 - Fuel Cell Subsystem

To minimize prospective development costs, only state-of-the-art fuel cells systems were considered for the multiple restart power pack. The operational characteristics of these cells were reviewed to ensure selection of the most appropriate system for use in prolonged space missions.

The use of hydrazine and hydrogen peroxide decomposition products as feeds may require fuel cell operation with impure or diluted reactants. This differs from current aerospace practice, where ultra-pure hydrogen and oxygen are available in cryogenic form. Therefore, the effect of impure gases on fuel cell performance was reviewed critically.

Finally, preliminary systems studies were conducted to define partially optimized fuel cell operating points. Fuel cell performance factors play a major role in defining reactant weight requirements.

Part a - Selection of Fuel Cell Systems

The choice of a fuel cell system was restricted to proven technology. Several systems, developed with NASA funding, are available. The salient characteristics of these systems were reviewed recently by Cohn (5). The following tabulation lists the potential choices for the hydrogen-oxygen fuel cell:

- General Electric ion exchange membrane fuel cells, used in the Gemini flight program (6,7).
- Pratt and Whitney modified medium temperature Bacon cells, used in the Apollo program (8,9).
- Pratt and Whitney "low" temperature cells, currently under development (10,11).
- Allis-Chalmers "low" temperature cells, currently under development and testing (12-17).
- Union-Carbide flowing electrolyte cells, adapted for zero G operation in a recent design study (18).

Thus, off-the-shelf hardware is available. Typical specific weights for these systems are shown in Figure 3. The primary differences among these systems are the operating temperature and the techniques used for heat balance and removal of water produced by the fuel cell reactions. These techniques were discussed by Cook (19). They include a wicking mechanism used by General Electric, a flowing recycle reactant stream used by Pratt and Whitney and Union Carbide, and a static moisture removal system used by Allis-Chalmers. Each system may also use circulating auxiliary coolants for thermal control. For unmanned missions, all of these cells would be operated in an open-cycle mode, with product water vented overboard.

Figure 3

SPECIFIC WEIGHT CHARACTERISTICS OF AEROSPACE FUEL CELL SYSTEMS

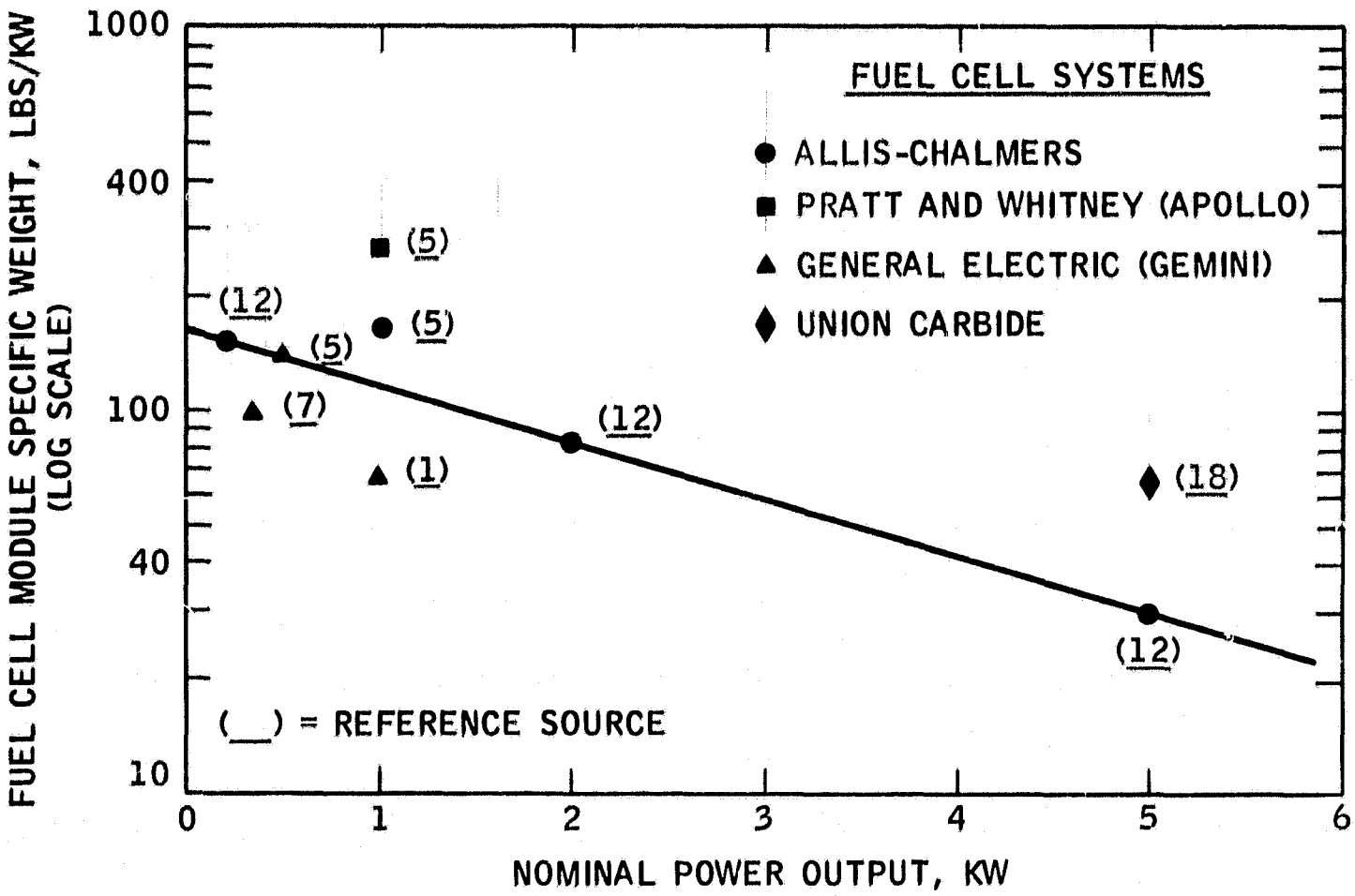

The Allis-Chalmers fuel cell module systems were selected as the most representative, advanced hydrogen-oxygen fuel cell system. The basis for this choice includes consideration of low specific weight, demonstrated boot-strap start-up capability and good resistance to the abuse that will be encountered in deep space, multiple-restart service. Furthermore, several module types are available, covering a net power range from about 150 to 5000+ watts. Platner has described the performance characteristics of these modules rather extensively (12). Subsequent systems studies in this program were conducted using these data.

The ion exchange membrane cells were rejected because of poor storage stability in the activated state and poor recovery from abuse (5). The medium temperature modified Bacon cell was excluded because of long start-up times to achieve steady state operation from prolonged storage at low temperatures and high specific weight. The Pratt and Whitney low temperature cells and the Union Carbide flowing electrolyte systems may be attractive choices in the future. Apparently, long-lived components have been found for circulating the reactant gas streams. The Pratt and Whitney cell was rejected primarily because of insufficient published performance details, including weight analyses and reactant consumption. The Union Carbide cell is an adaptation of a terrestrial system. This system was not not considered further because space qualification data are lacking.

It should be noted that most of the fuel cell systems discussed above have not been subjected to prolonged storage periods, ranging up to 3 years, prior to use. The ability to function after such storage has yet to be demonstrated.

Part b - Fuel Cell Operation with Impure Reactants

Ultra-pure hydrogen and oxygen are normally used as reactants in aerospace fuel cell systems. Under these conditions, the cells may be dead-ended, and reactant transport into the cell cavities may be accomplished by a combination of bulk flow induced by pressure differences and diffusive flow. Periodic purging is required to prevent the eventual accumulation of inert components within the cells. The transient characteristics of this process and its effect on the distribution of current generation across the face of the electrode have been studied by Allis-Chalmers (16,17), Gidaspow (20) and Maget (21) to establish an appropriate purge sequence. Clearly, excessive purging will result in substantial loss of unreacted feed gas. The reactant weight penalty imposed by this loss can be large.

The anticipated operation of a fuel cell using gases generated by the decomposition of hydrazine and hydrogen peroxide will aggravate the inerts build-up problem. Thus, substantial amounts of nitrogen diluent, roughly 33 mole percent, result from the stoichiometric conversion of hydrazine to hydrogen. The corresponding problem with oxygen generated from hydrogen peroxide is not as severe. Although the peroxide decomposition reactor effluent will contain 67 mole percent water, almost all of this diluent can be removed by the proper selection of condenser operating conditions. This approach cannot be used to remove non-condensible nitrogen from the hydrogen feed gas. Several strategies may be adopted for using this impure anode fuel. These include:

- Conventional dead-ended operation with more frequent purging.
- Once-through operation with venting of the spent feed gas.
- Recycle operation to increase the mass flow across the electrode face. A steady state purge is also required.
- Operation at elevated pressure, increasing hydrogen partial pressure to offset the diluent effect of nitrogen.
- Recovery of ultra-pure hydrogen via diffusion through a palladium-silver diffuser.

The first three options are variants on a theme and will be considered together. The relation between hydrogen utilization factor, Ψ, and intermittent purge cycling is defined by Equation (1):

$$\psi_H = 1 - \frac{(\text{Purge Flow Rate})\ (\text{Purge Time})}{(\text{Feed Flow Rate}\ (\text{Dead End Time})} \qquad (1)$$

$$\psi_H = \frac{\text{Moles } H_2 \text{ Consumed}}{\text{Moles } H_2 \text{ Feed}} = \frac{\text{Moles } H_2 \text{ Feed} - \text{Moles } H_2 \text{ Purged}}{\text{Moles } H_2 \text{ Feed}}$$

Typical purge flow rates used with ultra-pure reactants are about 2-6 times stoichiometric or feed flow rate (16). Under these conditions, purge times of about 6 seconds would be required to remove the inerts build-up. The effect of permissible dead-end time, before appreciable loss of cell performance, on hydrogen utilization is shown in Figure 4. These calculations show that hydrogen utilization drops sharply as the dead-end time is shortened. Clearly, very high utilizations are required for aerospace missions to reduce reactant storage requirements and overall system weight at lift-off.

Figure 4

EFFECT OF PURGING ON REACTANT UTILIZATION

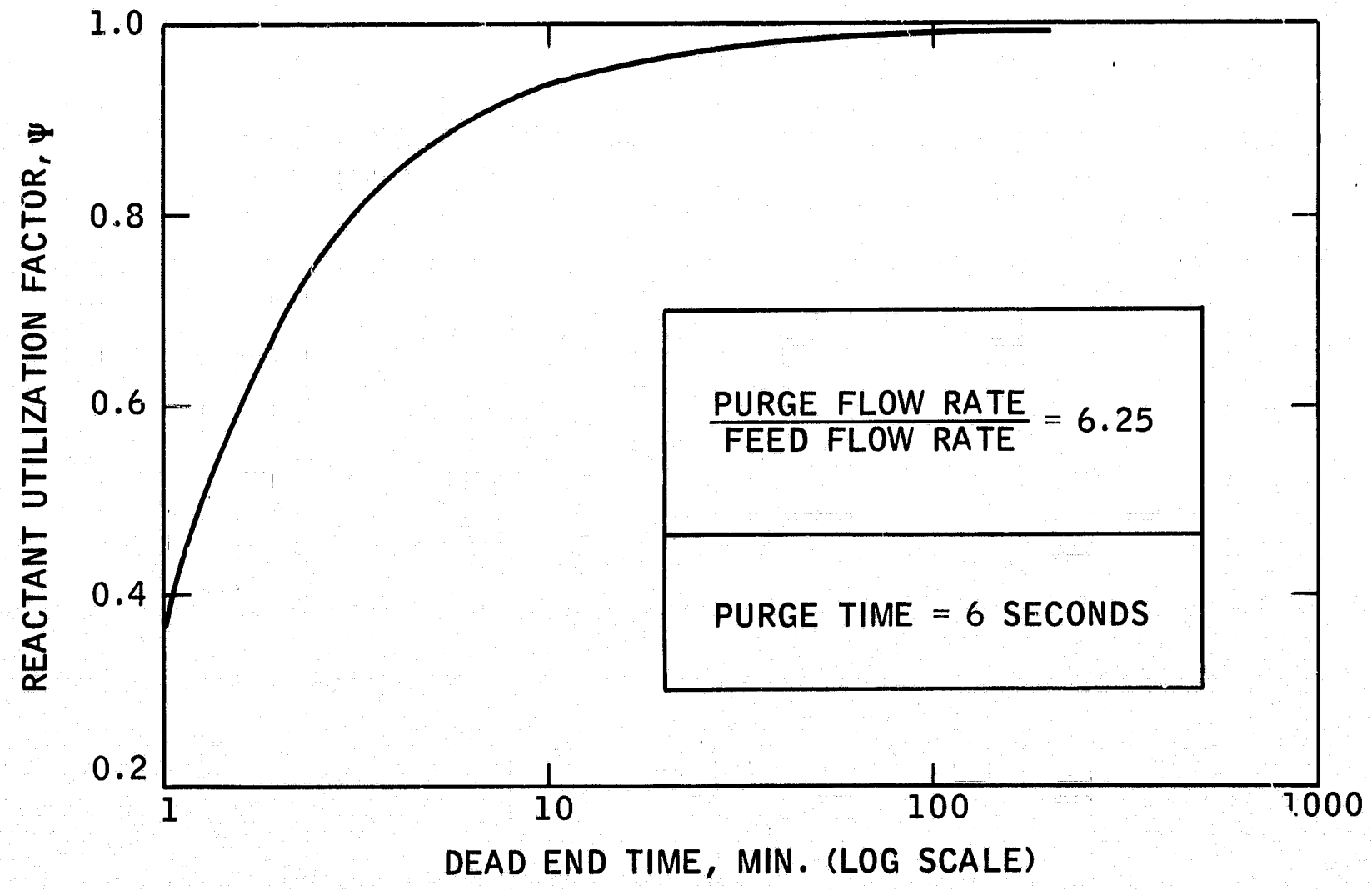

If cells are operated on a once-through basis, the requirement of high utilization can only be achieved by reducing the hydrogen content of the effluent to a minimum. In turn, this lowers the average hydrogen concentration within the anode cavity to values well below the feed concentration. This relationship is shown in Figure 5. A detailed derivation is given in Appendix 2.

Figure 5

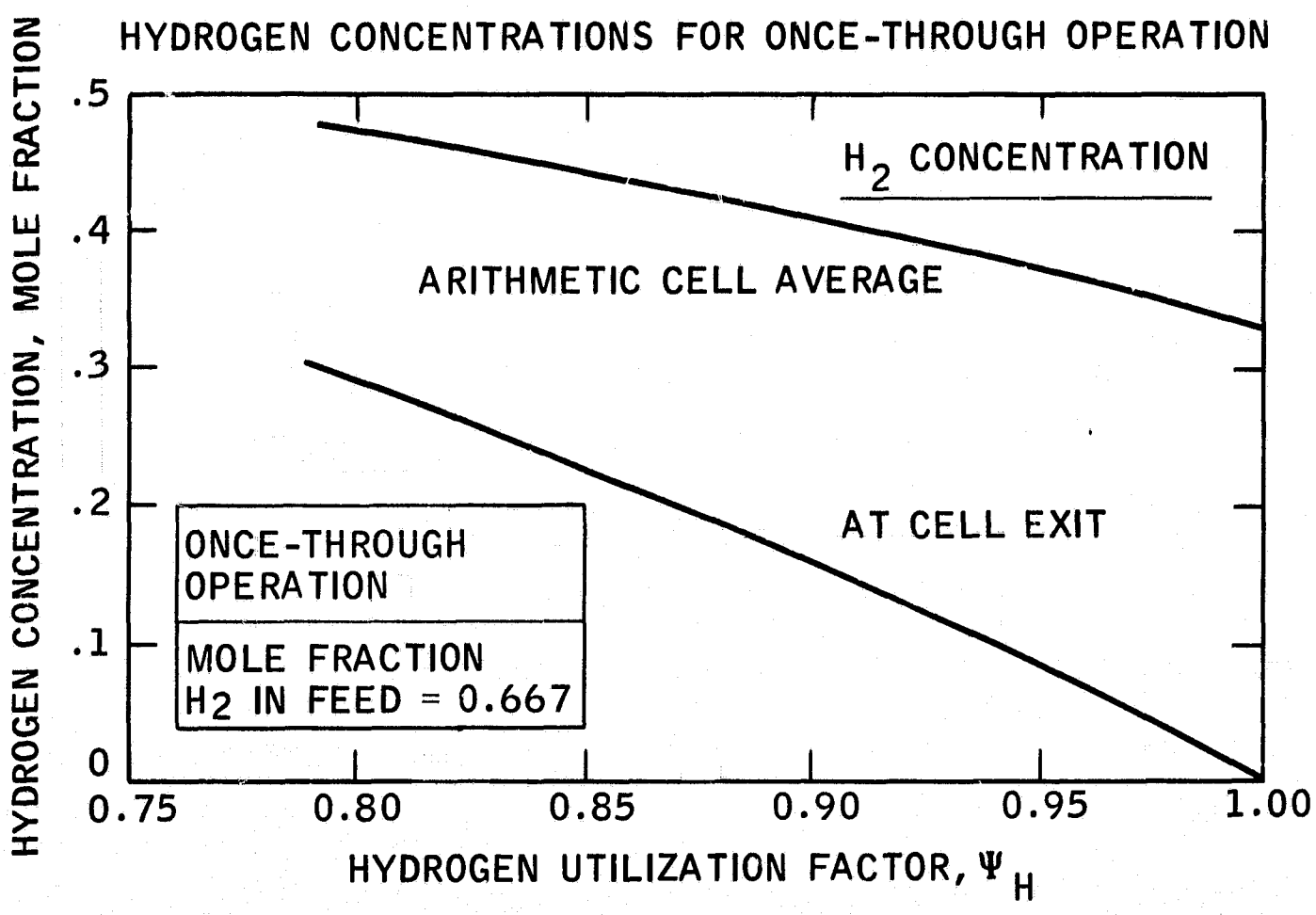

Recycling the cell effluent still requires a substantial purge, and aggravates the problem by further lowering the average hydrogen content, as shown in Figure 6.

Figure 6

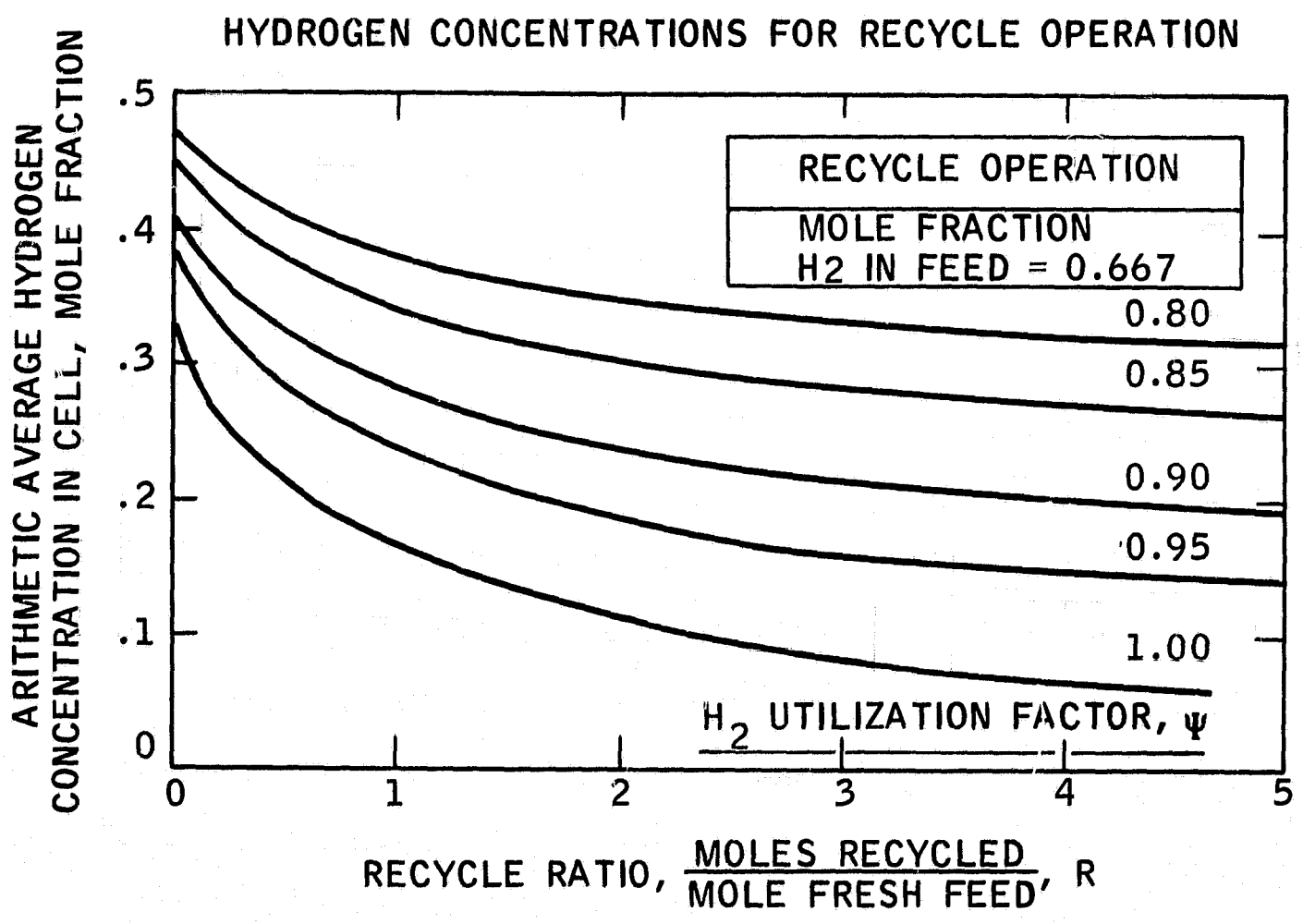

Operation with reduced hydrogen content can cause substantial loss in performance. The Nernst expression, Equation (2), predicts a 33 mv cell voltage debit when operating at a typical total pressure of 28 psia with an average hydrogen mole fraction of 0.066, instead of standard conditions of pure hydrogen at 14.7 psia (22,23). From Figure 6, this low hydrogen content would occur at a recycle ratio of 4 and hydrogen utilization factor of 1.00.

$$\Delta \mathcal{E} = \frac{RT}{nF} \ln \frac{P_1}{P_o} \qquad (2)$$

where:

$\Delta \mathcal{E}$	=	Performance debit, volts
R	=	Gas constant, 8.3 $\frac{\text{volt coulombs}}{\text{mole } °K}$
T	=	Temperature, °K
n	=	Reaction equivalents per mole
F	=	Faraday's constant, 96500 coulombs/eq
P_1	=	Average hydrogen partial pressure
P_o	=	Standard hydrogen partial pressure

These estimates are optimistic. The use of porous electrodes requires the diffusion of gaseous reactants down the length of the pore to the active reaction site. This impediment to mass transfer will further reduce the actual concentration of hydrogen at the active sites within the pore. Estimated performance debits for this process were calculated using methods described by Swinkels (24) and Austin (22). Here too, only small effects were predicted. Details are presented in Appendix 3. Actually, a complete evaluation of the effect of reduced hydrogen content on gas diffusion electrode performance is complex. One must consider the effects of counter-diffusion of reactant hydrogen and product water vapor through the nitrogen diluent present within pores of undefined geometry.

Available data suggest that severe performance debits will occur when operating at high utilization factors with dilute hydrogen feeds. For example, the in-house data shown in Figure 7 indicate that utilization factors above 0.80 cannot be achieved. These data were obtained in non-optimized, single test cells. Similar data obtained by Leitz, using reformed natural gas in an acid electrolyte cell, are shown in Figure 8 (25). It should be noted that these are not poisoning effects, but represent the loss in performance caused by reactant diffusion through the electrode structure.

Figure 7

HYDROGEN UTILIZATION AND PERFORMANCE DEBIT
USING DILUTE HYDROGEN

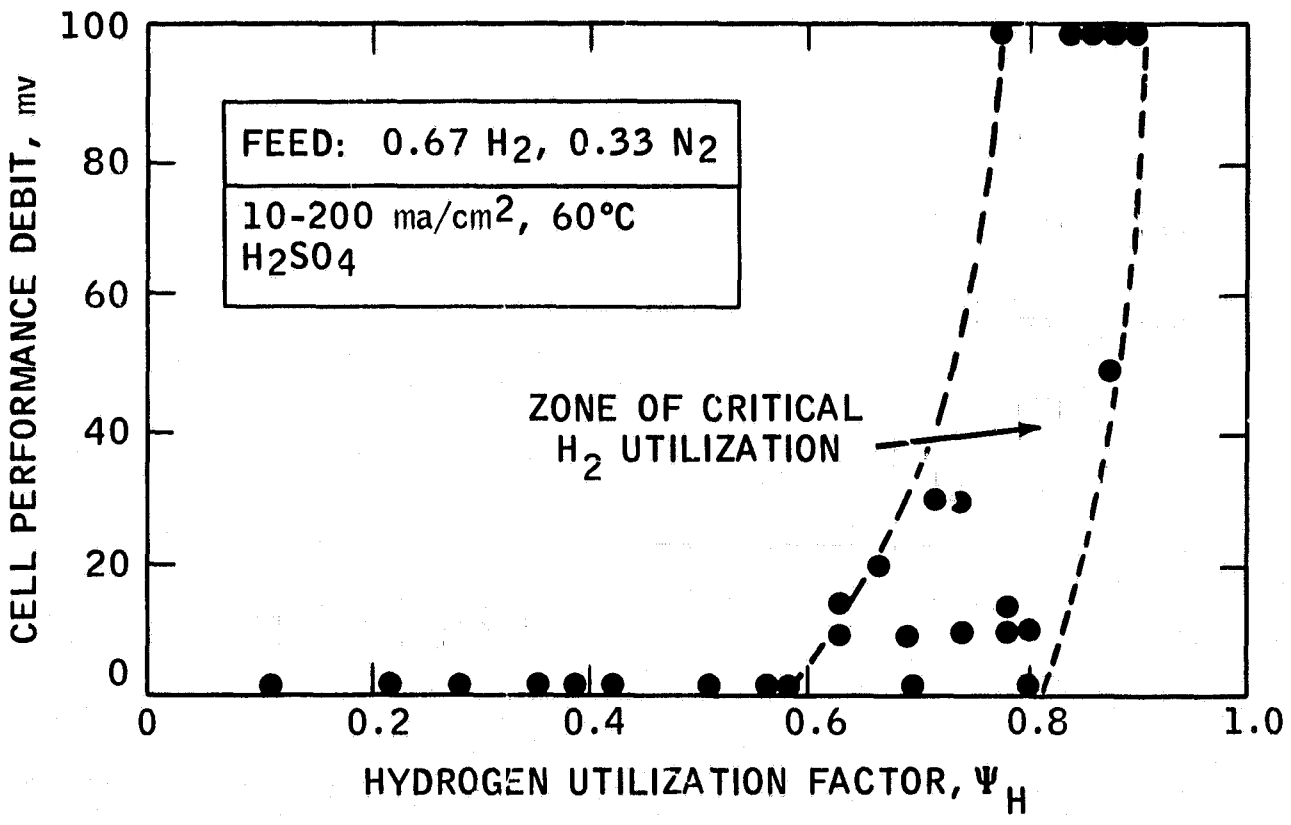

Figure 8

PERFORMANCE DEBIT FOR IMPURE HYDROGEN

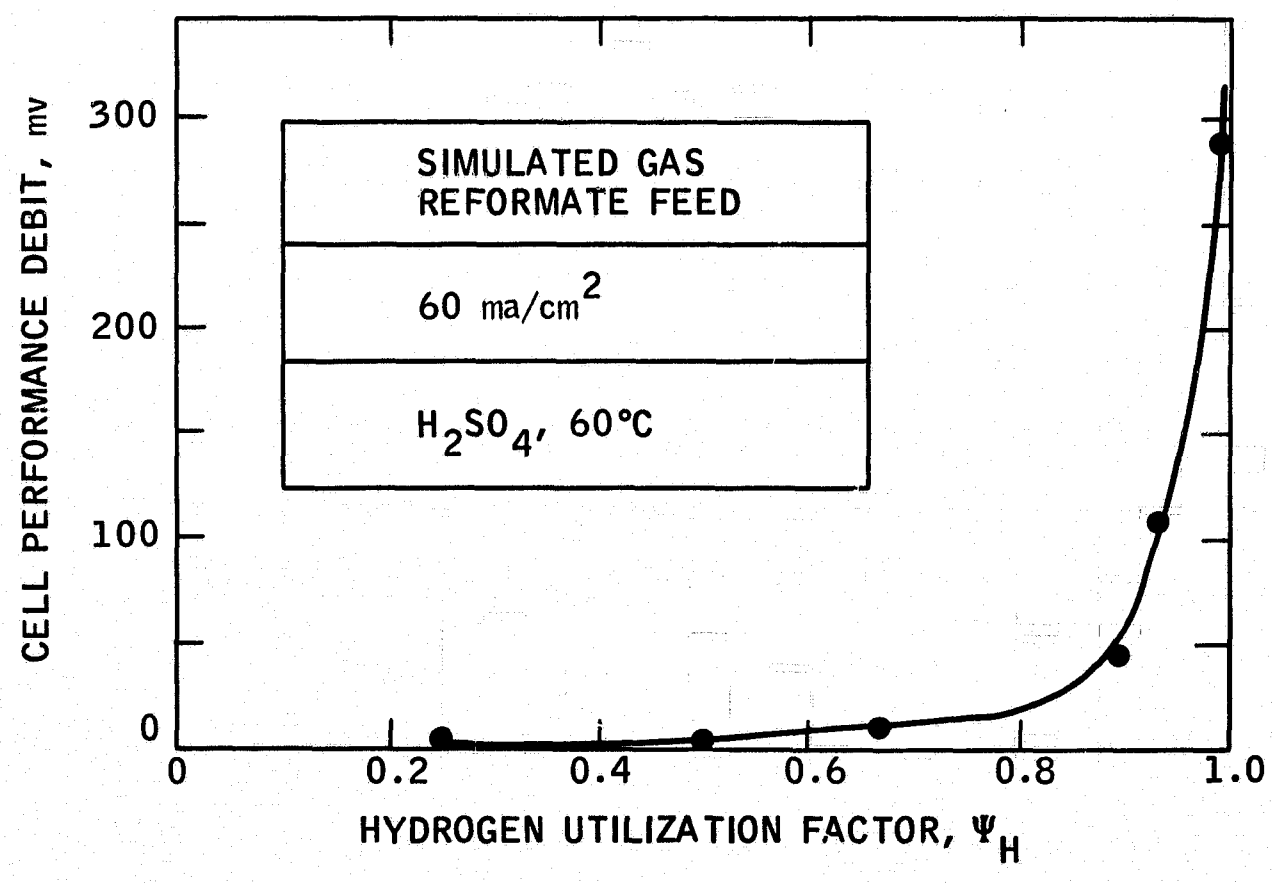

Finally, Winsel has presented data obtained with simulated cracked ammonia products in caustic electrolyte cells that also show poor performance at high utilization (26). These data are summarized in Table 1.

Table 1

Summary of Performance Debits for Operation with Dilute Hydrogen Feeds

Date Source	Hydrogen Content, Mol Fraction		Hydrogen Utilization Factor,	Performance Debit, mv
	Feed	Cell Average		
Esso	0.67	0.44	0.87	50
Leitz (25)	Variable	0.44	0.89	60
Winsel (26)	0.75	0.49 0.40	0.90 0.98	50 Dead

A recent analysis by Grune describes how fuel cell modules may be operated in cascaded series to improve reactant utilization when operating with impure feeds (27). However, this analysis is useful only for cases where individual cells in a module exhibit substantially greater than average flow resistance. The excess reactant supply required to feed the errant cell is used downstream in another module. It is assumed that modern fabrication and assembly techniques will reduce the variance of flow resistance among cells in a stack. Intrinsic cell operability at reduced reactant concentrations is the key limitation. New cell and electrode designs will be required to overcome these limitations.

Operation at elevated pressure can be used to improve fuel cell performance (16,28,29). This option is possible for the multiple-restart system because the decomposition reactors can be operated at elevated pressure. Although the Allis-Chalmers cells have been operated at about 40 psia (12,16), overall module design factors appear to favor a 30 psia working pressure. Imposition of higher pressures probably would require substantial redesign and tool-up costs.

On the basis of this evidence, one must conclude that fuel cell operation with the as-is product stream from the hydrazine decomposition reactor is unattractive. The use of a palladium diffuser to provide ultrapure hydrogen will improve the overall reactant utilization factor and will result in minimal distortion at the gas generator-fuel cell interface. The design of the diffuser is discussed in a later section.

Operation with dilute oxygen will also result in reduced performance. Data presented by Jones showed that reducing oxygen purity from 99.995 to 99.988 percent would roughly halve the allowable dead-end time in modified Bacon cells (9). Allis-Chalmers data showed that oxygen feeds containing 0.5 percent argon diluent would require purging after 5-10 minutes to limit the performance decay to 10 mv (16). As shown in Figure 4, purge losses at these short cycle times would decrease oxygen utilization.

The oxygen generator subsystem contains a condenser to reduce the water content of the product feed gas. As shown in Figure 9, a condenser effluent, saturated at 150°F (66°C) and 500 psia, would contain about 0.7 mole percent water vapor. The condenser temperature could be lowered if experimental studies showed that cathode performance decayed too rapidly at this concentration level. Alternatively, a modified form of Esso's heatless adsorption drying process could be used to produce bone-dry oxygen. Oxygen recovery factors may exceed 99 percent using this approach. Heatless drying technology was recently evaluated in our laboratories for NASA under Contract No. NAS1-6918 (30). The goal of these studies was to investigate the drying and purification of spacecraft atmospheres. This approach was not pursued further.

Figure 9

EFFECT OF CONDENSER OPERATING CONDITIONS ON OXYGEN CONCENTRATION

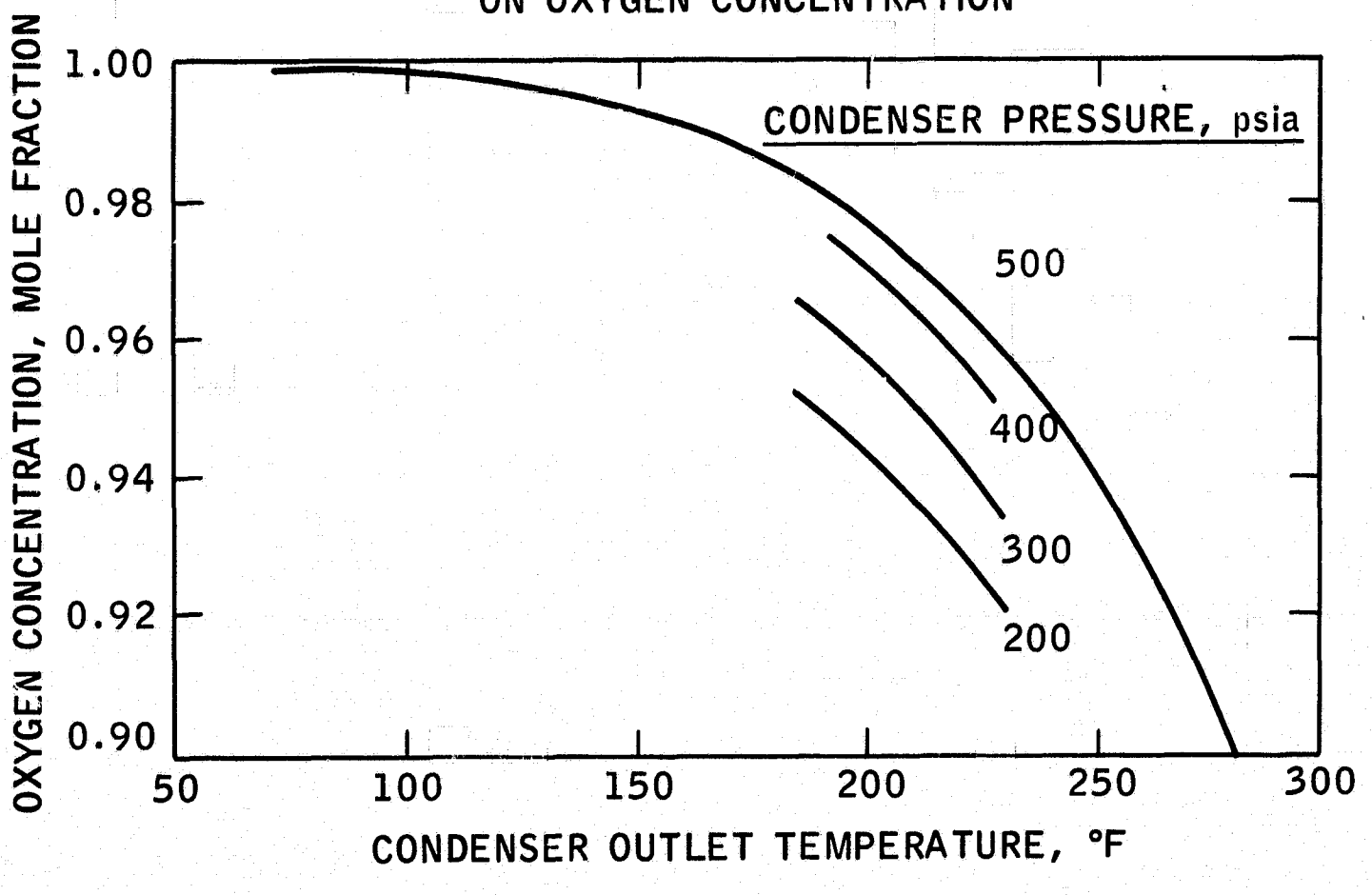

The presence of water vapor in the oxygen feed may also affect the static moisture removal mechanism employed in the Allis-Chalmers cells. Analytical and experimental studies at Allis-Chalmers have defined the water concentration gradients existing in the cell (15,16). Conventional cell operation results in water concentrations ranging from about 8 percent at the inlet port of the oxygen cavity to 11 percent at the exit port. In turn, a steady state transverse water gradient exists through the electrodes, capillary matrix, hydrogen cavity and water removal membrane. Detailed evaluation of the effect of additional water on the water balance system is beyond the scope of this study.

Part c - Selection of Fuel Cell Operating Points

Preliminary trade-off analyses were conducted to select the specific type and number of Allis-Chalmers fuel cell modules for a variety of potential on-load missions. These missions were assumed to require 200 to 5000 watts net power output for 100 or 1000 hours. The approach taken was to estimate the sum of stored reactant, tankage and fuel cell weight, using factors for tankage expulsion efficiency, storage stability, gas generator conversion efficiency, product recovery efficiency and feed gas utilization in the fuel cell. A conservative parasitic power factor of 10 percent above net power was used for these studies.

The basic characteristics of the fuel cell modules were described by Platner (12). These are summarized in Table 2. The trade-off studies showed that system weight was sensitive to variations in fuel cell voltage efficiency, particularly for the 1000 hour missions which are energy-storage limited. The radiation-cooled and liquid-cooled modules gave the lowest system weight projections. Occasionally, suitably down-rated multiple modules were found to be optimum. Table 3 contains a summary of the fuel cell design operating points. Conservative performance data, obtained after 50-60 days operation, were used for the designs. These data reflect the expected performance degrad tion rate of the Allis-Chalmers fuel cell modules. Details of the trade-off analysis are given in Appendix 4.

Table 2

Description of Allis-Chalmers Fuel Cell Modules

Module Performance Characteristic	Module Type		
	Radiation Cooled	Gas/Liquid Cooled	Liquid Cooled
Nominal Power Output, watts	200	2000	5000
Nominal Voltage, vdc	27	29	28
Weight(1), lbs	30	169	150
Overall Size, inches	7x7x17	16x21x32	11x11x32
Number of Cells	28	32 pairs	30 sections(2)
Parasitic Power Factor,(3)	0.01	0.05	0.015

(1) Ex reactants, associated tankage and space radiator, if required

(2) Four cells in parallel per section

(3) Parasitic Power Factor, π = $\frac{\text{Parasitic Power Required, watts}}{\text{Net Power Output, watts}}$

Table 3

Summary of Fuel Cell Operating Points

Mission On-Load Time, Hrs.	Power Output, Watts		Module Type and Number(1)	Module Power Output, Watts	Module Voltage(2)		Individual Cell Voltage at 50-60 Days
	Net	Gross			Initial	50-60 Days	
100	200	220	R(1)	220	26.4	25.0	0.893
	500	550	R(2)	275	25.9	24.4	0.875
	1000	1100	L(1)	1100	30.3	29.6	0.987
	5000	5500	L(1)	5500	27.0	26.2	0.873
1000	200	220	R(2)	110	27.6	26.2	0.936
	500	550	L(1)	550	30.8	30.1	1.003
	1000	1100	L(1)	1100	30.3	29.6	0.987
	5000	5500	L(4)	1375	30.0	29.3	0.977

(1) Allis-Chalmers Cells: R = Radiation-cooled module,
L = Liquid-cooled module

(2) 50-60 Day performance values chosen as design basis.

These studies assumed that unregulated output voltages would be acceptable for spacecraft use. The mean voltages will range from 28 to 31 volts, depending on the module and operating point. Voltage variations will be ±0.7 volts or less at steady state design conditions. In the absence of specific load profiles, the response of fuel cell performance to transient load factors was neglected. Suitable, lightweight voltage regulator designs are available, if required (31). These are integrated-circuit devices using high frequency pulse-width modulation. However, efficiencies do not exceed 90 percent and the parasitic power required to operate the regulator will increase reactant storage requirements.

Coulombic efficiency and reactant utilization factors were assumed equal to unity. These appear to be reasonable values based on eventually optimized purge cycles with pure reactants and the intrinsic capability of the Allis-Chalmers cells. Also, the internal heat and water balance operation of the fuel cell is assumed to be solved by the Allis-Chalmers design.

Reliability factors were neglected in this analysis. Obviously, increasing reliability by providing redundant modules will increase system weight, particularly for the shorter time missions. The 1000 hour mission weights will be relatively unaffected because the down-rated modules will operate at higher voltage efficiency, permitting some reduction in reactant tankage.

Other operational features of the Allis-Chalmers systems were reviewed briefly. Bootstrap startup capability and low temperature performance and storability are three critical characteristics of the multiple-restart, deep space fuel cells. Some Allis-Chalmers modules can withstand bootstrap startup from about 80°F (27°C) to a normal operating temperature of 190°F (88°C) in 6.5 minutes (12). This is accomplished by high current drain or short circuit operation, using internal self-heating to heat the module components. Platner states that startup can be achieved from temperatures as low as -20°F (-29°C) (12). The effect on module life of repeated startup under these conditions has not been demonstrated yet. Our feasibility study has assumed that bootstrap startup from +40°F (4°C) storage can be accomplished safely within 15 minutes.

The Allis-Chalmers cells can provide stable performance at temperatures as low as -35°C (14,16). The maximum sustained load at this temperature is about 5 ma/cm^2, rising to about 60 ma/cm^2 at -5°C. Gas leakage prevented operation below -40°C. The minimum storage temperature is reported as -40°C, probably set by the freeze point of the 38 wt. percent potassium hydroxide electrolyte (15). In turn, this sets a minimum level on the permissible dead-storage temperature for the multiple-restart power system.

The shelf life characteristics of these modules were also reported by Platner (12). Storage with internal cavities filled with inert gas for periods up to two years had no effect on performance. The modules appear storeable for at least 30 days at 80°F (27°C) with reactants in the cells at normal operating pressure, about 30 psia.

Both the radiation-cooled and gas/liquid-cooled modules have demonstrated the ability to withstand the extremes of launch and orbital flight environments. Evidently, the liquid-cooled module has not been space-qualified yet. From this analysis, the use of Allis-Chalmers fuel cells in the multiple restart power system appears feasible and justified. Minimum interface distortion is expected between the gas generator subsystems and the energy conversion subsystem.

Phase 3 - Hydrogen Generator Subsystem

The hydrogen generator subsystem contains the hydrazine storage tank, hydrazine decomposition reactor and hydrogen purifier, product coolers, accumulation tankage and associated hardware. The suitability of hydrazine as a storeable reactant was evaluated and preliminary systems analyses were performed to select the most appropriate hydrogen generation scheme. Experimental data were required to evaluate the activity of several decomposition catalysts required to convert hydrazine to hydrogen. These kinetic yield data were used in subsequent design studies.

Part a - Hydrazine Characteristics

Hydrazine has an established role in propellant technology, where it is used as a high specific impulse fuel in propulsion rockets and attitude-control thrust devices (32). Under suitable conditions, hydrazine may also be used as a source of hydrogen. Equation (3) describes the usual form of the overall stoichiometry of the hydrazine decompositon reaction. Neglecting the specific details of the reaction mechanism, a two-step sequence is often proposed. This is shown in Equations (4) and (5). As indicated, the decomposition of hydrazine is highly exothermic. Conversely, the associated ammonia decomposition reaction is endothermic. Catalysts are usually employed to decompose hydrazine, although Equation (4) can proceed as a non-catalytic homogeneous reaction.

$$N_2H_4 \longrightarrow \frac{4}{3}(1-x)NH_3 + \left(\frac{1+2x}{3}\right) N_2 + 2x\,H_2 \qquad (3)$$

Where: x = Fractional ammonia conversion

$$N_2H_4 \longrightarrow \frac{4}{3}NH_3 + \frac{1}{3}N_2 + 12.0\ \text{Kcal} \qquad (4)$$

$$NH_3 \longrightarrow \frac{3}{2}H_2 + \frac{1}{2}N_2 - 10.96\ \text{Kcal} \qquad (5)$$

Van Vorst has calculated the adiabatic reaction temperature for hydrazine decomposition as a function of ammonia conversion level (33). These data, shown in Figure 10, indicate that temperatures as high as 1380°C can be reached during the decomposition reaction and that complete conversion to hydrogen and nitrogen will yield a temperature of about 600°C. The use of diluted hydrazine feeds, such as hydrazine hydrate, will naturally yield lower decomposition temperatures.

Figure 10

HYDRAZINE ADIABATIC DECOMPOSITION TEMPERATURE

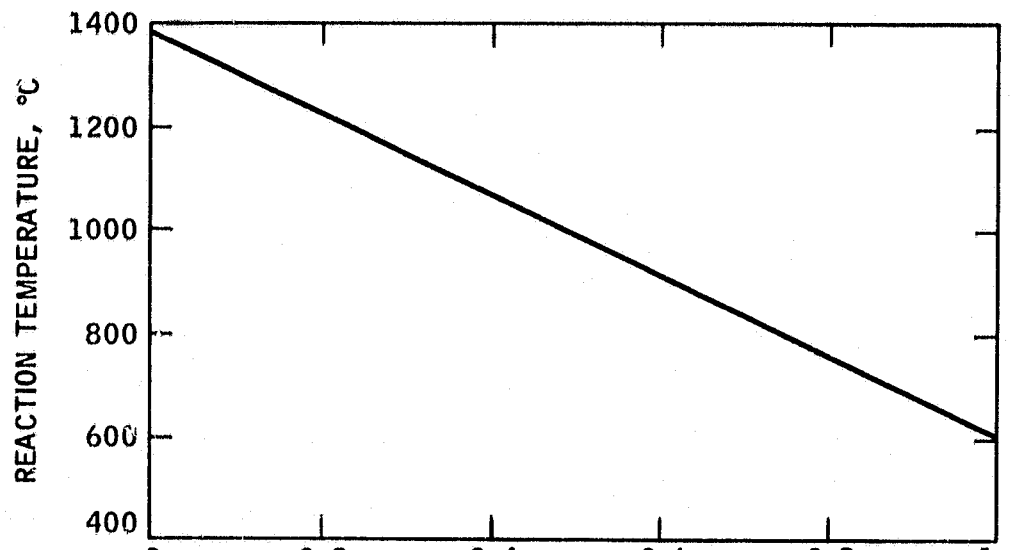

The storage stability of hydrazine has also received considerable attention. Data obtained by Axworthy show that propellant grade hydrazine, treated with barium oxide, is thermally stable in contact with 321 stainless steel at low temperatures (34). These data are shown in Figure 11.

Figure 11

HYDRAZINE STORAGE STABILITY

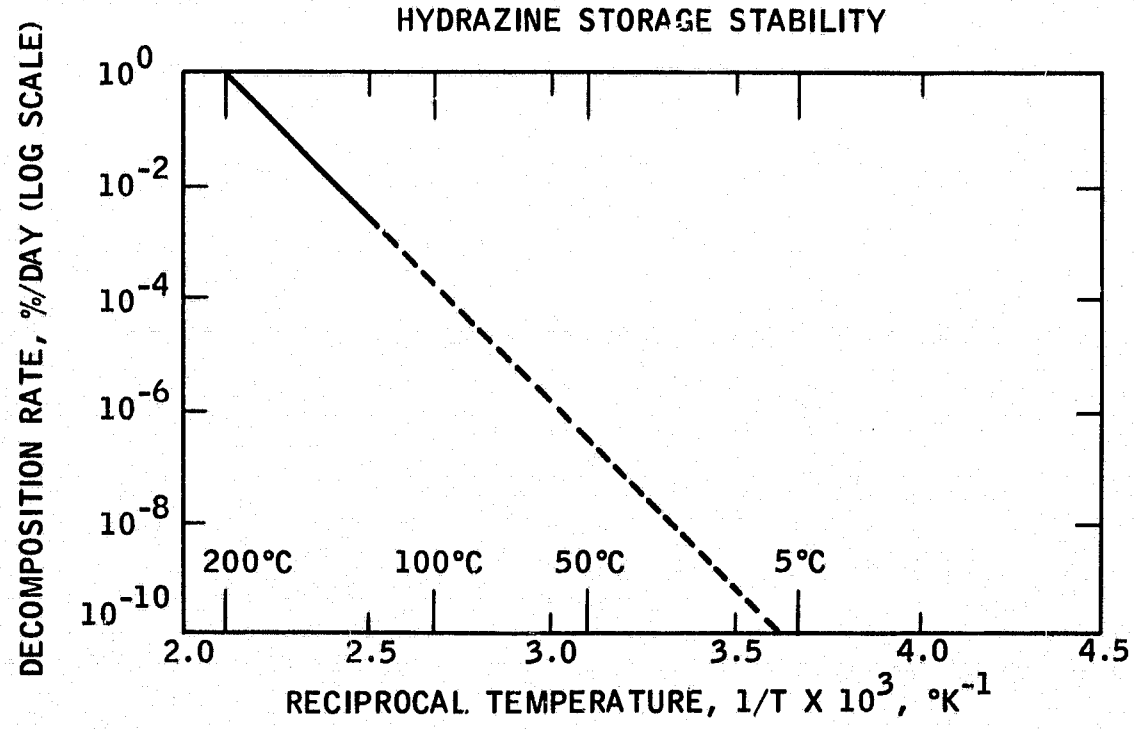

Indeed, the hydrazine tank pressure data, obtained from the Mariner IV flight, clearly show that hydrazine storage stability will not be a problem in an aerospace environment (32). Subsequent design studies will propose the use of plutonium 238 radioactive isotope heaters for overall thermal balancing in deep space. Calculations described in Appendix 5 show that the resulting radiolysis yields for hydrazine decomposition are trivial (35). Other studies of radiation effects indicate that hard X-rays may cause minor decomposition (36).

Additional information on hydrazine handling safety and general physical and thermochemical properties is also available (37,38).

Part b - Potential Systems Approaches

Several schemes may be used to generate hydrogen from hydrazine. The high temperature catalytic decomposition process was selected for the center-line design. This route will yield the simplest system with minimum reactant requirements. In this system, the use of a palladium-silver diffuser to recover pure hydrogen is feasible because the reactor product gases are available at high temperature. Earlier it was shown that pure hydrogen feed was required for effective fuel cell operation.

The center-line design uses neat hydrazine, rather than diluted mixtures, to reduce stored reactant weight. In turn, this fixes the minimum reactant storage temperature at +2°C, the freeze point of hydrazine. Dilute fuels, such as hydrazine hydrate with a -52°C freeze point, must be used if operability is required at -40°C, the minimum practical fuel cell storage temperature. Systems studies discussed later will show that much lower equilibrium temperatures will prevail in deep space missions. Hence some form of passive heating or thermal control will be required in any event. A possible low temperature approach would be to use intermediate tankage containing diluted start-up feed. This tank would be replenished during operation using recovered water from the fuel cell or the peroxide decomposition reactor. As discussed in Appendix 1, this approach was rejected because complex fluid management procedures are required. In addition, the safe melting of frozen neat hydrazine in the main reactant tanks is questionable.

An alternative, low temperature hydrazine decomposition reactor system was rejected on the basis of poor selectivity and probable excessive weight. This system used a potassium hydroxide moderator and is discussed more fully in Appendix 6.

Winsel has described another approach that uses electrodecomposition to produce stoichiometric yields of hydrogen and nitrogen (39). Unfortunately, the product is available at low temperatures that prevent the effective use of a palladium diffuser. Again, the use of impure hydrogen would decrease the utilization factor in the fuel cell, resulting in excessive reactant storage requirements.

Part c - Hydrazine Decomposition Studies

A number of hydrazine decomposition catalysts with spontaneous ignition capability are available. These catalysts are normally used in rocket firing applications using high bed loadings or mass flow rates of hydrazine feed (32). Predictable and repeatable ignition delay response, in the millisecond range, is required for this stringent application. The operational requirements for use in the hydrogen gas generator are less severe. Experimental data were obtained to define catalyst activity, kinetic yield data and to evaluate potential reactor design problems.

Most rocket reactors use Shell 405 catalyst, an iridium-based, spontaneous catalyst that has demonstrated activity at temperatures as low as -65°C (40 - 43). High cost is the major disadvantage of Shell 405 catalyst. In addition, catalyst shrinkage and fines production have been noted in rocket-firing tests (32). A stable, proprietary, non-noble metal catalyst Esso 104, is also available. Both Shell 405 and the lower cost Esso 104 were used in the experimental studies. Other non-strategically limited catalyst compositions are being developed in our laboratories under contract with the Air Force Rocket Propulsion Laboratory (43).

Hydrazine decomposition data were obtained in small tubular, packed bed reactors. Feed flow rates were increased gradually until breakthrough of unreacted hydrazine was noted. Generally this created a fog or mist in the product gas collection system. Hydrazine decomposition was complete for space velocities below visual breakthrough. At these space velocities, a maximum fractional ammonia conversion of x = 0.7 was observed with Esso 104 catalyst. These data are shown in Figure 12. Gas chromatographic procedures were used to analyze the product gases. Details of the reactor assemblies and conversion data are given in Appendices 7 and 8.

Figure 12

EFFECT OF HYDRAZINE FEED RATE ON AMMONIA CONVERSION

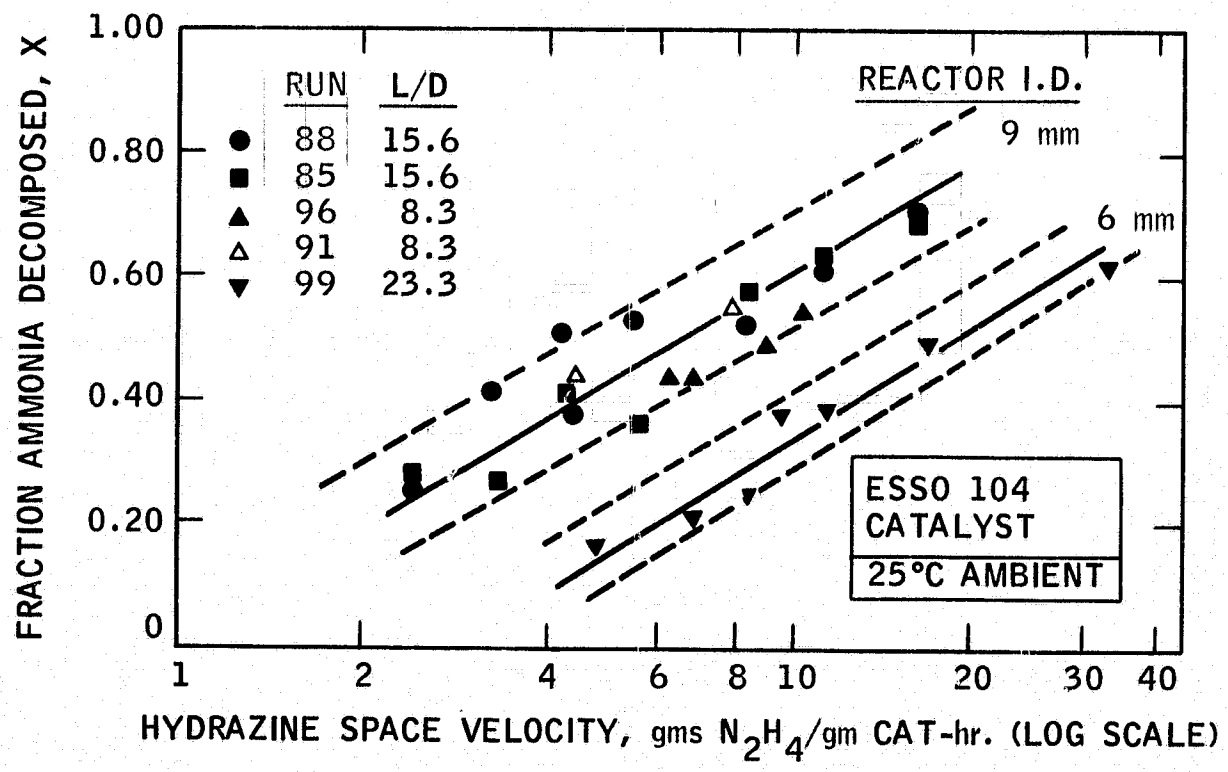

The maximum hydrazine space velocity for complete conversion is about 15 gms N_2H_4/gm cat-hr. The product gas composition at x = 0.7 is listed in Table 4. It is evident that further decomposition of ammonia is needed to raise the yield of hydrogen to a target value of about 98 percent of theory. Ammonia decomposition studies are discussed below.

Table 4

Product Gas Composition From Hydrazine Decomposition Reactor

Component	Mole Fraction
Hydrogen	0.538 (1)
Nitrogen	0.308
Ammonia	0.154

(1) Theoretical value is 0.667

Instantaneous start-up was achieved throughout these initial studies using room temperature hydrazine feed. The same batch of Esso 104 catalyst was used for over 15 hours in different reactor assemblies with no apparent performance loss or significant fines generation.

Initial reactor firings in 15-25 mm diameter Vycor reactors were terminated abruptly when the decomposition flame front receded into the fuel inlet line. In subsequent studies with 9 mm reactors, this problem was corrected by using a cooled, thin capillary feed line to reduce axial heat transport from the hot reaction zone. Also, dead zones of hydrazine hold-up were eliminated between the feed line and the active catalyst bed within the reactor. It is essential to prevent hydrazine vapor penetration into the feed line. Although hydrazine liquid is reasonably stable, explosive decomposition can occur in the vapor phase. Actually, the design of stable autothermal catalytic reactors is complex. This problem is discussed further in Part e of this Phase.

Part d - Ammonia Decomposition Studies

Initial hydrazine decompositon data, obtained with Esso 104 catalyst, showed that typical product gas streams contained a minimum of 15 percent ammonia. This corresponds to a fractional ammonia conversion level of x = 0.7. Additional decomposition of ammonia is required to increase hydrogen yields to the target value of about 98 percent of theory.

The synthesis of ammonia is an industrially significant process. As a result, the kinetics and catalysis of the ammonia synthesis and decomposition reactions have been studied in some detail. Extensive general reviews are available (44-47). Specific catalyst compositions also have been evaluated, particularly in Japan (48-55).

Ammonia decomposition was studied experimentally using Girdler G-47, an iron-on-sintered alumina catalyst. This catyst was selected because of its stability at the high temperatures expected in the hydrazine decomposition reactor. Runs were made with simulated hydrazine decomposition product gases containing 27% and 45% ammonia. Several space velocities and operating temperatures were studied at atmospheric pressure. Effective rate constants were calculated using the conventional Temkin-Pyzhev ammonia decomposition expression, together with integral reactor design equations (56). Details of the procedures used are given in Appendix 9. Complete data are listed in Appendix 10.

As shown in Figure 13, the activity of Girdler G-47 was rather low. Temperature levels in excess of 750-800°C are required to achieve the target levels of ammonia decomposition with reasonable catalyst loadings. These temperatures cannot be achieved in an adiabatic system because the theoretical flame temperature for the reaction of hydrazine to hydrogen and nitrogen, including complete decomposition of ammonia, is only 600°C. Supplying additional heat to the reactor to overcome the endothermic ammonia decomposition reaction will reduce overall system efficiency.

Figure 13

AMMONIA DECOMPOSITION WITH GIRDLER CATALYST

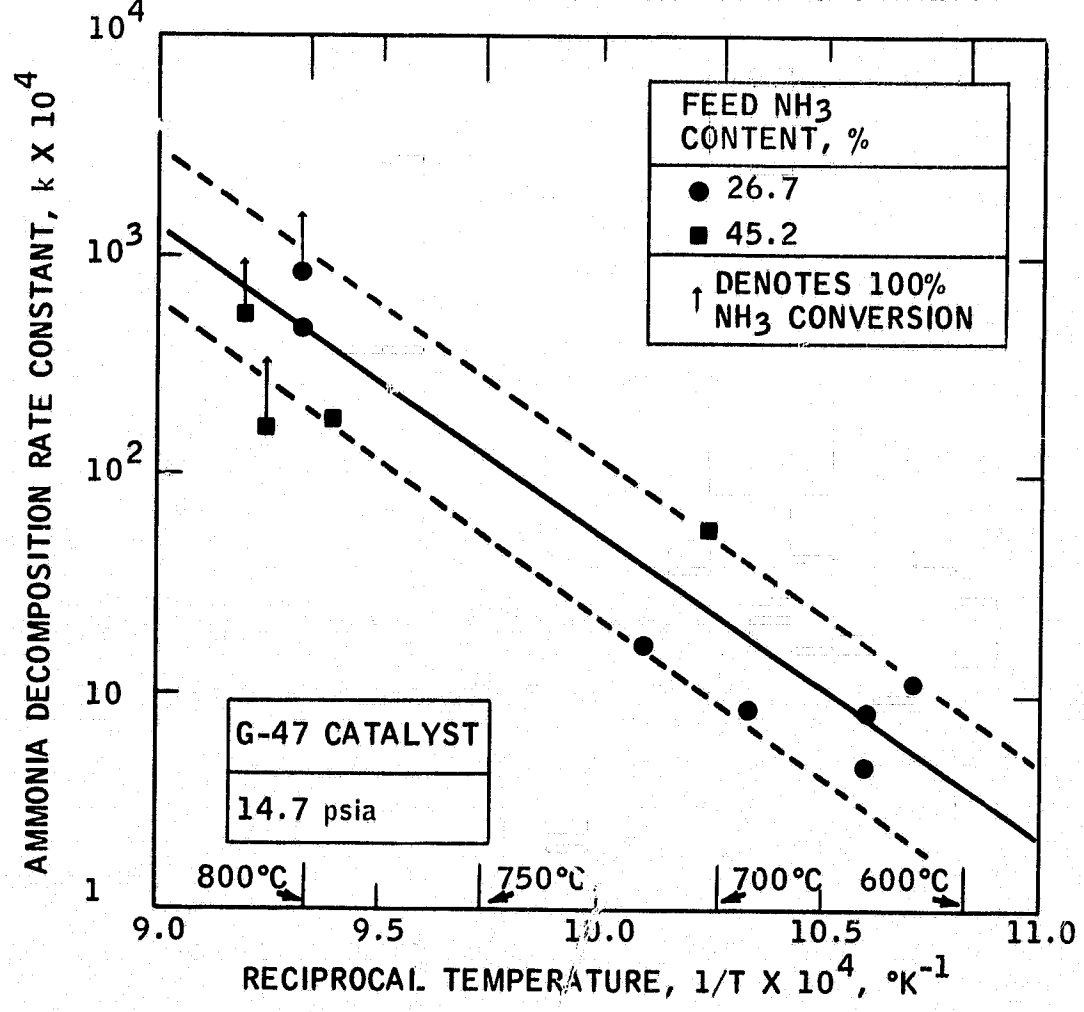

Catalysts with improved activity are required. Fortunately, a number of promoted iron-alumina catalysts, used for ammonia synthesis, are available. Typical literature data for these catalysts, shown in Figure 14, indicate that they are about 100 times more active than Girdler G-47 (54). These catalysts lose activity via sintering when operated at temperatures above 600°C. However, loss of catalyst activity should be low during the expected life of the multiple reserve power system. A typical ammonia synthesis catalyst, Haldor Topsoe KM-1R, was obtained and used in the composite reactor runs discussed in Part e.

Figure 14

COMPARISON OF AMMONIA DECOMPOSITION CATALYSTS

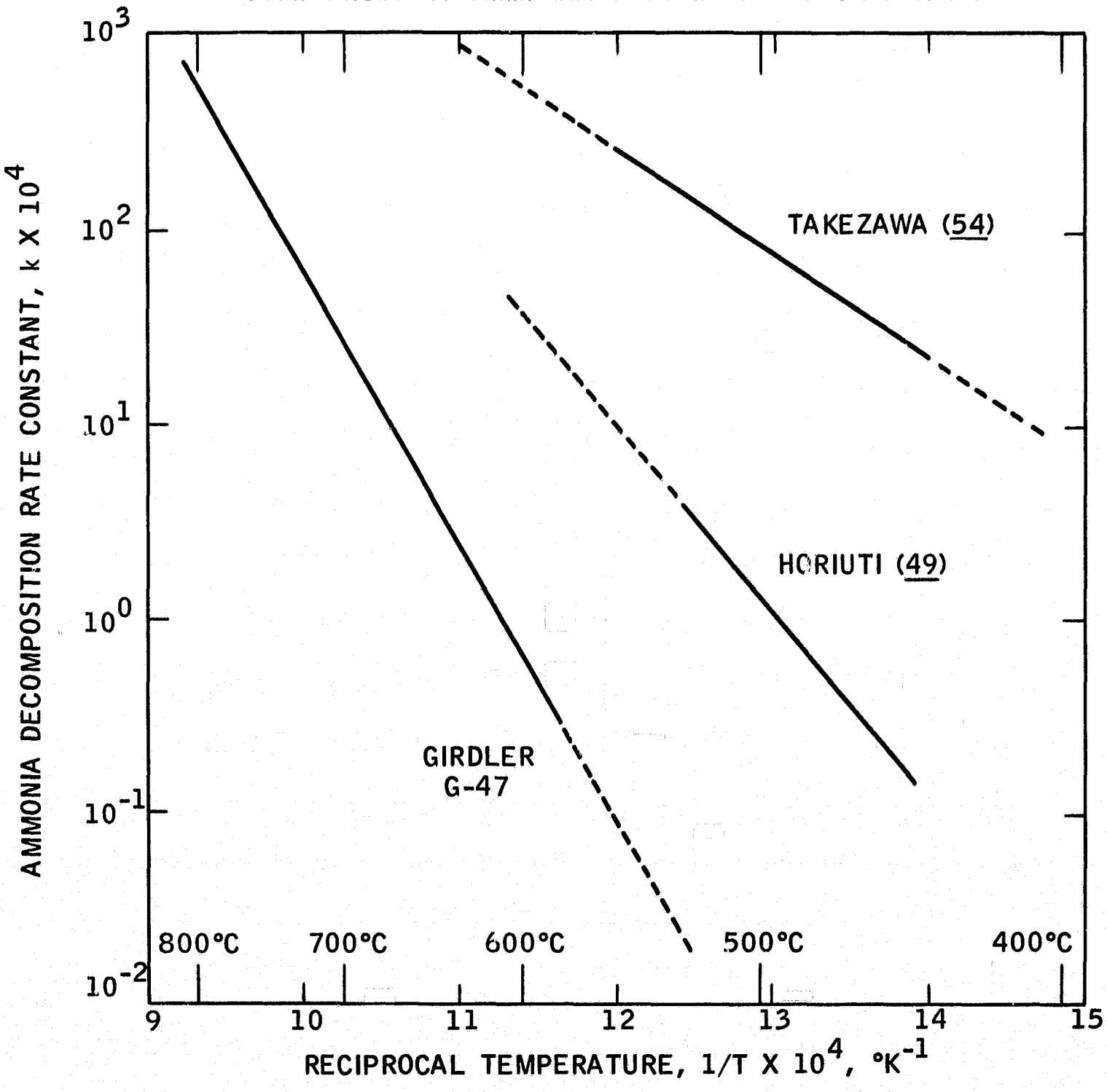

Part e - Composite Reactor Studies and Reactor Design

Hydrazine decomposition runs were made in composite reactors containing mixed catalyst charges. Esso 104 and Shell 405 hydrazine decomposition catalysts were used together with Girdler G-47 or Haldor-Topsoe KM-1R ammonia decomposition catalysts. The latter were activated in-situ. Reactor performance was studied at temperatures from 25°C down to -40°C.

As shown in Figure 15, the addition of G-47 and KM-1R catalysts substantially increased the extent of ammonia decomposition. The maximum conversion level, x = 0.85, was obtained with a mixed bed of Shell 405 and KM-1R. Feed system limitations prevented operation at higher space velocity. Complete data are listed in Appendix 8.

Figure 15

EFFECT OF CATALYST CHARGE
ON AMMONIA CONVERSION

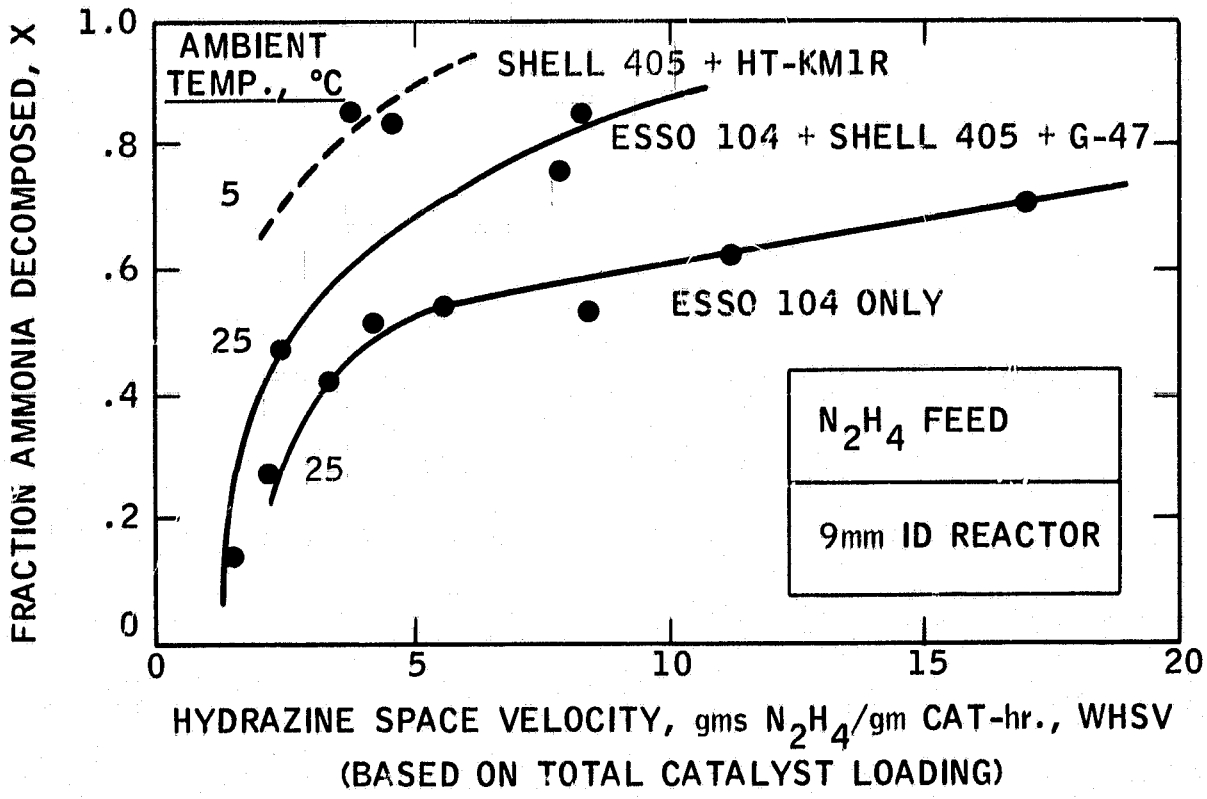

Ammonia decomposition levels must be increased still further. The Haldor-Topsoe catalyst is active and more rigorous adherence to commercial activation practice would probably improve activity. Nevertheless, average catalyst bed temperatures of 500-600°C are still required for maximum effectiveness. The performance characteristics of simple, in-line packed beds are inadequate, at least for the small reactors tested. For example, hydrazine feed rate had a pronounced effect on the temperature distribution within the reactor. The data in Figure 16 show that the intense hydrazine decomposition zone at low flow rates is localized at the reactor inlet. At higher flow rates the converse is true. Proper spacial distribution of the catalysts within the bed might reduce these variations in temperature. As it stands, the in-line reactor has poor throttling characteristics. This is shown in Figure 17. For these figures, hydrazine weight hourly space velocity, WHSV, is defined as gms N_2H_4/gm cat-hr, using the total reactor catalyst charge.

Figure 16

EFFECT OF FEED RATE ON REACTOR STABILITY

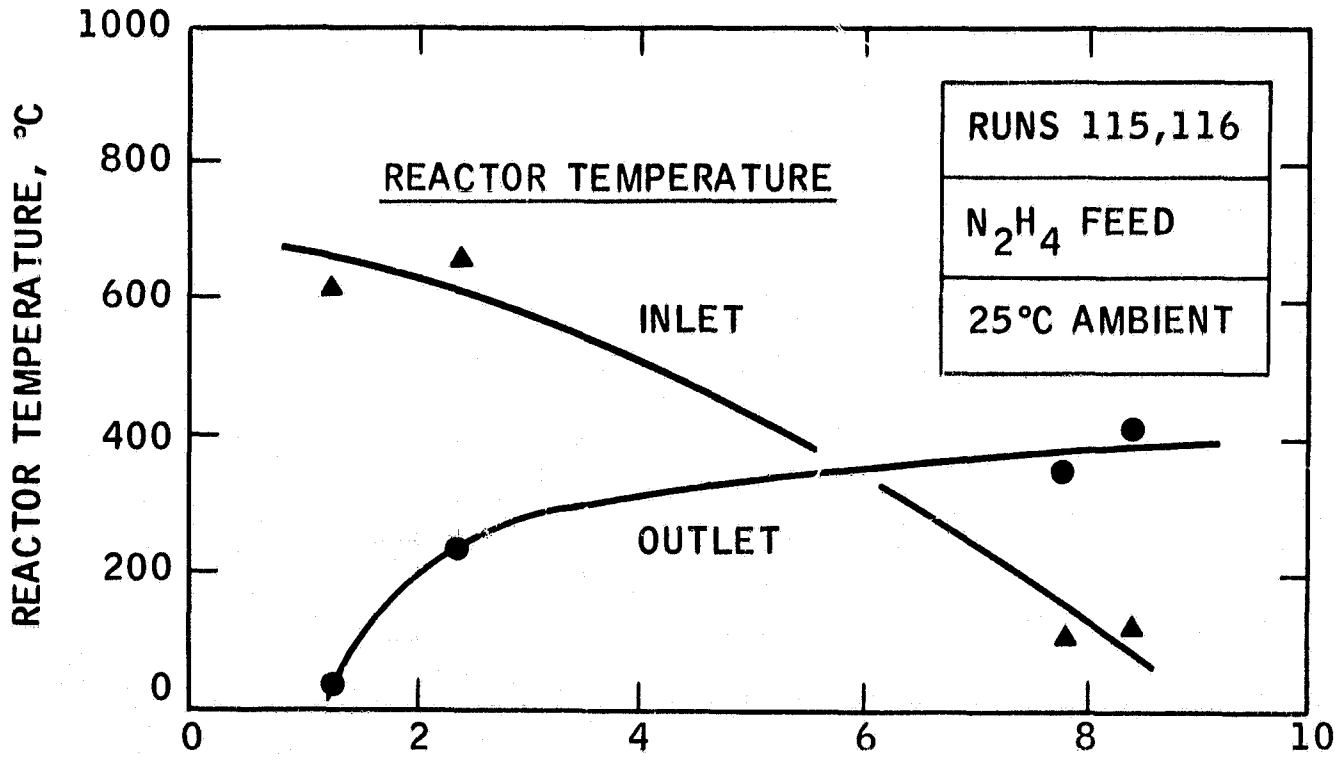

Figure 17

THROTTLING CHARACTERISTICS OF IN-LINE COMPOSITE REACTOR

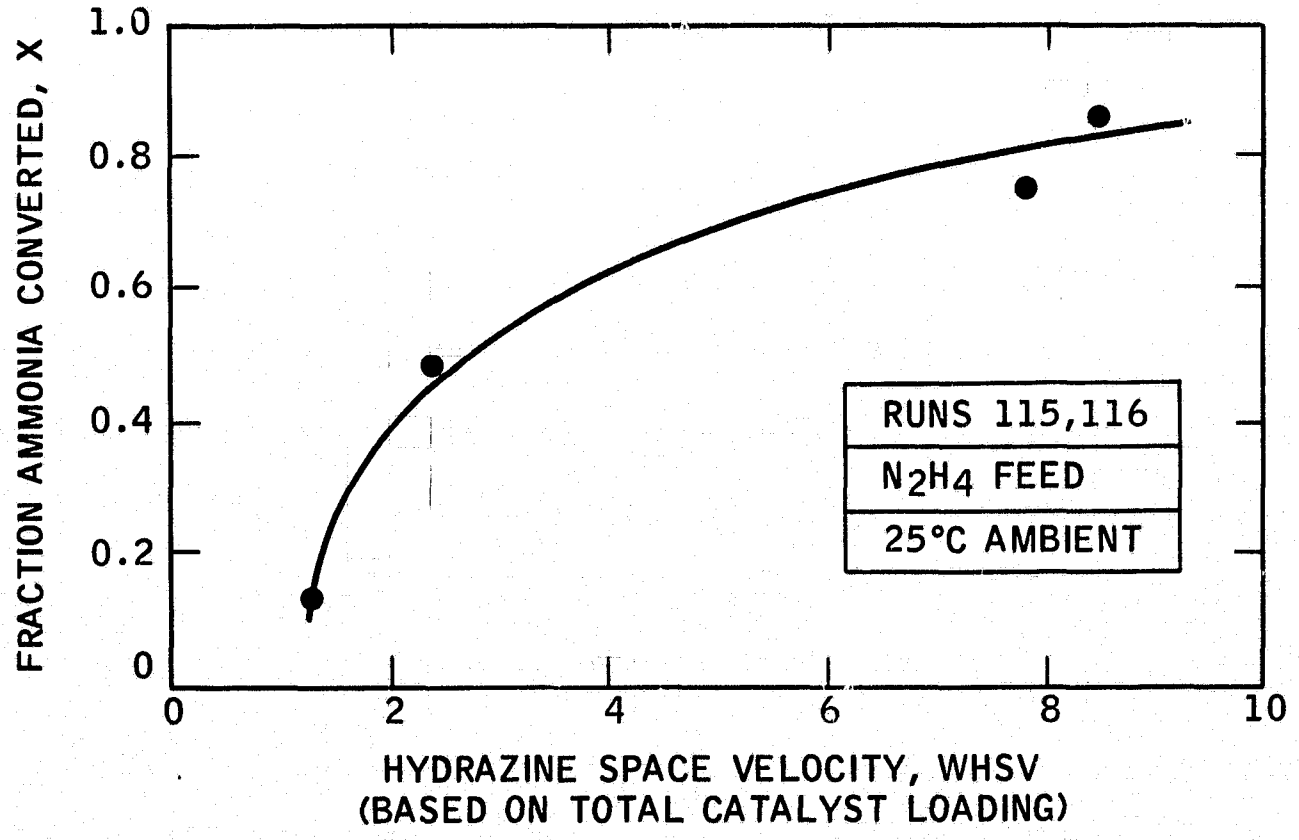

Optimization studies are required to define the effect of catalyst bed geometry and system heat loss on reactor stability and performance. The composite reactors were not operating adiabatically, despite the addition of conventional external insulation. Radial and longitudinal heat transfer effects play a critical role in establishing stable operation with autothermal reactors. Considerable effort has been devoted to defining the stable operating modes of these systems (57-65). Kesten has analyzed the performance of hydrazine-fueled rocket beds (66). The analysis is tedious, but crucial. These optimization studies were considered beyond the scope of the present contract.

It is assumed that reactor geometries can be developed to ensure essentially complete conversion of ammonia without excessive catalyst loadings. Subsequent design studies assumed that an average ammonia catalyst bed temperature of 500°C can be maintained by suitable design and insulation techniques. Typical geometries that may be used are shown schematically in Figure 18. An interesting "fail-safe" variant would be to develop an integrated reactor containing hydrogen peroxide decomposition zones within the ammonia catalyst beds, as shown in Figure 19. The peroxide reactors would act as heat sources to maintain the ammonia beds at 500°C or so. Erickson recently discussed a trimode propulsion device that involves the integration of hydrazine and peroxide reaction chambers (67).

Again, heat transfer characteristics will be critical. Predictions of the heat transfer coefficients between the packed catalyst bed and reactor interior walls showed that these coefficients would only be about 1-10 BTU/hr ft °F (68). Effective radial thermal conductivities for packed beds were not calculated, but adequate correlations exist (69,70). Finally, some form of internal area augmentation, such as extended surface finning, will probably be required to accomplish the necessary heat transfer (71).

The start-up characteristics of the in-line composite bed reactor were also evaluated at -40°C using hydrazine hydrate fuel. These data are given in Appendix 8.

Figure 18

REACTOR CONCEPTS

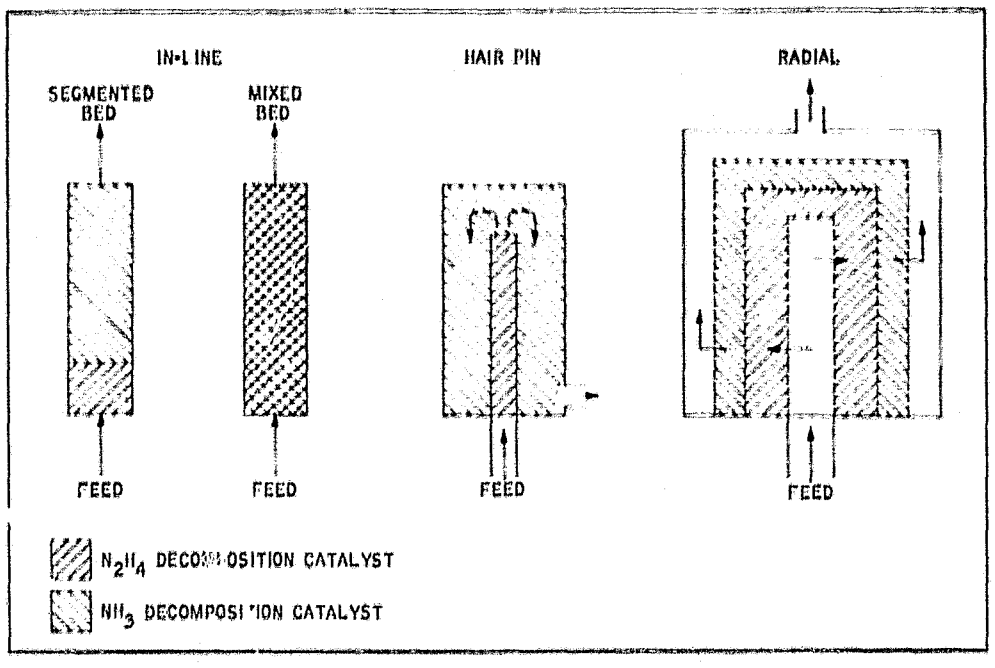

Figure 19

INTEGRATED REACTOR APPROACH TO HEAT CONSERVATION

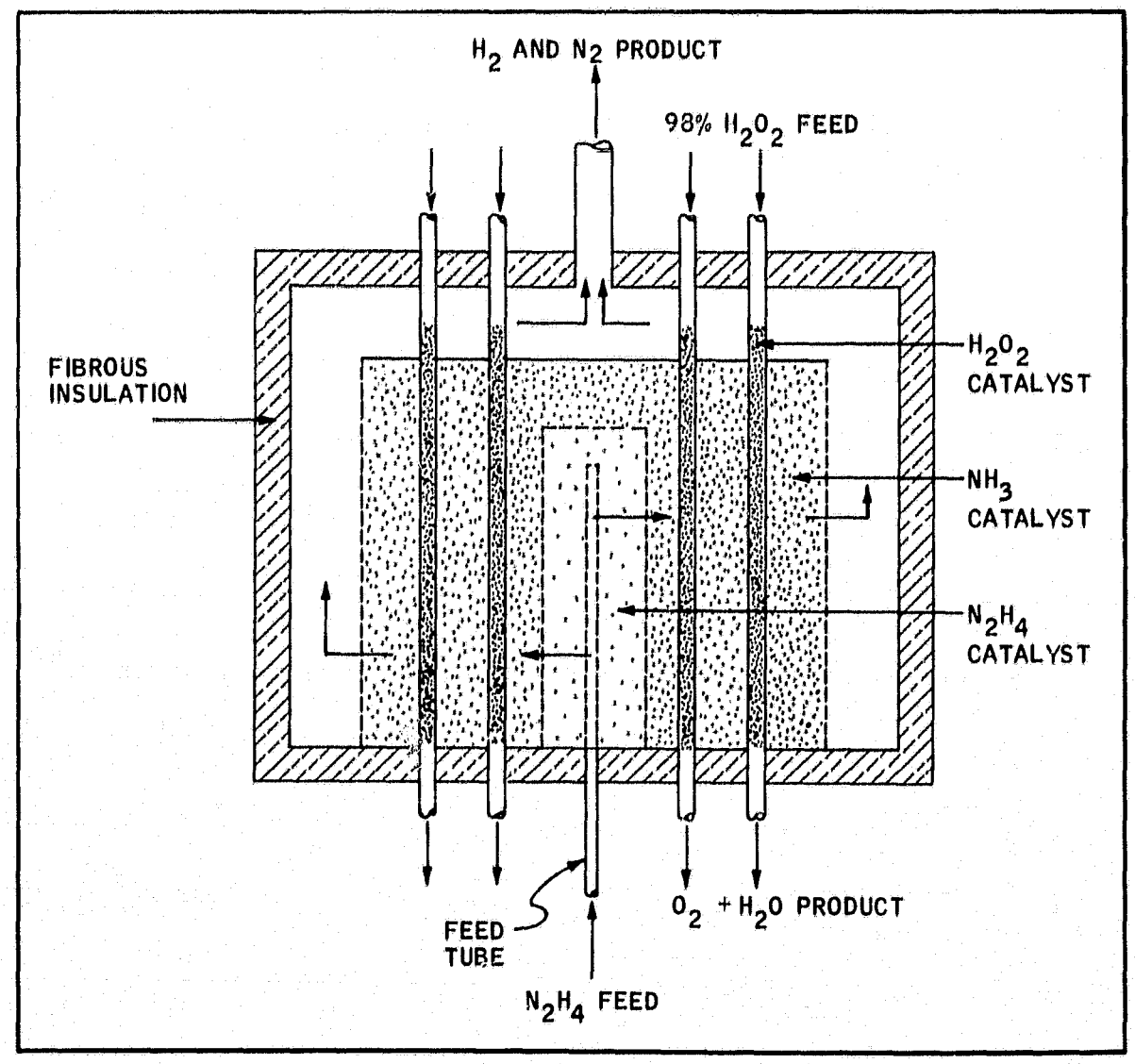

Part f - Hydrogen Generator Subsystem Design

Hydrogen generator subsystem designs were prepared for the assumed mission loads, ranging from 200 to 5000 net watts power output for on-load times of 100 and 1000 hours. Hydrazine feed rates were calculated using design values for the following variables:

- Hydrogen yield from the integrated hydrogen reactor
- Hydrogen recovery factor for the palladium diffuse
- Fuel cell voltage and coulombic efficiency
- Fuel cell hydrogen utilization factor
- System parasitic load factor

Required hydrazine flow rates ranged from 1.2 to 33.1 gms/min, depending on system power level. Calculation details are given in Appendix 11.

Hydrazine storage requirements were estimated using design values for the following factors:

- System hydrazine flow rate and mission on-load time
- Hydrazine storage stability
- Tankage expulsion efficiency

The system storage temperature was assumed to be about 5°C, or high enough to prevent hydrazine freeze-up. Potential thermal control systems to accomplish this are discussed in Phase 5. Stored hydrazine weights ranged from 19 to 4377 lbs. Complete data are presented in Appendix 12. A tankage weight analysis was carried out using two options, a positive expulsion bladder system or an advanced capillary action (Zero G) system. These are shown schematically in Figure 20.

Figure 20

SCHEMATIC DIAGRAM OF TANKAGE CONCEPTS

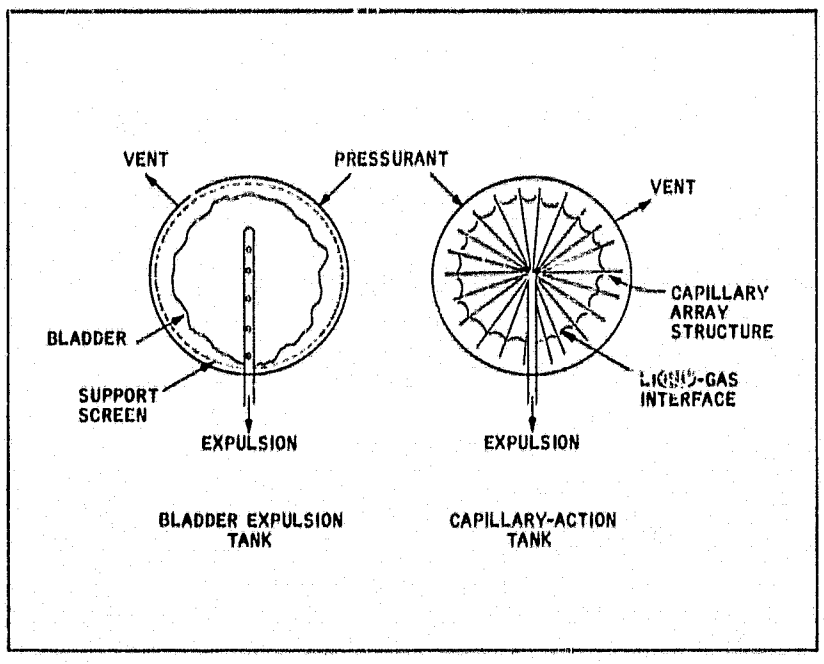

Experience with Mariner IV has shown that hydrazine may be safely stored in 6Al-4V titanium tanks containing butyl rubber bladders (32). The major problem encountered with these systems is probably accelerated hydrazine decomposition catalyzed by the bladder constituents (72). Sufficient ullage must be provided within the bladder to accomodate the gaseous decomposition products. Alternatively, an interior venting system may be provided to remove the gases or they may diffuse through the bladder wall into the space between the bladder and the tank wall.

Considerable progress has been made to develop other fluid management techniques for zero G environments (73-78). The most intriguing of these is the capillary-action tank that uses surface tension forces to control the location of the gas-liquid interface within the tank (73). Constant expulsion of liquid, rather than gas-liquid mixtures, is desirable for controlled operation of the hydrogen generator system. On the other hand, system requirements for constant quality feed are not as severe as those imposed by rocket propulsion reactors. Titanium capillary-action tanks were selected for the hydrogen generator system. Spherical tanks were assumed, although future optimization and packaging studies may show that cylindrical shapes will result in lower overall system volume. Estimated tankage weights ranged from 2.7 to 102 lbs, as discussed in Appendix 13.

An integral unit configuration was chosen for the decomposition reactor, similar to those discussed in Part e. Shell 405 catalyst was used, although Esso 104 would be equally suitable. Only small amounts of catalyst were required for complete hydrazine decomposition, ranging from 0.01 to 0.29 lbs. Ammonia decomposition catalyst requirements were estimated, assuming that the reactor geometry chosen would result in an average bed temperature of 500°C. Haldor-Topsoe KM-1R catalyst was selected, using extrapolated kinetic data on a well-reduced doubly-promoted iron catalyst (54). Atmospheric pressure rate data were used, although the reactor will operate at 500 psia. About 0.06 to 1.72 lbs of catalyst were required, depending on the system power output. The overall hydrogen generation efficiency factor was 0.98.

The reactor pressure is 500 psia, dictated by the operating characteristics of the palladium diffuser. A nominal 20 psia pressure drop was assumed across the reactor. Cast stainless steel, ACI Type HK, appears to have the necessary high temperature strength and corrosion resistance to withstand exposure to hydrogen and oxygen within the reactor (66,79). A fibrous insulation, suitable for high temperature operation was selected to minimize heat losses from the reactor, based on published NASA data (80). The final reactor weight estimates ranged from 3.9 to 9.6 lbs, a very small fraction of the overall system weight. Details are presented in Appendix 14.

Feed pumps will be required for reactor operation at 500 psia. Although a detailed study of pump selection was not performed, appropriate models appear available. These are discussed in Appendix 15.

The design of the palladium diffuser was carried out using the technique described by Hunter (81). Alternative procedures are available, but design data were not presented for their use (82). A hydrogen recovery factor of 0.966 was used, making the pure hydrogen stream available at 427°C and 30 psia pressure. It was assumed that the diffuser tube wall could be increased to 0.010 inches from the standard 0.003 inches to permit operation at 450 psi pressure differential. Start-up time for the diffuser should be less than 15 minutes, using a heat-conservation reactor-diffuser packaging appproach. Design details are given in Appendix 16.

Small filters may be required to remove catalyst fines in the high pressure reactor/diffuser product stream. The hot hydrogen and nitrogen effluents are cooled to about 66°C in separate, small space radiators. A simplified radiator sizing approach was selected, similar to the one described by Boretz (83). These designs are not critical, although optimized techniques are available (84,85). NASA experience indicates that these radiators weigh about 1.5 lbs/ft^2 (5). The calculation procedures are given in Appendix 17.

Product accumulation tanks were also sized. The non-optimized spherical tanks will be fabricated from 306 or 316 stainless steel with a wall thickness of 0.05 inches. Normal filling temperature will be 66°C, but the hydrogen tank is sized to deliver the required 15 minute start-up fuel at a system storage temperature of 5°C. The delivery pressure at this temperature would be about 24.6 psia, somewhat below the 30 psia required by the Allis-Chalmers fuel cell modules. Future trade-off studies would be required to optimize tankage sizes. The tanks would be filled at lift-off.

Hydrogen tank size is a critical factor requiring further study. Very large tanks are required to store the pure, low pressure hydrogen product obtained from the diffuser. Future studies may show that hydrogen recompression to about 150 psia may result in lower system weight, even though parasitic power will be required to operate the compressor.

The high pressure nitrogen tank design is not critical. A suitable size was assumed, sufficient to provide hydrazine feed tank pressurant. Excess nitrogen is vented overboard. Also, an overall weight estimate was made for the ancillary tankage hardware, pressure regulators, vent check valves and associated piping. Details of the tankage system design are presented in Appendix 13.

The design, construction and operation of the hydrogen generator subsystem is judged to be feasible, using current technology. A summary of the specific component weight analysis is presented in Phase 5.

Phase 4 - Oxygen Generator Subsystem

The fuel cell oxygen supply is obtained from the decomposition of stored hydrogen peroxide. The oxygen generator subsystem consists of appropriate tankage and auxiliary hardware, closely resembling the components of the hydrogen generator assembly. Again, considerable propellant-based technology is available for design studies (86-88). Hydrogen peroxide decomposition is an intrinsically simpler problem. Therefore, only limited experimental studies were made to confirm system operability.

Part a - Hydrogen Peroxide Characteristics

Hydrogen peroxide decomposes cleanly to form oxygen and by-product water, as indicated in Equation (6).

$$H_2O_2 \longrightarrow \frac{1}{2}\ O_2 + H_2O + 23.4\ \text{Kcal} \qquad (6)$$

The reaction is strongly exothermic and is usually carried out in the presence of an appropriate heterogeneous catalyst.

The extent of peroxide decomposition is limited only by the availability of catalyst surface and essentially stoichiometric yields of oxygen are obtained. Williams (89) has calculated the adiabatic decomposition temperature as a function of feed peroxide content. These data are shown in Figure 21.

Figure 21

HYDROGEN PEROXIDE ADIABATIC DECOMPOSITION TEMPERATURE

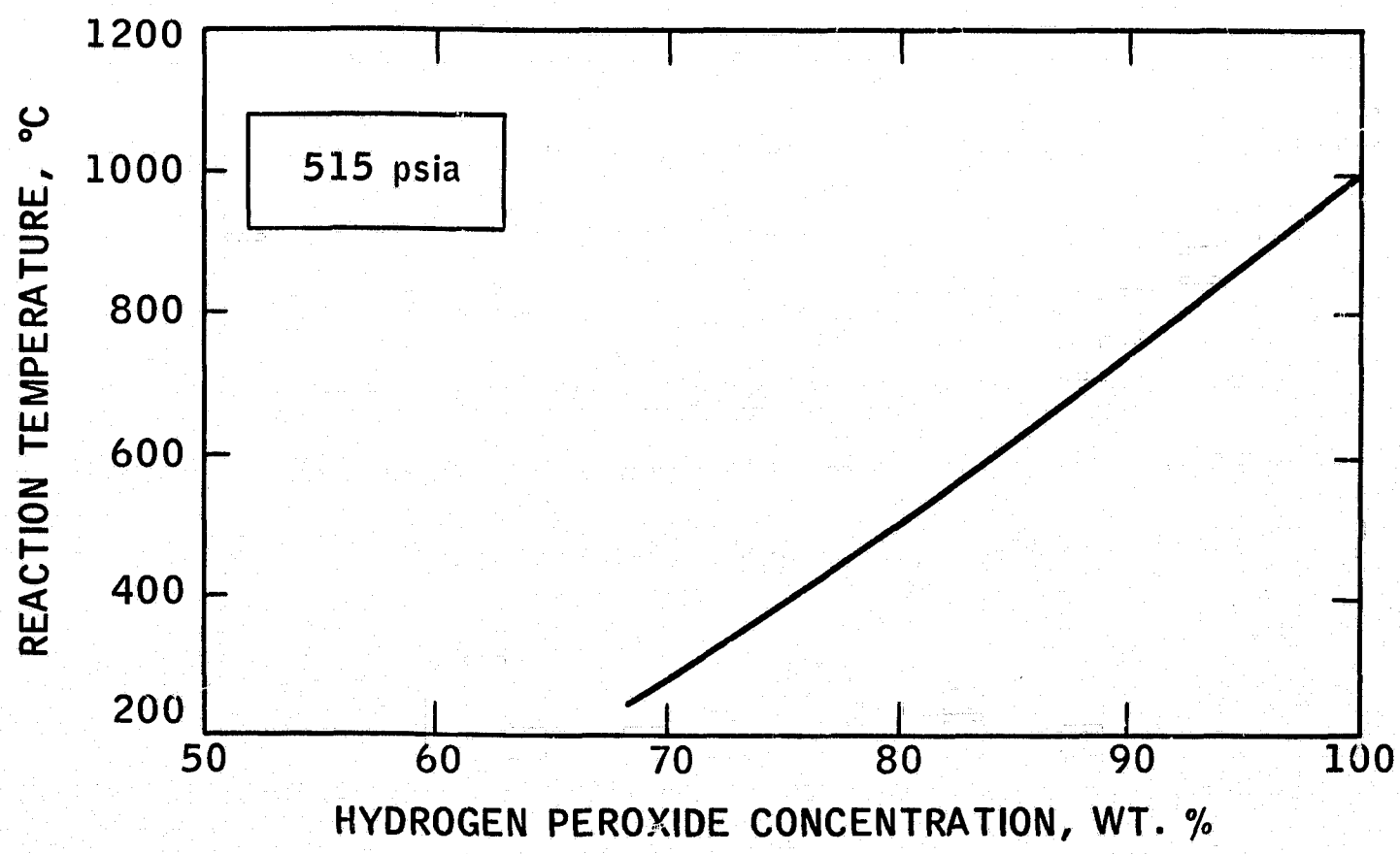

Concentrated hydrogen peroxide solutions, ranging from 70 to 98 wt. percent, are available for aerospace usage (90). The data in Figure 21 show that temperatures exceeding 1000°C result from the decomposition of 98 wt. percent peroxide solutions. The ease with which these solutions decompose often poses safety problems. Considerable effort has been spent to define safe peroxide handling techniques (37,90,91). In essence, rigorous cleaning and passivation procedures must be used on all surfaces that come in contact with the peroxide solutions.

Hydrogen peroxide storage stability is acceptable in the absence of specific catalytic surfaces. Homogeneous decomposition rates for liquid peroxide solutions are low, particularly at low temperatures, as shown in Figure 22 (37). The presence of nearby alpha radiation from plutonium 238 radioisotope heating elements will not affect peroxide stability because the radiolysis yields are low (91,92).

Figure 22

HYDROGEN PEROXIDE STORAGE STABILITY

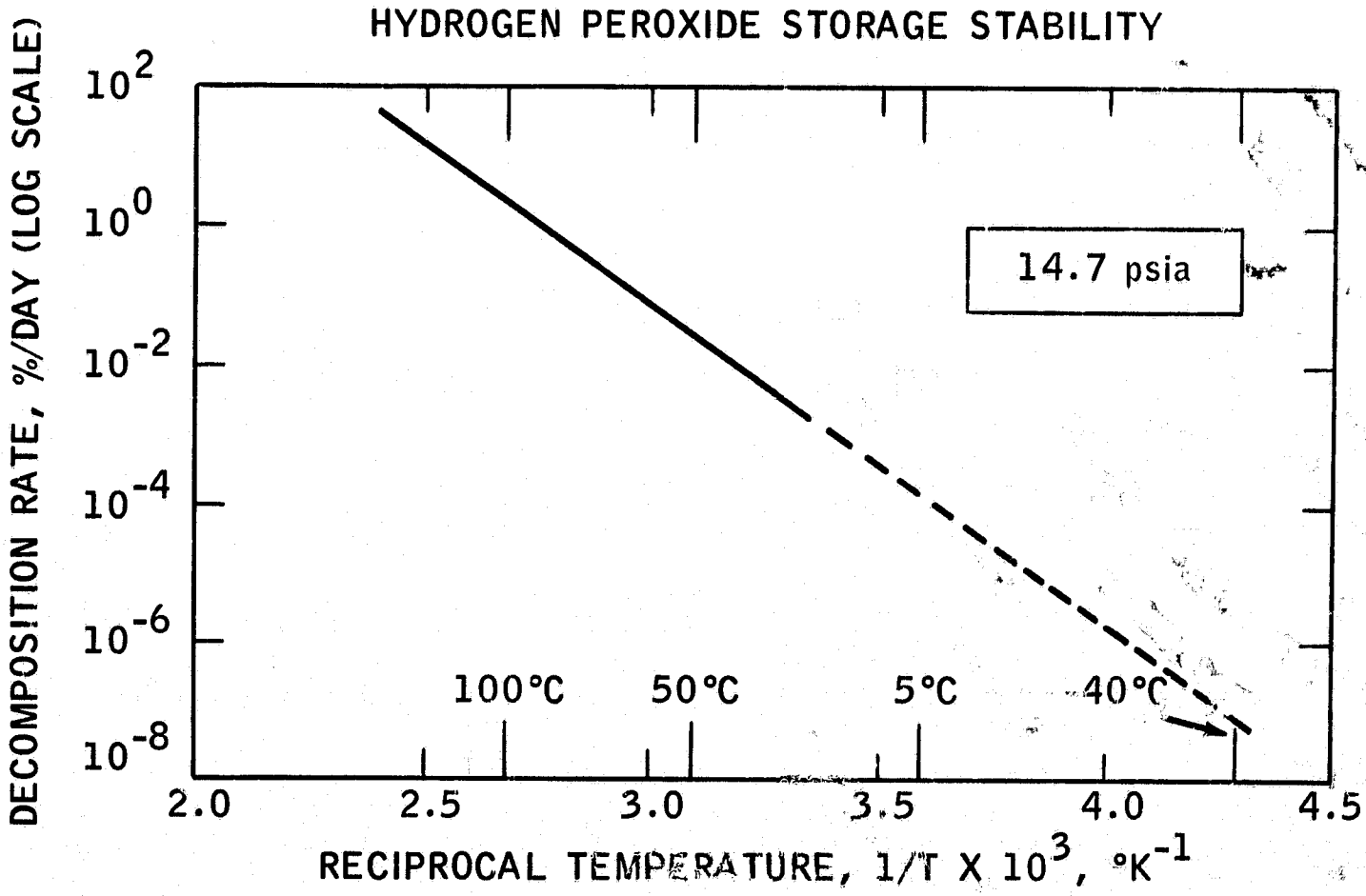

Finally, the physical and thermochemical properties of hydrogen peroxide have been summarized in definitive form by Schumb (91).

Part b - Potential Systems Approaches

The direct decomposition of concentrated hydrogen peroxide solution, using appropriate catalysts, will provide the simplest and most reliable oxygen generator system. This technique has been demonstrated in previous studies to develop on-board life support systems for spacecraft (93).

Once again, a minimum system storage temperature must be chosen. The lowest possible temperature would be -40°C, the minimum fuel cell storage temperature. However, 98 wt. percent peroxide "freezes" at about -2°C. Thus storage at -40°C would entail the dual tankage approach, using diluted feeds, that was discussed previously in Phase 3. Solutions containing 39 to 70 wt. percent hydrogen peroxide have freeze points below -40°C. This approach increases system complexity and was rejected, as discussed in Appendix 1. A minimum storage temperature of about +5°C was selected, based on the freeze, point of neat hydrazine.

Part c - Hydrogen Peroxide Decomposition Studies

The catalytic decomposition of concentrated hydrogen peroxide solutions was studied briefly to evaluate catalyst activity and reactor yield characteristics. Silver screen is usually used as a peroxide decomposition catalyst (93). However, the melting point of silver is 961°C, below the maximum adiabatic reaction temperature obtainable with 98 wt. percent peroxide. Munday has disclosed a number of confidential compositions developed to provide high temperature stability (94,95). One of these, designated sample I-6A, was prepared and used in the form of 1/8 inch pellets. Several runs were also made with pressed silver oxide pellets to assess low temperature reactor capability.

A simple packed bed reactor was used with feeds ranging from 70 to 98 wt. percent peroxide. Ambient system temperatures ranged from -40 to +25°C. The experiments were run at atmospheric pressure. The data in Figure 23 show that complete peroxide decomposition and stoichiometric yields of oxygen were obtained up to a space velocity of about 60 gms H_2O_2/gm cat-hr. The precision of these data leaves much to be desired, but the use of this space velocity as a design criterion is probably adequate. Reactor stability problems are not critical here. Experimental details and data are presented in Appendices 18 and 19.

Figure 23

HYDROGEN PEROXIDE DECOMPOSITION DATA

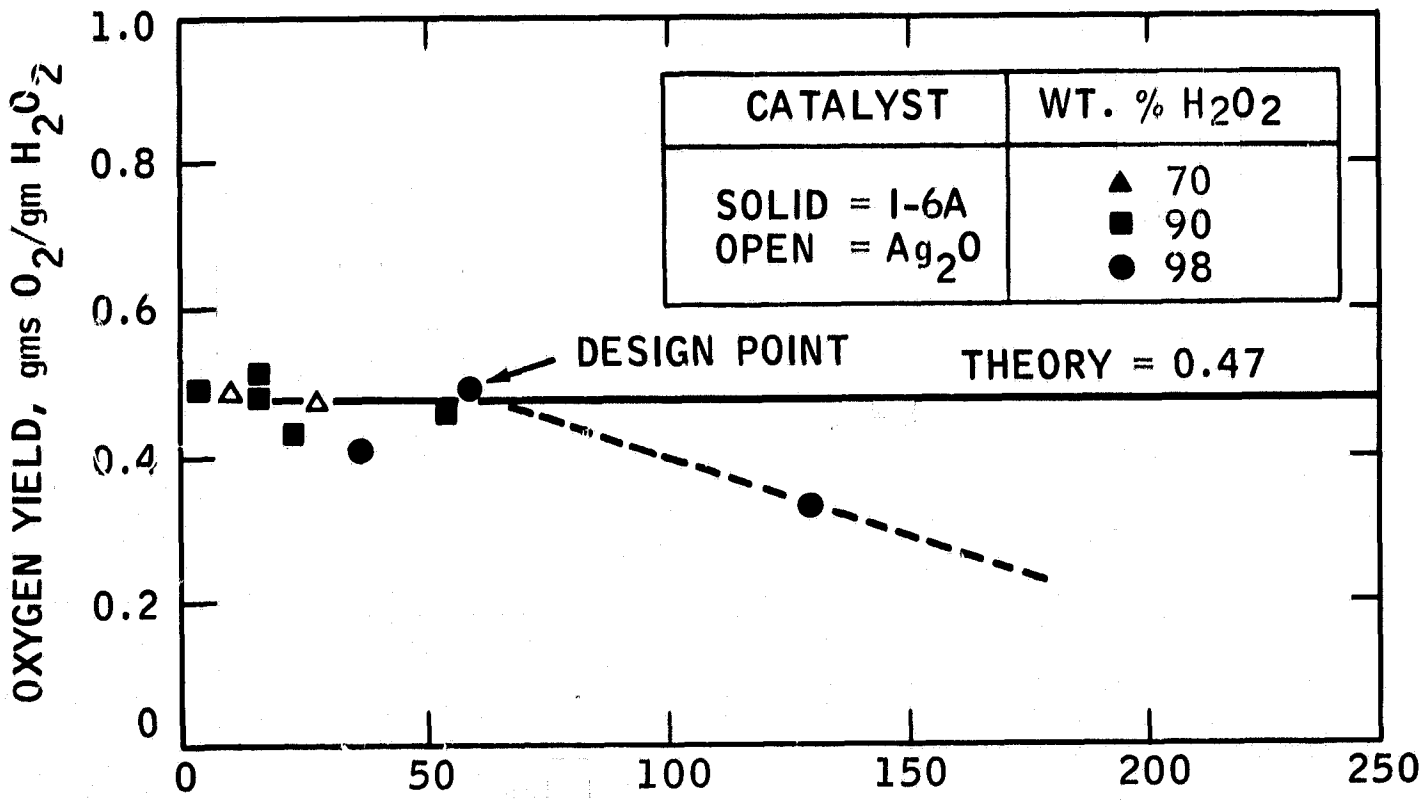

Reactor startup was instantaneous with catalyst I-6A and 98 wt. percent peroxide feed at 25°C and with 90 wt. percent peroxide at 5°C. It is assumed that 98 wt. percent peroxide will auto-ignite at 5°C, but this was not demonstrated because the feed supply was exhausted. Subsequent reactor and catalyst inspection showed that this catalyst had good high temperature stability. Bench-scale tests indicated a slight drop-off in low temperature activity. Silver oxide was the only active catalyst at -40°C, but operation at temperatures in excess of 100°C caused extensive breakdown to elemental silver, which formed a mirror on the Vycor reactor walls.

Part d - Oxygen Generator Subsystem Design

Design studies were conducted to size the components of the oxygen generator system. These include reactant storage requirements and tankage, peroxide decomposition reactor, by-product water condenser and separator, and oxygen accumulation tankage.

The reactant chosen was 98 wt. percent hydrogen peroxide, on the basis of minimum excess water storage weight and demonstrated operability. Peroxide solution flow rate requirements were calculated for the selected missions considering the following factors:

- Oxygen yield from the decomposition reactor
- Fuel cell voltage and coulombic efficiency
- Fuel cell oxygen utilization
- System parasitic load factor

Peroxide flow rates ranged from 2.6 to 68 gms/min. Calculation details are presented in Appendix 11.

Again, peroxide storage requirements were estimated using design values for the following factors:

- System peroxide flow rate and mission on-load time
- Peroxide storage stability
- Tankage expulsion efficiency

Stored peroxide weights range from 39 to 8941 lbs, as discussed in Appendix 12. Bladder expulsion and capillary-action tankage were also considered for the peroxide storage system. Studies by Schmauch indicate that Teflon or Fluorel are suitable bladder materials for long time storage of peroxide (93). Properly passivated aluminum 1060 is the preferred tankage material (37). Again, the capillary system was chosen because it should be easier to vent the decomposition products formed during storage from the periphery of the tank interior. Projected weight differences between the two systems appear small. Estimated weights for the spherical tanks ranged from 2 to 78 lbs, as described in Appendix 13. Good design practice indicates that vented valves should be used for safety in the peroxide flow system (37).

Catalyst requirements for the peroxide decomposition reactor were small, ranging from 0.006 to 0.15 lbs. As noted earlier, a single integrated reactor is used to conserve heat required for ammonia decomposition. Additional details are presented in Appendix 14. The peroxide reactor will operate at 500 psia, defined by the water removal requirements of the downstream condenser. This design feature was discussed earlier in Phase 2.

The hot reactor off-gas is cooled to 66°C (150°F) in a condenser/radiator. Schmauch has described a simple pin-finned stainless steel tube radiator that should be adequate. Studies under zero G conditions indicate that two-phase flow problems will not interfere with the condensation mechanism (96). The condenser wall temperature must be kept above 0°C, the freeze point of water. Operability of this unit would be ensured by mounting the radiator within the system envelope, where a storage temperature of 5°C will prevail. Condenser weights ranged from 0.09 to 2.3 lbs. Details are presented in Appendix 17.

The selective separation of condensed water from the oxygen product is essential to maintain a high oxygen recovery factor. A number of schemes are possible. The use of an induced-vortex cyclone separator seems feasible, based on studies made by AIResearch for the Union Carbide 5 KW flowing electrolyte fuel cell system (18). Alternative approaches include the use of a

hydrophobic porous Teflon bladder wall, mounted within a tank, to permit the selective transport of gaseous oxygen. Studies have shown that the Teflon adsorbs contaminants and becomes hydrophilic, or non-selective, after prolonged storage (96). A condenser/separator may also be used, with interior wicking facilities and pressure balances for water separation. AIResearch also presented designs for this unit (18). However, an auxiliary coolant is usually used as heat transfer medium, thus adding system complexity. The cyclone approach was selected on the basis of passive operation, simplicity and low weight. Detailed fluid-mechanical designs were considered beyond the scope of the current program. The separator weight was estimated by down-rating the AiResearch design. The procedure is discussed in Appendix 17.

A stainless steel tank is used to accumulate product oxygen at 66°C (150°F) and 150 psia. This tank also provides pressurant for the hydrogen-peroxide storage tank. The accumulation tank would be fully charged at lift-off. The tank weights ranged from 0.8 to 6.6 lbs. Design details are listed in Appendix 13.

The design, construction and operation of the oxygen generator subsystem is considered feasible, using available technology. A summary of the specific component weight analysis is presented in Phase 5.

Phase 5 - Systems Integration and Final Design Studies

The feasibility study of the multiple-restart fuel cell power supply was completed by integrating the component subsystem assemblies. Final projected weights were calculated for the integrated systems. The critical problem of thermal control was studied briefly. Finally, alternative approaches to the deep-space power supply problem were reviewed.

Part a - Systems Integration Studies

The power system components, including the fuel cell module, hydrogen generator and oxygen generator, were integrated into a single package. A simple, in-line component configuration was selected, illustrated schematically in Figure 24. The inertial characteristics of this packaging concept should minimize problems arising from eccentric loads. However, the system has not been optimized to yield a minimum capsule volume or sheath weight.

Figure 24

IN-LINE COMPONENT PACKAGING

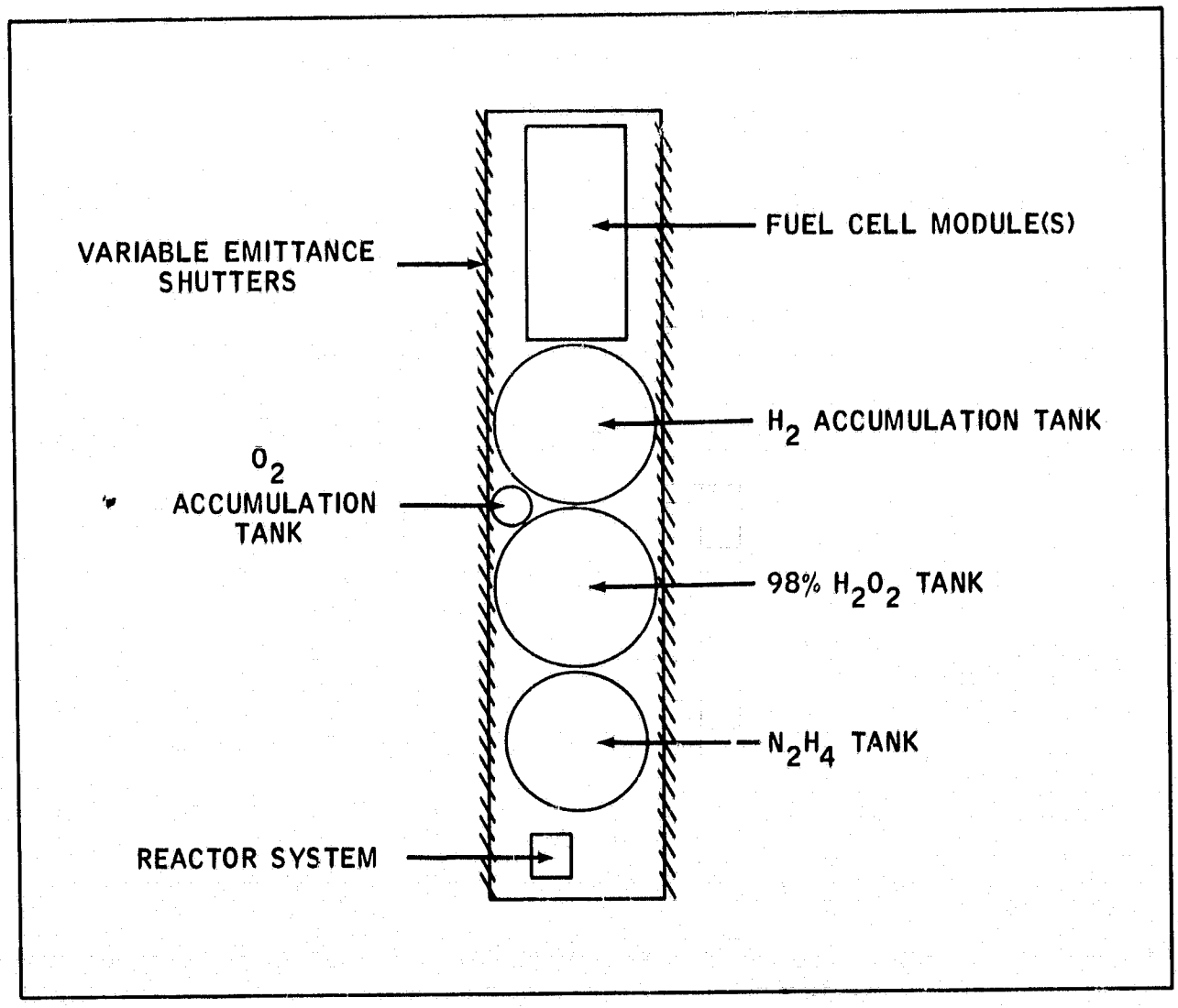

The entire system is enclosed in a capsule sheath, that contains integral space radiators for the product gas coolers and the fuel cell coolant fluid, where required. The capsule sides will be required to perform a semi-passive thermal control function, as discussed below in Part b.

Minimum integration problems are anticipated between the fuel cell module and the gas generators. The latter have been designed to provide the module with pure reactants that are compatible with effective fuel cell performance. The coolant space-radiator area and weight requirements for the Allis-Chalmers liquid-cooled fuel cell module in deep-space were estimated as 12 ft^2/KW and 1.5 lbs/ft^2, respectively. These values were reported by Cohn (5), and are evidently based on space experience and analytical studies. Detailed calculations have been reported by Allis-Chalmers, but these are for near-earth missions (13,15). Optimum configurations can be designed (84,85), but these are not required for this study. On the other hand, care must be taken to prevent freeze-up of the glycol coolant during initial introduction into the radiator network. The capsule exterior surface will undoubtedly fall below -60°F (-51°C), the freeze point of typical ethylene glycol-water coolants. Some form of radiator pre-heating should be provided. Substitution of gaseous coolants is a possibility, but will involve fuel cell module weight penalties.

The dynamic characteristics of the coupled systems have not been considered. It is assumed that the response characteristics of the gas generator subsystems to variations in load and multiple restart will be adequate. Future optimization studies would be required to evaluate potential problems in this area. In particular, the start-up "duty cycle" should be defined. If 10 starts are required for the 100 hour mission, approximately 150 minutes will be spent in the start-up mode. During this time, the gas generator reactors may be operating inefficiently. The effect of this inefficiency on overall reactant storage requirements was not considered in this study.

Part b - Thermal Balance Studies

The control of spacecraft thermal environment is critical, and much effort has been devoted by others to solve this problem. Passive control procedures are desirable because of their inherent reliability (97). The feasibility studies discussed above have assumed that the simplest and lowest weight system will result if the power system capsule can be maintained above the freezing point of hydrazine and below the temperatures where significant reactant auto-decomposition occurs. In turn, the heat generated during lift-off and the variations of solar flux encountered during deep-space missions will place a heavy burden on any thermal control system designed to meet these demands.

Typically, passive temperature management for spacecraft or lunar components involves the selection of exterior surfaces having appropriate thermal radiation characteristics, coupled with necessary auxiliary insulation (98-100). Many surface coatings are available, covering a range of solar absorptivity, α_s, and thermal emissivity, ε_t. Characteristic values are listed in Table 5 (98,101).

Table 5

Thermal Radiation Properties of Typical Materials

Finish	Solar Absorptivity, α_s	Thermal Emissivity, ε_t	Ratio, α_s/ε_t (1)
Aluminum 0.01 Oxide	0.21	0.82	0.26
Al-Pigmented Polyester	0.25	0.25	1.00
Dull Black Enamel	0.91	0.85	1.08
Clean 7075 Aluminum	0.55	0.11	5.00
410 Stainless Heated to 1300°F, Smooth	0.76	0.12	6.13

(1) At room temperature

The data in Figure 25 illustrate the nature of the problem. Equilibrium surface temperatures of an insulated flat plate exposed to the sun can vary from +600°F at AU=1 to -300°F at AU=9, depending on the ratio, $\frac{\alpha_s}{\varepsilon_t}$. Calculations indicate that this ratio must be 19.8 to achieve the desired storage temperature of +40°F at AU=9. The highest value available, obtained with a stainless steel surface, is only 6.1, as shown in Table 5. Therefore, an auxiliary heat source and interior insulation must be provided to maintain the target storage temperature.

Figure 25

POTENTIAL CAPSULE SURFACE TEMPERATURE EXCURSIONS

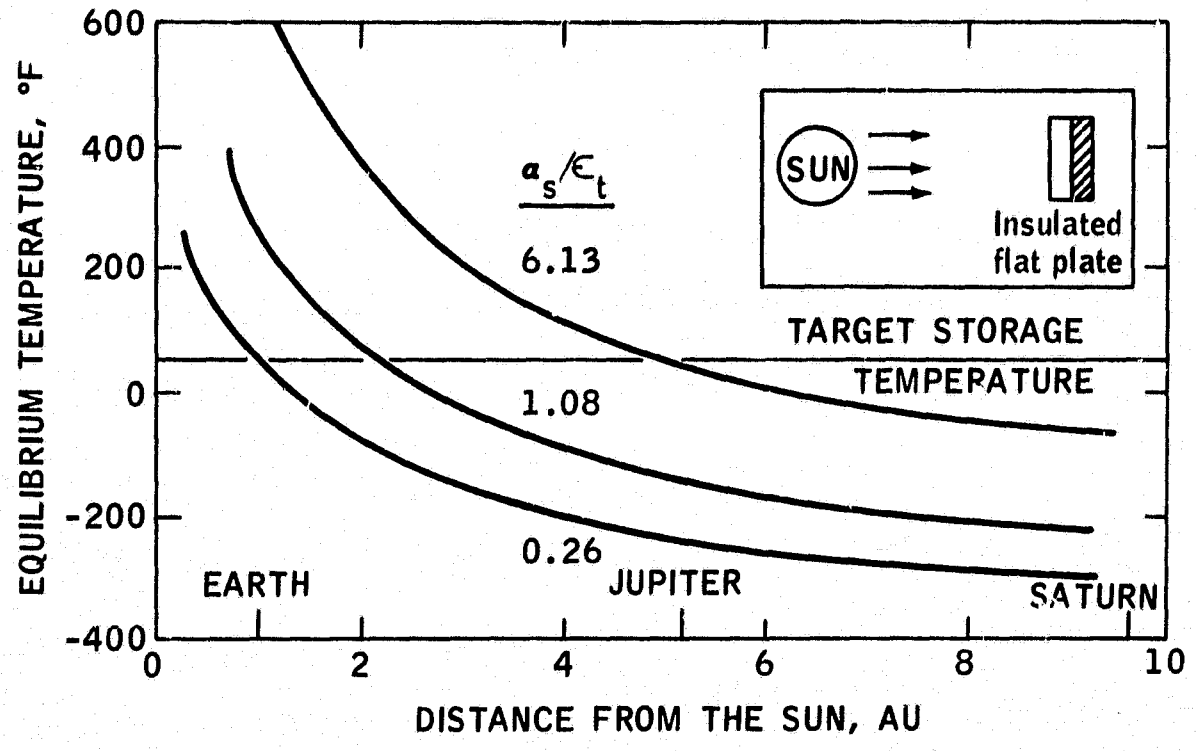

Small plutonium 238 radioisotope heaters are proposed (102). This isotope, in the oxide form, generates about 1.23 BTU/hr gm (103). The AEC transfer price to other Federal agencies for this material is about $1400/gm (103). Thermal control studies have assumed that the cost of 10 gms of the isotope will be an acceptable burden. Potential reactant radiolysis yields from the isotope alpha radiation are negligible.

A grossly simplified calculation procedure, detailed in Appendix 20, was used to estimate the insulation requirements and thermal response of the power plant capsule. Exterior temperatures were estimated for a surface with $\alpha_s = \varepsilon_t = 0.25$, considering the entire capsule area to be exposed to the solar flux. The heat balance assumed that the interior temperature could be maintained at 40°F (4°C) by the combined use of space-age super-insulation (80) and the radioisotope heaters. Although the capsule interior was maintainable at 40°F (4°C) at AU=9, severe high temperature excursions existed closer to the sun, as shown in Figure 26.

Figure 26

DEAD-STORAGE TEMPERATURE EXCURSIONS FOR POWER PLANT CAPSULE

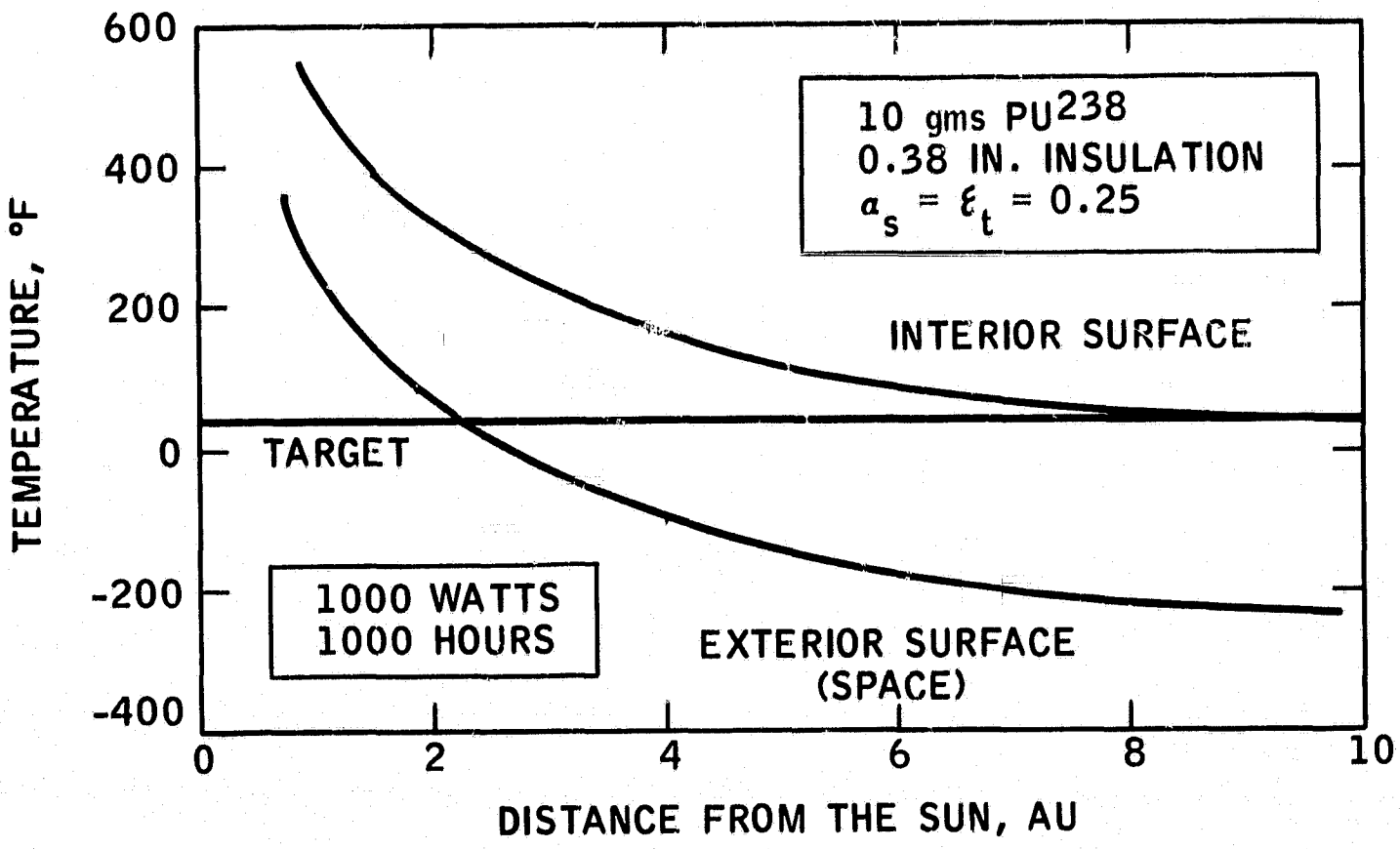

Time limitations prevented further analysis of this problem. However, a solution must be found, not only to ensure the operability of the proposed multiple restart power plant, but also to ensure that on-board electronic instrument packages are workable. In addition, sufficient flexibility must exist to dissipate the heat released from the gas generator reactors and water condenser during on-load operation. Potential solutions might consist of:

- Provision of expanding wax, piston-activated louvres or shutters to vary the thermal radiation emittance of the entire capsule. This system is similar to that used in the Allis-Chalmers thermal radiation fuel cell module.

- Use of multiple internal insulation shields or insulated tankage having appropriate thermal radiation characteristics. These shields may be jettisoned over-board as the distance from the sun increases.

- Use of suitably modified heat pipes to control interior temperatures near the sun.

- Adoption of a low-power requirement dynamic cooling system. A small RTG device could be used as power supply, or solar cells may be used during the initial exposure time near the sun.

Additional optimization studies are required to develop a reliable thermal technique to compensate for variations in solar flux, planetary albedo and overall spacecraft reflection. These problems have been analyzed extensively for NASA by other contractors. A NASA literature search, Number 8203, uncovered 462 references to "Spacecraft Thermal Control" from 1962 through March 10, 1969. Again, time limitations prevented a review of these previous studies.

Part c - Final Weight Analysis

The design studies were completed by estimating integrated power system weights. The projected weights are listed in Table 6 as a function of mission "on-load" time and net power output. These estimates place the entire capsule weight and thermal balance burden on the power system. Clearly, trade-off studies between the instrument package and the power system should result in some weight sharing. The weight estimates include a 10% increment for internal structural members and an additional 5% gross contingency factor. A small weight allowance was made for control components, but no attempt was made to define the control requirements in detail. Further, it was assumed that the spacecraft receiver antenna system could be powered continuously with a small RTG or even down-rated solar cells.

Table 6

Final Component Weight Analysis

Design Point and Component Weight	Mission On-Load Time, hrs.							
	100				1000			
	Net Powerplant Output, watts							
	200	500	1000	5000	200	500	1000	5000
Design Point								
Fuel Cell Module(s)(1)	R(1)	R(2)	L(1)	L(1)	R(2)	L(1)	L(1)	L(4)
Design Cell Voltage, volts(2)	0.893	0.875	0.987	0.873	0.936	1.003	0.987	0.977
Gross Power per Module, watts	220	275	110	5500	110	550	1100	1375
Component Weight, lbs.								
• N_2H_4 Reactant	19.0	48.8	86.5	489	182	425	865	4377
N_2H_4 Tankage	2.7	5.0	6.8	23.5	12.2	21.5	35	102
N_2H_4 Feed Pump	2.0	2.0	3.0	4.0	2.0	2.0	3.0	4
Integrated Reactor	3.9	5.0	5.9	9.6	3.7	4.9	5.9	9.3
Pd Diffuser	1.4	1.6	2.1	8.2	1.4	1.6	2.1	7.7
N_2 Radiator	0.03	0.08	0.14	0.79	0.03	0.08	0.14	0.79
N_2 Pressurant Tank	1.1	2.1	3.1	9.7	5.1	8.9	14.3	45
H_2 Radiator	0.06	0.15	0.27	1.52	0.06	0.13	0.27	1.36
H_2 Accumulation Tank(3)	6.8	12.8	18.5	59.0	6.6	11.6	18.5	55
• 98% H_2O_2 Reactant	39.1	99.5	177	998	374	872	1771	8941
98% H_2O_2 Tankage	2.1	4.0	5.8	18	9.6	16.6	26.6	78
98% H_2O_2 Feed Pump	2.0	2.0	3.0	4.0	2.0	2.0	3.0	4.0
H_2O Condenser/Radiator	0.09	0.23	0.45	2.3	0.09	0.23	0.45	2.3
H_2O Separator	1.0	1.5	2.0	3.0	1.0	1.5	2.0	3.0
O_2 Accumulation Tank	0.76	1.42	2.1	6.6	0.75	1.3	2.1	6.1
Total Piping, Regulators, etc.	10.0	11.0	12.0	20.0	10.0	11.0	12.0	20.0
• Fuel Cell	30.0	60.0	150	150	60	150	150	600
Fuel Cell Radiator	--	--	18	90	--	9	18	90
Control Package	2.0	2.4	2.7	3.0	2.0	2.4	2.7	3.
• Capsule Shell	17.1	30.2	45.3	69	55.4	81.4	117	287
• Capsule Insulation	0.5	1.6	5.1	21.9	5.2	12.7	28.3	195
• Total Weight ex. Structure	141.6	291.4	549.8	1991	733	1636	3077	14832
Structure @ 10%	14.2	29.1	55.0	199	73	164	308	1483
Weight plus Structure	155.8	320.5	604.8	2190	806	1800	3385	16315
Contingency @ 5%	7.8	16.0	30.2	110	40	90	169	816
Gross Total Weight	163.6	336.5	635	2300	846	1890	3554	17131
• Specific Energy, WH/lb	122	148	157	217	236	265	281	292

(1) Allis-Chalmers modules, R = Variable emittance module, L = Liquid cooled module
(2) Selected from 50-60 day performance curves
(3) Addition of compressor would permit storage at 150 psi instead of 30 psi, thus lowering tank weight.

As shown, the specific energy of these power plants ranged from 122 to 292 WH/lb, compared to a theoretical value of 584 WH/lb for a system using hydrazine and hydrogen peroxide as a source of hydrogen and oxygen. Future optimization studies may change these estimated specific energy characteristics. Although conservative fuel cell performance data were used, no provision was made for system redundancy to increase reliability. As noted earlier, this will not necessarily increase the overall weight of long duration (on-load) missions, but the weight for shorter time missions would increase. Ultimate capsule sheath and thermal control requirements are the major areas of uncertainty. If the capsule sheath and thermal control insulation weights are doubled, overall system specific energy will decrease by about 10%. In addition, detailed analysis is required to develop a light weight support structure capable of withstanding launch stresses. Furthermore, prospective lander missions would probably require a system with heat sterilization capability. Reactant decomposition losses, particularly hydrogen peroxide, would be severe during sterilization. It appears that fly-by missions would be a more appropriate application.

Part d - Comparison with Alternative Approaches

The storable-fuel, multiple restart fuel cell system studied in this program is not the only power system approach. The literature abounds with alternative solutions. Many attempts have been made to retain elemental hydrogen and oxygen as primary system reactants. Although major advances have been made to develop effective superinsulation materials, the boil-off losses associated with cryogenic storage of hydrogen and oxygen makes their use unattractive for missions exceeding about 2-3 months (104-109). Continuous refrigeration has been proposed as a solution, but the power requirements for this system would probably be high. In addition, the refrigeration power system must operate continuously for the expected duration of Jovian missions, exceeding three years.

The choice of hydrazine and hydrogen peroxide reactants leads to storage and tankage weights that compare favorably with available hydrogen-oxygen system designs. This is shown in Figure 27, taken from data presented by Koslover (110) and Cohn (5).

Figure 27

COMPARISON OF ALTERNATIVE FUEL CELL REACTANT STORAGE MODES

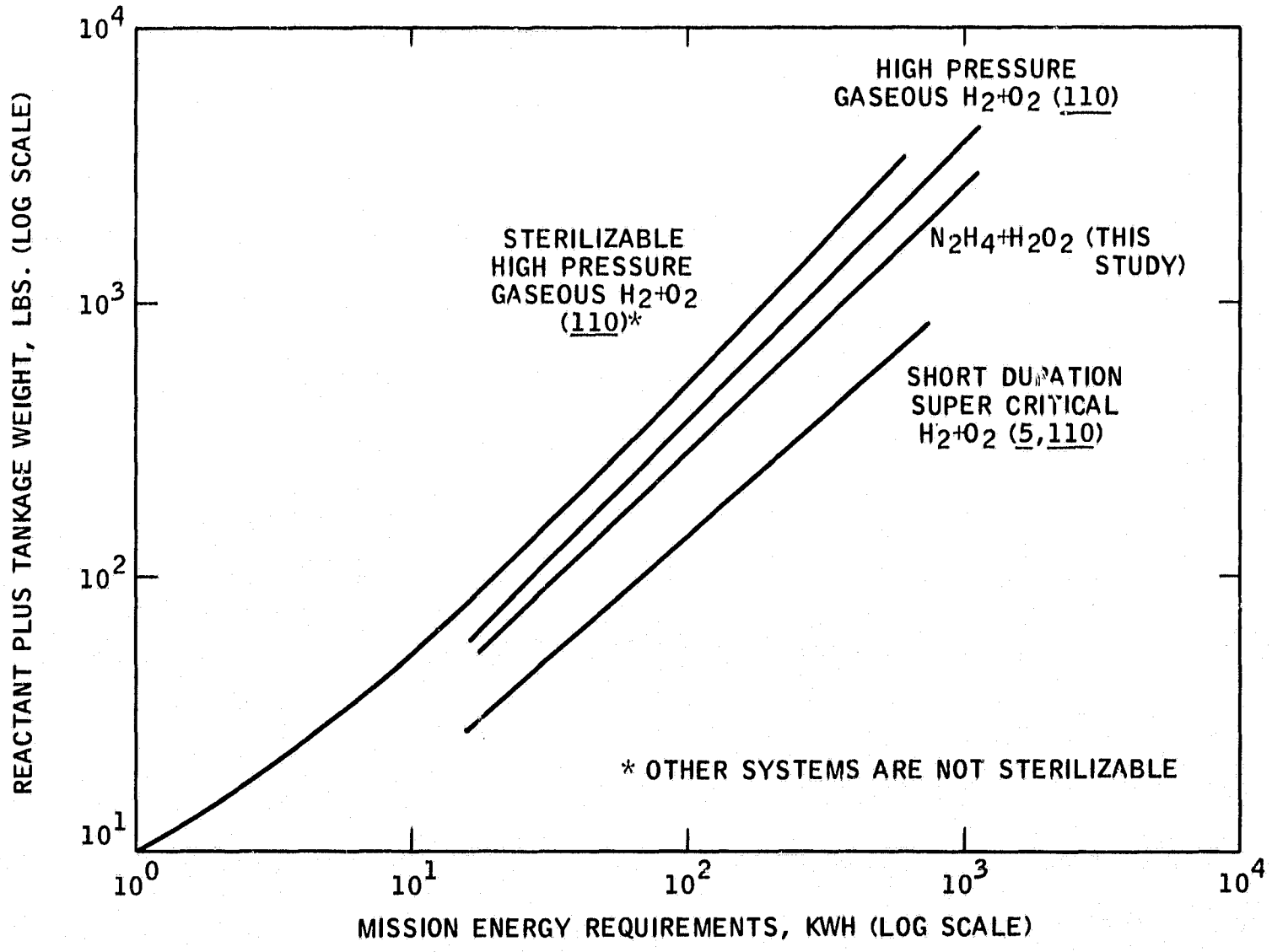

Another interesting approach is the coupled solar cell-fuel cell hybrid. This hybrid extends the application range of fuel cell systems to 16-24 weeks without reactant regeneration or more than 24 weeks with reactant regeneration by electrolysis (111, 112). The approach would be useful for near-sun missions only.

Alternative fuel supplies were considered briefly. The hydrogen yield per weight of reactants is low if one selects lithium hydride or boro-hydride as a source of hydrogen. Ammonia maybe an attractive fuel for some missions, but detailed calculations must be made to estimate boil-off losses for this fuel. Ammonia boils at -33.4°C and presents a less critical storage problem than either hydrogen or oxygen. On the other hand, the vapor pressure exceeds 80 psia at only 6.8°C, so that tank wall thicknesses will be higher than those needed for hydrazine. A suitable radioisotope source could probably be designed to provide heat required for the endothermic ammonia decomposition reaction.

Similarly, the production of oxygen from chlorates, such as $LiClO_4$, may be attractive. Additional studies would be required to devise suitable control schemes to start-up and quench the decomposition reaction.

Finally, hydrazine and hydrogen peroxide may be used directly as fuel cell reactants (113,114). Unfortunately, the poor coulombic efficiency noted for these systems would increase reactant storage weights excessively for long duration missions.

Major competitive power sources for the deep space missions will probably be radioisotope thermoelectric generators (RTG), solar cells and, perhaps, advanced batteries with multiple-restart capability. The energy storage characteristics of these systems are compared in Figure 28. The performance of RTG systems is about 1 watt/lb (103) and in-flight testing indicates that useful system life will exceed four years (115). Normally, plutonium 238, with a half-life of 90 years, is used as the energy source. The projected performance of advanced solar cells arrays is about 30 watts/lb at AU=1 (3). However, deep-space operation would require severe down-rating to accomodate the reduced solar constant. A value of 0.37 watts/lb was used for operation at AU=9, assuming that the fall-off in solar flux is proportional to $\left(\frac{1}{AU}\right)^2$. In addition, attitude control must be invoked to ensure maximum cell utilization. Battery performance has been assigned a range from about 50 to 180 WH/lb.

Figure 28

COMPARISON OF POWER SYSTEM CHARACTERISTICS

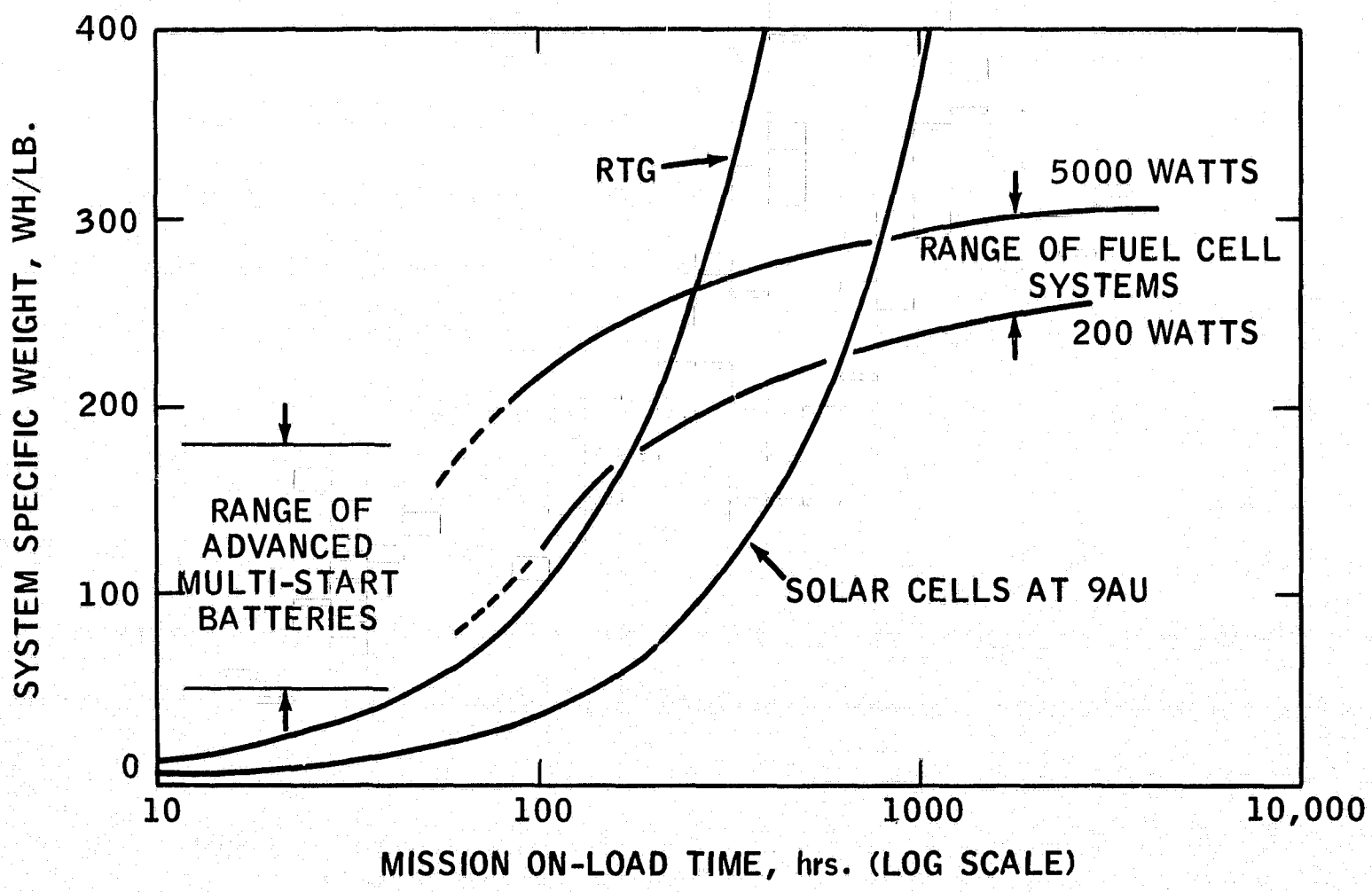

The fuel cell system looks attractive for missions having on-load times of 50 to 600 hours, depending on power output level. This appears to confirm the traditional role of fuel cell power in aerospace missions, as shown in Figure 1. However, there is another aspect that should be considered carefully. System specific weight characteristics affect mission costs by controlling the lift-off load. The cost of the selected power system also must be considered. The projected systems cost, shown in Figure 29, indicate that the fuel cell/gas generator approach may be the cheapest solution. These cost estimates were made using the data shown in Table 7. Further study of the fuel cell system approach is clearly justified.

Figure 29

PROJECTED POWER SYSTEM COST TRADE-OFF

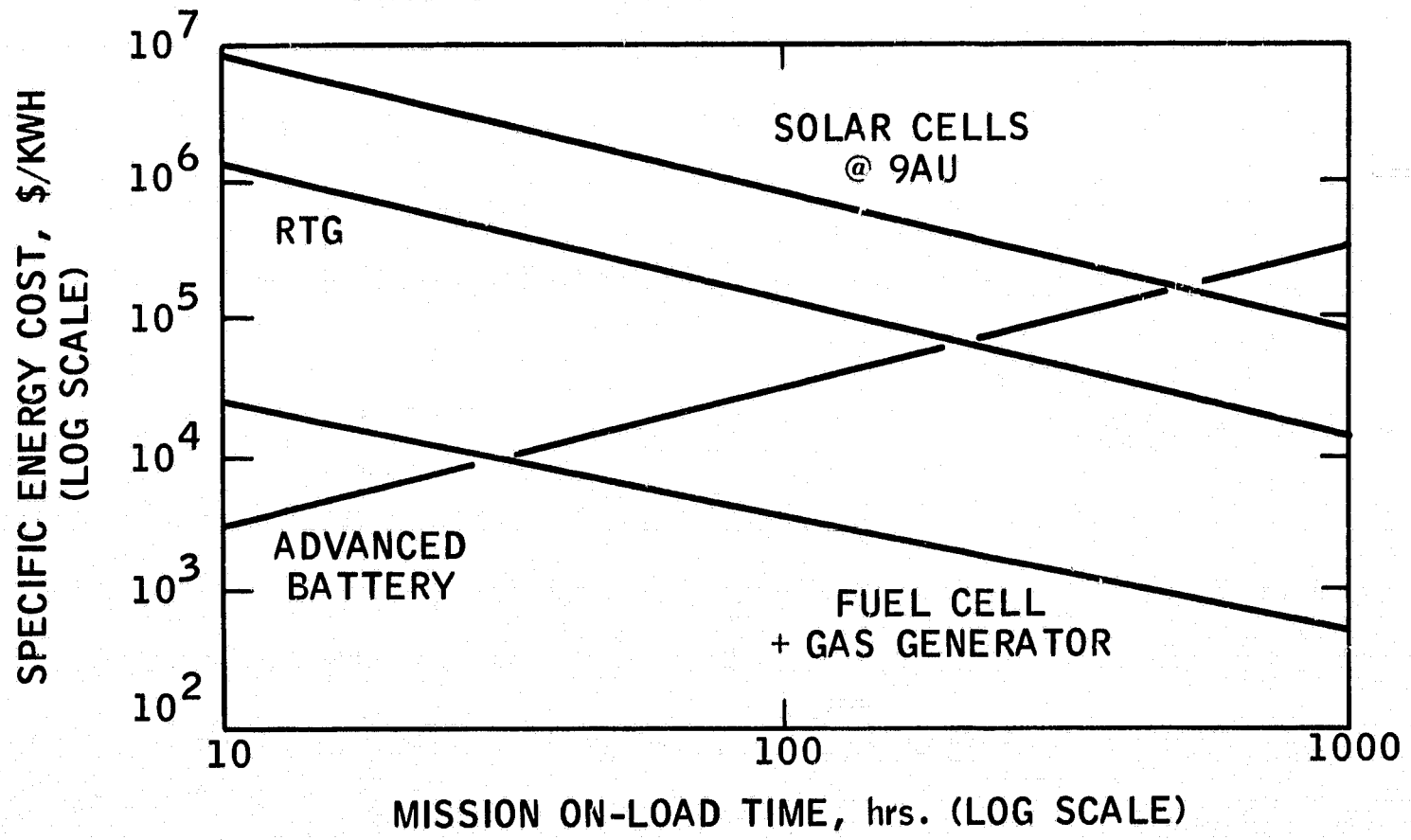

Table 7

Cost Factors for Power System Analysis

Power System	Basic Cost
Radioisotope Thermoelectric Generator	$13,000/watt(e) (1)
Solar Cells at AU=9	$81,000/watt(e) (2)
Fuel Cell/Gas Generator at 1000 watt level	$200,000/KW for Cell + $200,000/KW for Gas Generator (3)
Batteries	$300/KWH (4)

(1) Direct scale-up, since major cost item is fixed Pu^{238} charge (103)

(2) Mounted arrays of Si cells cost $1000/watt at AU=1 (115). (Eventual cost for CdS cell may be as low as $50/watt at AU=1) Direct scale-up used.

(3) Typical assembled fuel cell cost (5). This was doubled for gas generator system plus capsule costs. A 0.6 exponential scaling factor was used to estimate gas generator costs for other power output levels.

(4) Assumes zinc-oxygen batteries, using base cost of $60/KWH derived for zinc-air cells (116). Costs were escalated by a factor of 5 to reflect aerospace qualification. Sequential modular use of batteries was assumed, so costs rise linearly with KWH requirements.

SECTION 3

REFERENCES

1. "Planetary Exploration 1968-1975", Report of a Study by the Space Science Board, National Academy of Sciences, National Research Council, Washington, D.C., July 1968.

2. Murray, B. C., "A New Strategy for Planetary Exploration", Astronautics and Aeronautics, 6, No. 10, 42 (1968).

3. Barber, T. A., et al., "Spacecraft Electric Propulsion--Now?", Astronautics and Aeronautics, 6, No. 6, 38 (1968).

4. Szego, G. C. and Cohn, E. M., "Fuel Cells for Aerospace Application", Astronautics and Aerospace Engineering, 1, No. 4, 107 (1963).

5. Cohn, E. M., "Primary Hydrogen-Oxygen Fuel Cells for Space", 29th Meeting of AGARD Propulsion and Energetics Panel, NATO, Liege, Belgium, June 12-16, 1967, p. 557.

6a. Russell, J. H., "Gemini Fuel Cell System", 19th Annual PSC, May,1965 p. 35.

6b. Cohen, R., "Gemini Fuel Cell System", 20th Annual PSC, May, 1966, p. 21.

7. Maget, H. J. R., "The Ion Exchange Membrane Fuel Cell", Chapter in "Handbook of Fuel Cell Technology", Carl Berger, ed., Prentice-Hall, Engelwood Cliffs, New Jersey, 1968, p. 489.

8. Morrill, C. C., "Apollo Fuel Cell System", 19th Annual PSC, May, 1965, p. 38.

9. Cox, J. E. and Jones, J. C., "Experimental Determination of the Effect of Oxygen-Supply Impurities on Fuel Cell Performance", Second Annual IECEC Meeting, August, 1967, p. 407.

10. Connors, J. W., "System Selection for a Low-Temperature Fuel Cell Power Plant", CEP Symposium Series, Vol. 63, No. 75, 9 (1967).

11. McKee, J. M., et al., "Operating Characteristics of a Liquid-Cooled Contained-Electrolyte Low-Temperature Fuel Cell System Over a Period of 1500 Hours", Third Annual IECEC Meeting, August, 1968, p. 69.

12. Platner, J. L., "Allis-Chalmers Capillary Matrix Fuel Cell Systems--An Advanced Aerospace Power Source", Third Annual IECEC Meeting, August, 1968, p. 52.

13. Desai, R., et al., "Research and Development of Open-Cycle Fuel Cells", Report NAS 8-5892-QPR-003, Allis-Chalmers, Contract NAS 8-5392, May 15, 1965.

14. Platner, J. L., "Research and Development on Fuel Cell Systems", Report NAS-8-2696-QPR-005, Allis-Chalmers, Contract NAS8-2696, September 30, 1965.

15. Desai, R., et al., "Study of Energy Conversion Systems", Report NAS8-5892-SR-001, Allis-Chalmers, Contract NAS8-5892, January 15, 1966.

16. Platner, J. L., "Research and Development on Fuel Cell Systems", Report NAS8-2696-SR-002, Allis-Chalmers, Contract NAS8-2696 Mod. 6 and 9, October 17, 1966.

17. Bjorkman, H., "Research and Development on Fuel Cell Systems", Report NAS 8-29573-SR-002, Allis-Chalmers, Contract NAS 8-20573, March 28, 1968.

18. Grigsby, J. D., et al., "Development of Fuel Cell Electrodes. Task 2--Preliminary System Design", Report NASA CR-72305, Union Carbide Corporation, Contract NAS 3-9430, June 30, 1967.

19. Cook, N. A., "Hydrogen-Oxygen Fuel Cell System Design Parameters", Third Annual Conference on Energy Conversion and Storage, Oklahoma State University, October 28, 29, 1965, p. 2-1.

20. Gidaspow, D., et al., "Electrochemical System Heat and Mass Transfer", Report NAS 8-21159-SR-001, Institute of Gas Technology, Contract NAS 8-21159, August, 1968.

21. Maget, H. J. R., "Gas Phase Transport Processes - Their Influence on Electrode Current Density Distribution", Abstract 148A, Electrochemical Society Meeting, Dallas, Texas, Spring, 1967, p. 22.

22. Austin, L. G., "The Electrochemical Theory of Fuel Cells", Chapter in "Handbook of Fuel Cell Technology", Carl Berger, ed., Prentice-Hall, Englewood Cliffs, New Jersey, 1968, p. 1.

23. Liebhafsky, M. A. and Cairns, E. J., "Fuel Cells and Fuel Batteries", Wiley, New York, 1968.

24. Swinkels, D. A. J., "Impurity Effects in High Current Density Cl_2 Electrodes", J. Elect. Soc., 114, 812 (1967).

25. Leitz, F. B., et al., "Performance of a Reformed Natural Gas - Acid Fuel Cell System, Part II. Fuel Cell Battery", Chapter in "Hydrocarbon Fuel Cell Technology", B. S. Baker, ed., Academic Press, New York, 1965, p. 37.

26. Winsel, A. W., "Improved Calculation of Polarization of Porous Electrodes", Advanced Energy Conversion, 3, 427 (1963).

27. Grune, H., "Operation of Fuel Cells with Impure Gases", Chem. Ing. Tech., 40 185 (1968).

28. Coleman, W. P., et al., "Light-Weight Fuel Cell Electrodes. Part 1", 19th Annual PSC, May 1965, p. 14.

29. Kordesch, K. V., "Light-Weight Fuel Cell Electrodes. Part 2", 19th Annual PSC, May 1965, p. 17.

30. Skopp, A. and Micelli, J. V., "Investigation of Heatless Adsorption Technology for Carbon Dioxide Control for Manned Spacecraft", Report NASA CR-66582, Esso Research and Engineering Company, Contract NAS1-6918.

31. Heath, C. E., et al., "Methanol-Air Fuel Cell", Report ECOM-02387-F, Esso Research and Engineering Company, Contract DA-28-043-AMC-02387(E), February, 1968.

32. Price, T. W. and Evans, D. D., "The Status of Monopropellant Hydrazine Technology", Tech. Rept. 32-1227, JPL, Cal Tech, NASA, February 15, 1968.

33. VanVorst, W. D. and Ahlert, R. C., "Thermodynamic Properties of the Decomposition Products of Hydrazine", J. Chem. Eng. Data, 9, 345 (1964).

34. Axworthy, A. E., et al., "Research on Hydrazine Decomposition", Report AFRPL-TR-68-138, Rocketdyne Division of North American Rockwell Corp., Contract FO4611-67-C-0087, July, 1968.

35. Bolt, R. O. and Carroll, J. G., "Radiation Effects on Organic Materials", Academic Press, New York, 1963.

36. Lucien, H. W., "Preliminary Study of the Effects of Ionizing Radiations on Propellants; The X-Irradiation of Ammonia and Hydrazine", NASA Tech. Note D-1193, February, 1962.

37. "The Handling and Storage of Liquid Propellants", Office of the Director of Defense, Research and Engineering, January 1963.

38. Audrieth, L. F. and Ogg, B. A., "The Chemistry of Hydrazine", Wiley, New York, 1951.

39. Winsel, A., "Hydrogen-Oxygen Fuel Cells - Varta Fuel Cell Systems", 39th Meeting of AGARD Propulsion and Energetics Panel, NATO, Liege, Belgium, June 12-16, 1967, p. 575.

40. Poole, D. R., "Development of Low Temperature Gas Generator Technology", Report AFRPL-TR-66-226, Rocket Research Corporation, Contract AF 04(611)-11376, December, 1966.

41. Armstrong, W. E., et al., "Development of Catalysts for Monopropellant Decomposition of Hydrazine (U)", Report S-13947, Shell Development Company, Contract NAS 7-97, December, 1964.

42. Dake, J. O., "Catalytic Monopropellant Decomposition of Hydrazine-Blend Fuels at -65°F (U)", Report NOTS-TP-4141, United States Naval Ordnance Test Station, China Lake, California, Contract FO4611-67-C-0013, May, 1966.

43. Taylor, W. F., et al., "Development of a Low Cost Catalyst for Hydrazine (U)", Report AFRPL-TR-68-235, Esso Research and Engineering Company, Contract FO4611-68-C-0044, December 15, 1968.

44. Bond, G. C., "The Catalytic Synthesis and Decomposition of Ammonia and Related Reactions", Chapter 16 in "Catalysis by Metals", Academic Press, New York, 1962.

45. Nielsen, A., "Latest Development in Ammonia Synthesis", Chapter in "Advances in Catalysis", Vol. 5, P. H. Emmett, ed., Academic Press, New York, 1953, p. 1.

46. Bokhoven, C., et al., "Research on Ammonia Synthesis Since 1940", Chapter 7 in "Catalysis", Vol. 3, P. H. Emmett, ed., Reinhold, New York, 1955, p. 265.

47. Nielsen, A., "An Investigation on Promoted Iron Catalysts for the Synthesis of Ammonia", 3rd Edition, Jul. Gjellerups Forlag, Copenhagen, Denmark, 1968.

48. Love, K. S. and Emmett, P. H., "The Catalytic Decomposition of Ammonia over Iron Synthetic Ammonia Catalysts", J.A.C.S.63 3297 (1941).

49. Horiuti, J. and Toyoshima, I., "The Mechanism of Catalyzed Decomposition of Ammonia in the Presence of Doubly Promoted Synthetic Catalyst. Part I: Observation of the Decompositon Rate", J. Res. Inst. Cat., Hokkaido Univ., 5, No. 3, 120 (1957).

50. Tanaka, K., et al., "The Rate-Determining Step of Ammonia Synthesis and Decompositon over Singly- and Doubly-Promoted Iron Catalysts", Proc. Int. Cong. Cat., Vol. I, 676 (1968).

51. Tanaka, K., "The Rate-Determining Step of Ammonia Synthesis and Decomposition. Part I: Study of the Reaction Over Singly-Promoted Iron Catalyst at 305 and 340°C. Part II: The Effect of Ammonia Adsorption on Experimental Value for the Stoichiometric Number of the Rate Determining Step", J. Res. Inst. Cat., Hokkaido Univ., 13, No. 2, 119 (1965); 14, No. 2, 153 (1966).

52. Takezawa, N. and Toyoshima, I., "The Effect of Alkaline Promoter on Decomposition Over the Doubly Promoted Iron Catalyst", J. Cat. 6, 145 (1966).

53. Ibid., "The Change of the Rate-Determining Step of the Ammonia Decomposition Over an Ammonia Synthetic Iron Catalyst", J. Phys. Chem., 70 594 (1966).

54. Ibid., "The Rate-Determining Step of Ammonia Decompositon Over a Well-Reduced Doubly Promoted Iron Catalyst", J. Res. Inst. Cat., Hokkaido Univ., 14, No. 1, 41 (1966).

55. Ibid., "The Mechanism of Catalyzed Decomposition of Ammonia in the Presence of Commercial Doubly Promoted Iron Catalyst", J. Res. Inst. Cat., Hokkaido Univ., 15, No. 2, 111 (1967).

56. Levenspiel, O., "Chemical Reaction Engineering", Wiley, New York 1962 p. 449.

57. Kramers, M. and Westerterp, K. R., "Elements of Chemical Reactor Design and Operation", Chapman and Hall, London, 1963, p. 111, 118.

58. Aris, R., "The Optimal Design of Chemical Reactors", Academic Press New York, 1961, p. 281.

59. Brotz, W., "Fundamentals of Chemical Reaction Engineering", Addison-Wesley Reading, Massachusetts, 1965, p. 248.

60. Petersen, E. E., "Chemical Reaction Analysis", Prentice Hall. Englewood Cliffs, New Jersey, 1965, p. 200.

61. Vanderveen, J. W., et al., "Stability of Adiabatic Packed Beds and Reactors. Effect of Flow Variations and Coupling Between the Particles", Preprint 8D, Presented at 63rd National Meeting, AIChE, St. Louis, Missouri, February 18-21, 1968.

62. Inoue, M. and Komiya, T., "On the Stability of Autothermal Reactors", Int'l Ch.E. 8, 749 (1968).

63. Friedman, R., "Kinetics of the Combustion Wave", ARS Jnl 23, 349 (1953).

64. Adler, J. and Vortmeyer, O. D., "Stability of Exothermic Chemical Reactions in a Flow Tube", Chemie. Ing. Techn. 40, 849 (1968).

65. Wicke, E., et al., "Thermische Instabilitaten bei Exothermen Katalischen Gas-Reaktionen in Adiabitsche Kontact Schicht, 4th Eur. React Eng Symp Preprint, 1968.

66. Kesten, A. S., "Analytical Study of Catalytic Reactors for Hydrazine Decomposition", Hydrazine Monopropellant Technology Symposium (U), November 28-30, 1967, Johns Hopkins, CPIA Publication 160. December 1967.

67. Erickson, P. C., "Trimode Rocket Propulsion Feasibility Decomposition (U)", Bell Aerospace Systems, Contract FO4611-67-C-0020, Abstracted in "Air Force Rocket Propulsion Laboratory Semi-Annual Progress Report (U), AFRPL-TR-68-21, July, 1968, p. 157.

68. Perry, J. H., ed., "Chemical Engineers Handbook", Fourth Edition, McGraw-Hill, New York, 1963.

69. Argo, W. B. and Smith, J. M., "Heat Transfer in Packed Beds", CEP 49, 443 (1953).

70. Baddour, R. F. and Yoon, C. Y., "Local Radial Effective Conductivity and the Wall Effective in Packed Beds", CEP Symp. Series, Vol. 57, No. 32, p. 35, (1961).

71. Kraus, A. D., "Extended Surfaces", Spartan Books, Baltimore, Md., 1964.

72. Toth, L. R. and Keller, O. F., "Liquid Propulsion Systems", JPL Space Programs Summary 37-44, Vol. IV, April 30, 1967, p. 175.

73. DeBrock, S. C., "Surface Tension Devices for Management of Space Propulsion System Propellants", Paper 670558, SAE Preprints 76, Sect. 3, 2052 (1968).

74. Otto, E. W., "Static and Dynamic Behavior of the Liquid-Vapor Interface During Weightlessness", CEP Symp. Series 62, No. 61, 158 (1966).

75. Gluck, D. F., et al., "Distortion of the Liquid Surface During Tank Discharge Under Low G. Conditions", CEP Symp. Series 62, No. 61, 150 (1966).

76. Gluck, D. F. and Gille, J. P., "Fluid Mechanics of Zero-G Propellant Transfer in Spacecraft Propulsion Systems", Trans. ASME, Jnl of Engineering for Industry, 87B, 1 (1965).

77. Lundeen, H. R., "Subcritical Liquid Oxygen Storage and Supply System for Use in Weightless Environments", Report AMRL-TR-66-178, Bendix Corporation, Contract AF 33(615)-2308, April, 1967.

78. Warren, R. P. and Anderson, J. W., "A System for Venting a Propellant Tank in the Absence of Gravity", Paper B-4, "Advances in Cryogenic Engineering", Vol. 12, K. D. Timmerhaus, ed., Plenum Press, New York, 1967, p. 63.

79. Materials Engineering, "Materials Selector Issue", 68, No. 5 (1968).

80. Glaser, P. E., et al., "Thermal Insulation Systems", Report NASA SP-5027, Office of Technology Utilization, NASA, Washington, D.C., 1967.

81. Hunter, J. B., "Ultra-Pure Hydrogen by Diffusion Through Palladium Alloys", Preprints, Div. Pet. Chem., ACS, 8, No. 4B, B-49, September 8-13, 1963.

82. Cohn, G. and Straschil, H. K., "The Role of Platinum Metals in the Purification of Hydrogen", Preprints, Div. Pet. Chem., ACS, 8, No. 4B, B-43, September 8-13, 1963.

83. Boretz, J. E., "Isotope Dynamic Space Power Systems", Second Annual IECEC Meeting, August, 1967, p. 615.

84. Chapman, A. J., "Heat Transfer", 2nd Edition, Macmillan, New York, 1967.

85. Rubin, I. and Imber, M., "Optimization Study of Space Radiators", AIAA Jnl, 2, 353 (1964).

86. Bloom, R., Jr., et al., "Hydrogen Peroxide as a Propellant", ARS Jnl No. 80, 3 (1950).

87. Grelecki, C. J. and Tannenbaum, S., "Survey of Storable Propellants", ARS Jnl, 32, 1189 (1962).

88. Davison, W. R. and Carstens, J. P., "An Evaluation of the Space Storability of Propellants", Pyrodynamics 2, 275 (1965).

89. Williams, G. C., et al., "Calculation of Adiabatic Decomposition Temperatures of Aqueous Hydrogen Peroxide Solutions", ARS Jnl, 22, 70 (1952).

90. "Concentrated Hydrogen Peroxide - 70%, 90%, 98%", Technical Data Bulletin No. 46., FMC Corporation, New York.

91. Schumb, W. C., et al., "Hydrogen Peroxide", Reinhold, New York, 1955.

92. Dainton, F. S. and Rowbottom, J., "Primary Radiation Yield in Liquid Water", Nature 169, 370 (1952).

93. Schmauch, G. E. and Bailey, B., "Oxygen Supply System for Manned Space Enclosures", Report AMRL-TR-66-169, Air Products and Chemicals, Inc., Contract AF 33(615)-3335, December, 1966.

94. Munday, T. C. F.,"Investigation of Decomposition Catalysts for 98% Hydrogen Peroxide (U)", Report AFRPL-TR-67-229, FMC Corporation, Contract F 94(611)-67-C-0068, August, 1967.

95. Ibid., Report AFRPL-TR-67-141, May, 1967.

96. Siegel, R., "Effects of Reduced Gravity on Heat Transfer", Chapter in "Advances in Heat Transfer", Vol. 4, J. P. Hartnett and T. F. Irvine, Jr., eds., Academic Press, New York, 1967, p. 144.

97. Corliss, W. R., "Space Probes and Planetary Exploration", Van Nostrand, Princeton, New Jersey, 1965.

98. Knoll, R. H. and Oglebay, J. C., "Lightweight Thermal Protection Systems for Space Vehicle Propellant Tanks", SAE Trans. 72, 286 (1964).

99. Siegel, R. and Howell, J. R., "Thermal Radiation Heat Transfer, Vol. 1", Report NASA SP-164, Office of Technology Utilization, NASA, Washington, D.C., 1968.

100. Ogden, D. H., "Study and Design Optimization of a Water Electrolysis System", Report HGS-R47-68, Chrysler Corporation, Contract NAS8-21190, June, 1968.

101. Rittenhouse, J. B., "Materials For Spacecraft Systems", Preprint 18A, AIChE Materials Conference, March 31 - April 4, 1968.

102. Plant, A. F., "Another Peaceful Use of Atomic Energy", Ind. Res., November, 1968, p. 41.

103. "Radioisotopes... Production and Development of Large-Scale Uses", Report WASH No. 1095, A.E.C., May, 1968.

104. Sollami, B. J., "Weight Optimization of Flight Type Cryogenic Tankage Systems", Chapter 3 in "Atmosphere in Space Cabins and Closed Environments", K. Kammermeyer, ed., Appleton-Century-Crofts, New York, 1966, p. 32.

105. Cook, G. A. and Dwyer, R. F., "Fluid Hydrogen Slush - A Review", Paper D-3, "Advances in Cryogenic Engineering", Vol. 11, K. D. Timmerhaus, ed., Plenum Press, New York, 1966, p. 202.

106. Romero, J. B., et al., "Thermal Analysis and Optimization of Cryogenic Tanks For Lunar Storage", Paper D-7, "Advances in Cryogenic Engineering, Vol. 11, K. D. Timmerhaus, ed., Plenum Press, New York, 1966, p. 231.

107. Sedgwick, T. A. and Middleton, R. L., "Extraterrestrial Cryogenic Propellants Reliquifaction", Paper D-8, "Advances in Cryogenic Engineering, Vol. 11, K. D. Timmerhaus, ed., Plenum Press, New York, 1966, p. 241.

108. Anon., "Apollo 7 Cryogenic Gas Storage System", Cryogenic Engineering News, 3, NO. 11, 24 (1968).

109. Vance, R. W., "Space Applications of Cryogenic Technology", Proceedings of the First Cryogenic Engineering Conference, Tokyo, Japan, April 9-13, 1967, p. 43.

110. Koslover, M., "Comparative Studies of an Electrical Power Generator for a Mars Probe/Landar", First Annual IECEC Meeting, September, 1966, p. 60.

111. Schulman, F. and Smith, A. M., "Lunar Power Systems--A Long View", Astronautics and Aeronautics 6, No. 11, 62 (1968).

112. Silverman, R. V., "Space Power Supply", Tech. Rept. No. NSSA-R40-68-5, Navy Space Systems Activity, Los Angeles, May 1968.

113. Gruneberg, A. and Weddeling, F., "Hydrazine-Hydrogen Peroxide Fuel Cells", 29th Meeting of AGARD Propulsion and Energetics Panel, NATO, Liege, Belgium, June 12-16, 1967, p. 599.

114. Warszawski, B., "Pile de 2 KW de Haute Compacite", Proceedings of Deuxieme Journees Internationales d'Etude des Piles a Combustible", June 19-23, 1967, Brussels, Belgium, p. 108.

115. Shure, L. I. and Schwartz, H. J., "Survey of Electric Power Plants for Space Applications", CEP Symposium Series, Vol. 63, NO. 75, 95 (1967).

116. Morse, R. S., Chairman, "The Automobile and Air Pollution: A Program for Progress. Part II", U.S. Department of Commerce, December, 1967, p. 66.

117. Weast, R. C., ed., "Handbook of Chemistry and Physics", 45th Edition, Chemical Rubber Co., Cleveland, Ohio, 1964, p. F88.

118. Bird, R. B., et al., "Transport Phenomena", Wiley, New York, 1960.

SECTION 5

APPENDICES

APPENDIX 1

ANALYSIS OF LOW STORAGE TEMPERATURE SYSTEM

Low temperature storage is a potential design option for the multiple reactant fuel cell power system. The minimum permissible storage temperature is probably -40°C, set by the freezing point of the aqueous potassium hydroxide electrolyte within the fuel cell electrode matrix. It was assumed that lower temperatures could seriously damage the fuel cell. Also, Allis-Chalmers data showed that -40°C was the minimum temperature that small, but useful, power output could be obtained from the fuel cell. Therefore, system design problems were evaluated for a dead-storage temperature of -40°C.

Storage at -40°C requires the use of auxiliary tankage containing diluted, low freeze point reactants for startup. The modified feed delivery system is shown in Figure A-1. The auxiliary feed tanks would be filled at launch. Upon command in space, the startup feed valve would open and liquid feed would be pumped to the reactor, generating hot product gases. These gases would bypass the space radiator cooling system during the startup mode. Instead, the gases would be passed through a heater located within the main reactant storage tanks to melt the frozen contents.

Figure A-1

LOW TEMPERATURE START SYSTEM

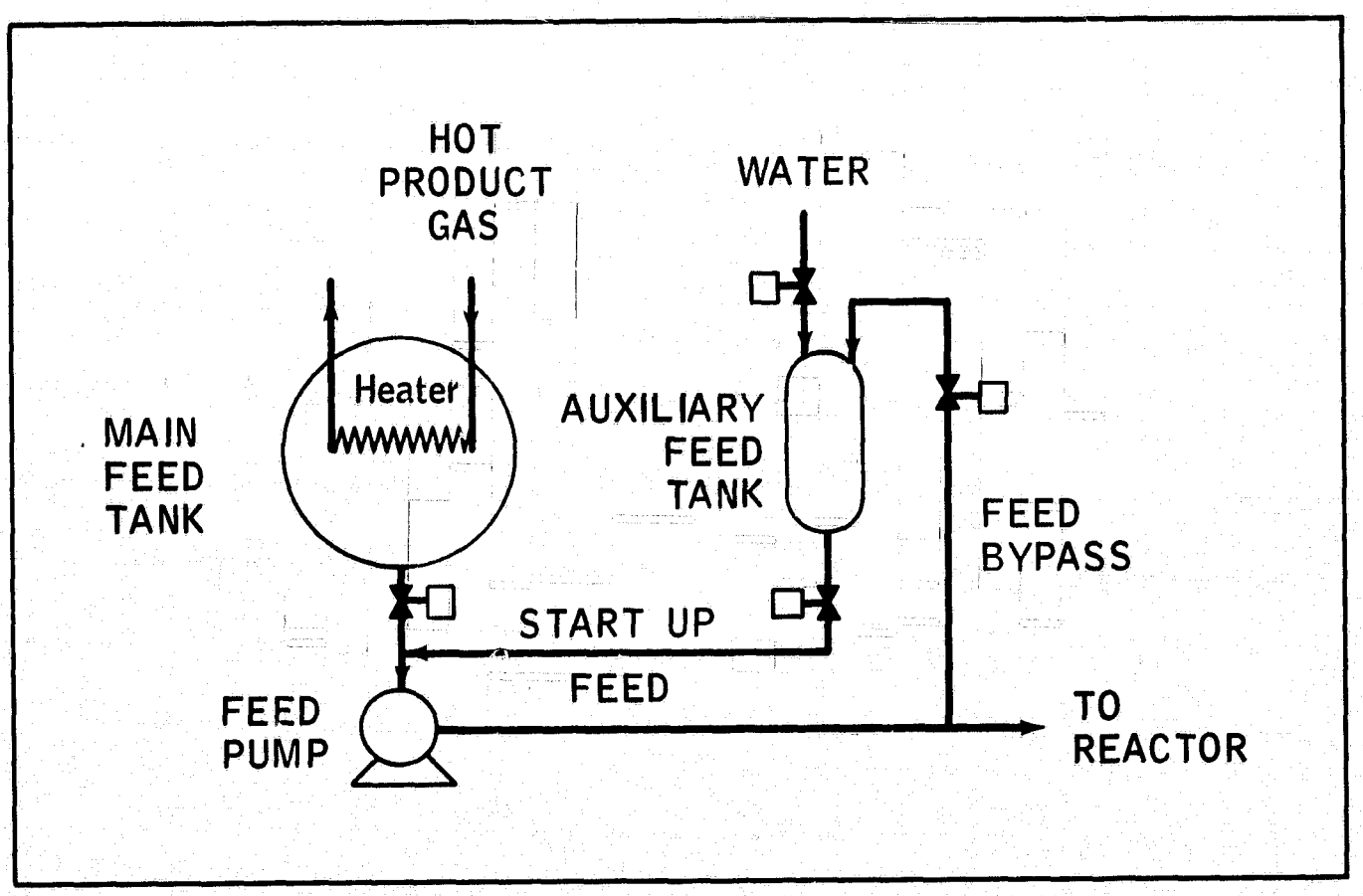

The availability of melted, concentrated feed would be sensed, say by thermistors, thus opening the main feed valve. During steady state operation with the main feed tankage, a timed bypass valve would be opened to permit recharging of the auxiliary feed tank. At the same time, a water diluent stream also would be added. These bypass streams would be shut off when the auxiliary tank was fully charged.

The data shown in Figures A-2 and A-3 indicate that solutions containing about 20-70 wt. % hydrazine and 40-70 wt. % hydrogen peroxide will have freeze points below -40°C. Therefore, the flow rates of concentrated reactants and water into the auxiliary tankage must be adjusted to provide mixtures within these ranges. It should be noted that peroxide solutions can be subcooled as glasses to much lower temperatures than indicated in Figure A-3. However, for design safety, the literature freeze point data were used.

Figure A-2

HYDRAZINE SOLUTION FREEZE POINT DATA

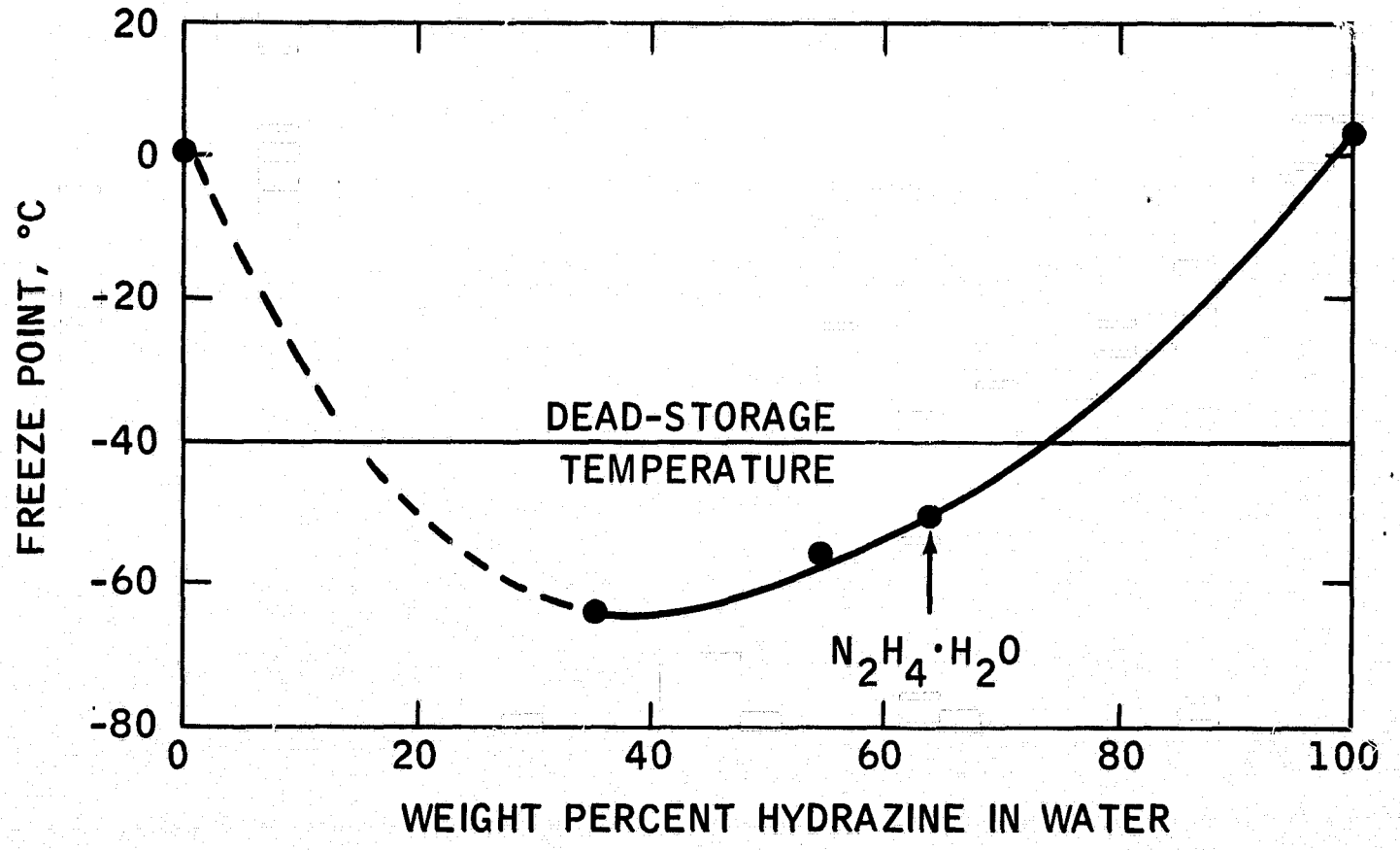

Figure A-3

HYDROGEN PEROXIDE SOLUTION FREEZE POINT DATA

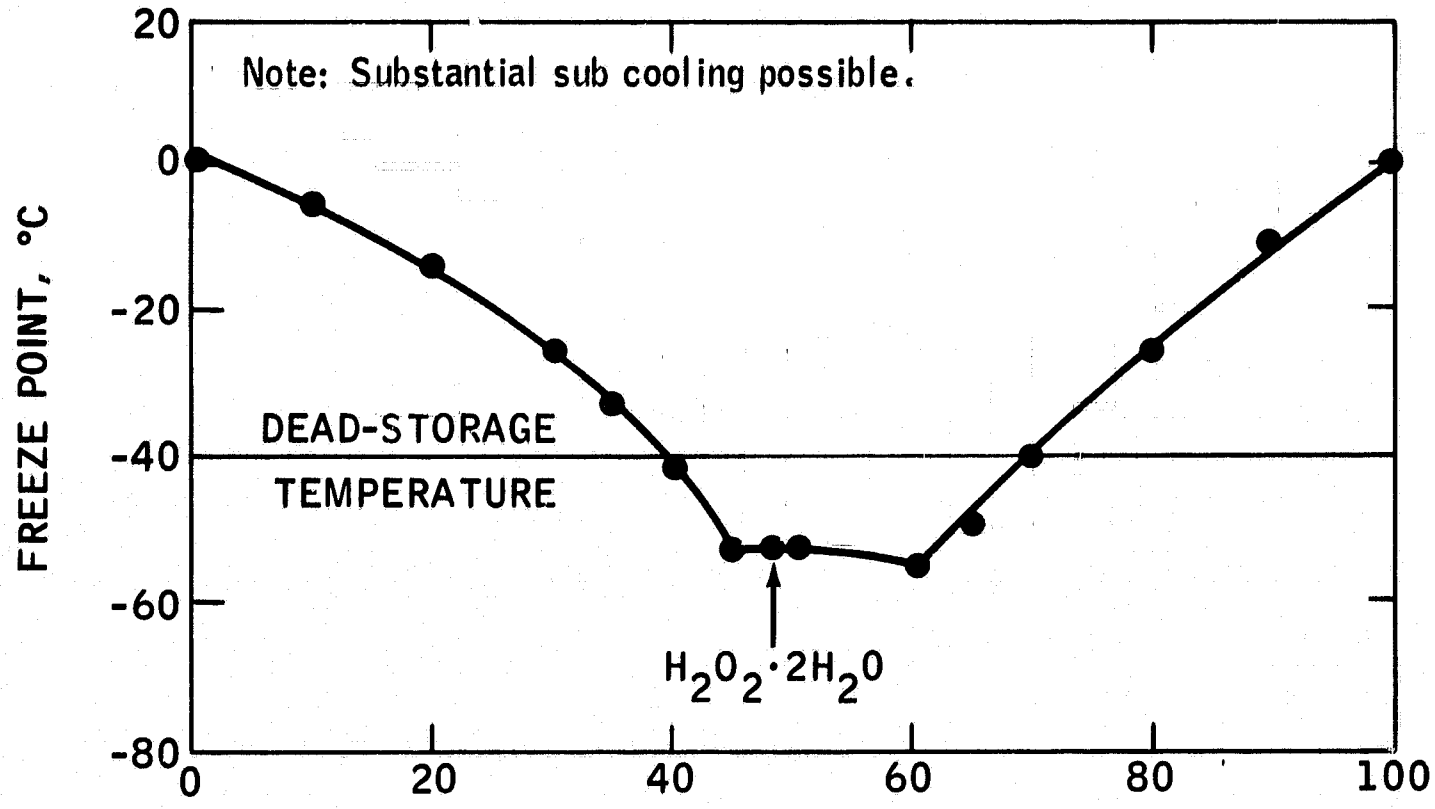

This system option was judged impractical for the following reasons:

- The piping and auxiliary tankage system are complex and would decrease system reliability.
- A source of water is required. The by-product water stream from the hydrogen peroxide decomposition reactor could be used, but trace amounts of unreacted hydrogen peroxide may be present, particularly during start-up. Additional decomposition catalyst beds, operating on the recovered water stream, would be required to ensure an uncontaminated water supply. The presence of unreacted hydrogen peroxide in the dilute hydrazine storage tank could be hazardous, to say the least. Alternatively, water could be recovered from the fuel cell modules. This means that the fuel cells would have to be operated as closed-cycle systems, complicating their design.

- Simple heat balance calculations showed that transferring sensible heat from the hot product gases to the main feed tank would not provide melted concentrated feed at a sufficiently fast rate to permit rapid startup. This means that the auxiliary feed tanks would have to be large, thus increasing system weight. In addition, the adiabatic decomposition temperatures of the diluted feeds are low, particularly for hydrogen peroxide startup feeds. The presence of heat transfer surface within the main feed tanks would considerably increase the tankage design problem. Lastly, under zero G conditions, thermal convection gradients would be missing in the molten reactant fluid adjacent to the hot heat transfer surfaces (96). This means that the latent heat of fusion would be supplied by a conduction mechanism, requiring very high local temperatures. In turn, excessive reactant decomposition would occur if these hot spots persisted.

- Cold start data obtained with dilute fluids showed that active catalysts are available for the hydrazine reactor, but the problem is more complex for hydrogen peroxide. Here, only silver oxide appeared active at -40°C. Unfortunately, it decomposes at temperatures above about 200°C, making it unsuitable for steady state operation with 98 wt. % hydrogen peroxide feed. Additional data are presented in Appendices 8 and 19.

- Although the entire system could be operated at -40°C using dilute fuels only, the weight penalty imposed by the excess water content is enormous.

APPENDIX 2

HYDROGEN CONCENTRATION DURING ONCE-THROUGH AND RECYCLE OPERATION

High reactant utilization is essential for effective aerospace fuel cell systems. Operation with dilute feeds will reduce the reactant concentration within the fuel cell. The relationship between utilization and concentration was calculated for typical once-through or recycle operation of the hydrogen anode cavity. A basis of 1 mole hydrogen consumed per unit time (C=1, referring to Figure A-4) was used for these calculations.

Figure A-4

RECYCLE OPERATION

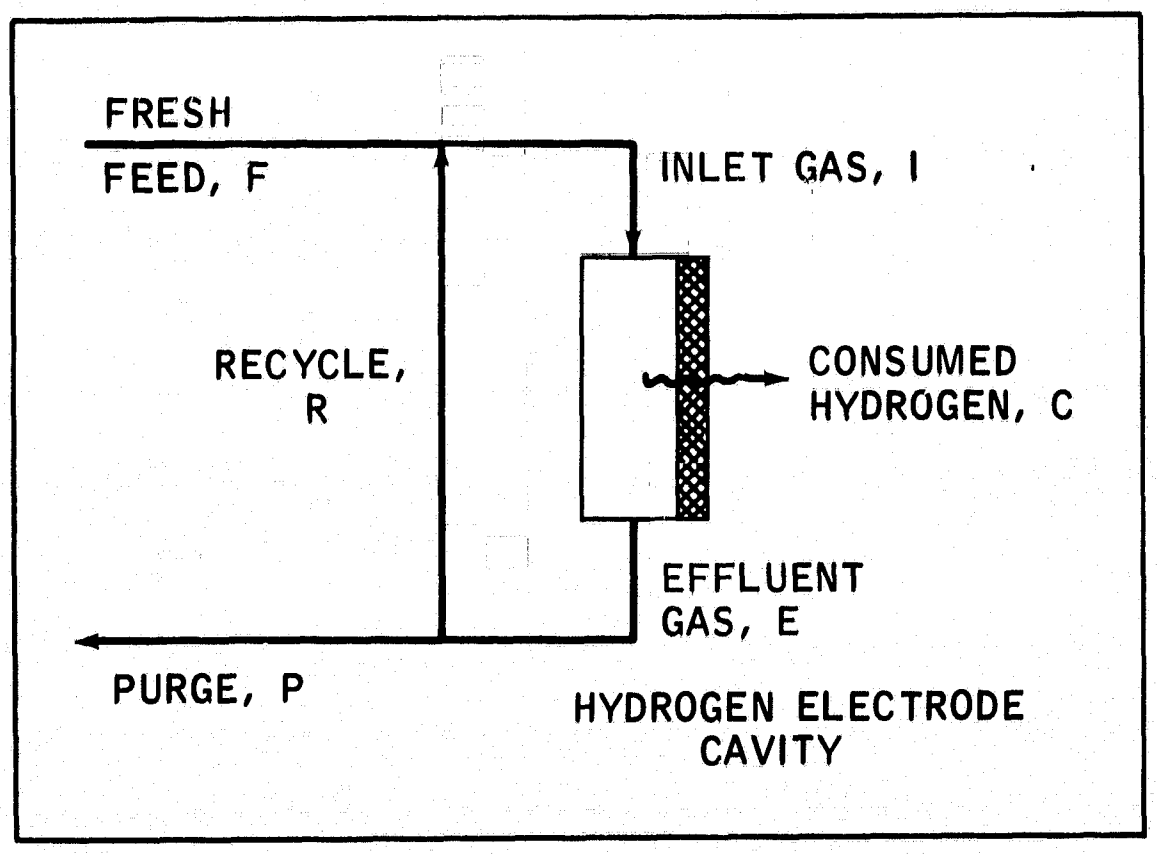

The following definitions were used:

- Utilization, $\Psi = \frac{C}{X_F F}$

  where X_F = reactant content of feed, mole fraction

- Recycle ratio, $r = \frac{R}{F}$ (based on total molal flow)

The corresponding total molal flow rates and hydrogen molal flow rates for each of the streams in Figure A-4 are listed in Table A-1. Appropriate material balances were used to simplify the hydrogen flow expressions.

Table A-1

Stream Flow Rates

Stream	Total Molal Flow/Unit Time	Hydrogen Flow/ Unit Time(1)
Feed	$F = \frac{C}{\Psi X_F}$	$\frac{C}{\Psi} = \frac{1}{\Psi}$
Cell	$C = 1$	$C = 1$
Effluent	$E = R + F - C$ $= C\left[\frac{1}{\Psi X_F} - 1\right] + R$	$X_R\left[\frac{C}{\Psi X_F}(1 + r) - 1\right]$
Recycle	R	$X_R R = \left(\frac{X_R}{X_F}\right)\left(\frac{r}{\Psi}\right)$
Inlet	$I = F + R = \frac{C}{\Psi X_F} + R$	$\frac{X_R r + X_F}{1 + r}$
Purge	$P = F - C = C\left[\frac{1}{\Psi X_F} - 1\right]$	$X_R\left[\frac{1}{\Psi X_F} - 1\right]$

(1) $X_E = X_R = X_P$ = mole fraction hydrogen in effluent, recycle and purge streams, respectively.

An overall hydrogen balance yields:

$$\frac{1}{\Psi} = 1 + X_R \left[\frac{1}{\Psi X_F} - 1 \right]$$

or,

$$X_R = \frac{X_F \left[1 - \Psi \right]}{\left[1 - \Psi / X_F \right]}$$

The cell inlet composition is:

$$X_I = \frac{X_R R + X_F F}{R + F} = \frac{X_R r + X_F}{1 + r}$$

The cell outlet composition is:

$$X_R = X_P = X_E = \frac{\Psi X_F \ (1 - \Psi)}{(1 - \Psi X_F)} = \frac{X_F \ (1 - \Psi)}{1 - \Psi X_F}$$

The average hydrogen composition within the cell is:

$$\bar{X}_{cell} = \frac{X_I + X_R}{2}$$

Values of X_I, X_R and $\bar{X}_{cell}$ were computed for the expected hydrogen feed content, $X_F = 0.667$, as a function of Ψ and r.

The results are listed in Table A-2.

Table A-2

Hydrogen Compositions in Recycle Operation

Hydrogen Utilization Factor, H	Recycle, Ratio, r	Hydrogen Composition, Mole Fraction		
		Inlet, X_I	Effluent or Recycle, X_R	Cell Average $\bar{X}_{cell}$
0.80	0	0.667	0.286	0.476
	1	0.476	↓	0.381
	2	0.413		0.350
	3	0.381		0.334
	4	0.362		0.324
	5	0.350		0.318
	6	0.340		0.313
0.85	0	0.667	0.231	0.449
	1	0.449	↓	0.340
	2	0.376		0.303
	3	0.340		0.285
	4	0.318		0.274
	5	0.304		0.267
	6	0.293		0.262
0.90	0	0.667	0.150	0.409
	1	0.409	↓	0.280
	2	0.322		0.236
	3	0.279		0.215
	4	0.254		0.202
	5	0.236		0.193
	6	0.224		0.187
0.95	0	0.667	0.091	0.379
	1	0.379	↓	0.235
	2	0.283		0.187
	3	0.235		0.163
	4	0.206		0.148
	5	0.187		0.139
	6	0.173		0.132
1.00	0	0.667	0	0.333
	1	0.333	↓	0.167
	2	0.222		0.111
	3	0.167		0.084
	4	0.133		0.066

APPENDIX 3

ELECTRODE PERFORMANCE WITH IMPURE HYDROGEN

Estimates of the effect of nitrogen diluent on hydrogen electrode performance were made using methods described by Swinkels (24) and Austin (22). Swinkels treated the problem as linear back-diffusion of impurities in the electrode pore against a flowing reactant stream, deriving the following expression:

$$P_s(i) = P_o \exp\left(\frac{iRT\tau t}{nF\ P_T\ \emptyset D}\right)$$

where: $P_s(i)$ = Impurity pressure in the gas at the gas-liquid interface within the pore, atm

P_o = Impurity pressure in the incoming gas, atm

i = Current density, amps/cm^2

R = Gas constant, 82.1 cm^3 atm/gm mole °K

T = Absolute temperature, °K

τ = Electrode tortuosity factor, dimensionless

t = Electrode thickness, cm

n = Reaction equivalents/mole

F = Faraday's constant, 96,500 coulombs/eq

P_T = Total pressure, atm

$\emptyset$ = Electrode porosity, dimensionless

D = Mutual diffusivity of H_2 and N_2, cm^2/sec

Typical values were assumed for these parameters in the proposed alkaline electrolyte fuel cell using hydrazine decomposition products directly as feed. These are listed below:

P_o = 0.680 atm, based on inlet gas at 30 psia containing 0.333 mole fraction N_2

i = 0.1 amps/cm^2, based on cell operation at 100 ma/cm^2

T = 373°K, based on operation near 212°F (actually cells should operate near 190°F)

τ = 2, assumed

t = 0.015 cm, based on typical electrode thickness of 0.006 inches

n = 2 for hydrogen oxidation

P_T = 2.04 atm, based on operation at 30 psia

$\emptyset$ = 0.5, assumed

D = 0.627 cm^2/sec calculated using the method of Bird (118):

$$\frac{P\,D_{AB}}{\left(P_{c_A}\,P_{c_B}\right)^{1/3}\left(T_{c_A}\,T_{c_B}\right)^{5/12}\left(\frac{1}{M_A}+\frac{1}{M_B}\right)^{1/2}} = 2.745 \times 10^{-4}\left(\frac{T}{\sqrt{T_{c_A}\,T_{c_B}}}\right)^{1.823}$$

where: A = Hydrogen

B = Nitrogen

P = atm

T = °K

M = Molecular weight, gms/mole

The following critical properties were used:

	H_2	N_2
P_c, atm	12.8	33.5
T_c, °K	33.3	126.2
M, gms/mole	2	28

A value of $P_s(i) = 0.68$ atm was predicted. The corresponding concentration polarization of the electrode during operation was calculated to be 6 mv using:

$$\eta_G(i) = \frac{RT}{nF}\ \ln\ \frac{P_T}{P_T - P_s(i)}$$

where: R = Gas constant, 8.3 volt coulombs/mole °K

Recalculation for end-of-cell conditions, where the nitrogen partial pressure may be as high as $0.9\left(\frac{30}{14.7}\right) = 1.84$ atm, gave only a 37 mv debit. If, in addition, a stagnant water vapor layer is assumed, equal to the vapor pressure of water over the electrolyte at a cell operating temperature of 190°F, a predicted debit of 40 mv is calculated.

The Austin analysis calculates the effect of inert gas content on the predicted limiting current. The following form of the equation was used, comparable to a corrected simple Fick's low expression:

$$i_L = \left(\frac{n\,F\,D_{eff}}{L}\right)\ C_{lb}\ f$$

where: D_{eff} = Effective diffusivity = $\frac{D_{free}}{\nearrow}$

$\nearrow$ = Pore labyrinth factor = 0.1 (assumed)

L = Pore length = 0.0254 cm (assumed equal to electrode thickness of 0.01 inches)

C_{1b} = Bulk concentration of reactant, gm moles/cm^3

$$= \frac{y_{H_2} P_T}{RT} = \frac{(.066)\ (2.04)}{(82.1)\ (373)} = 4.4 \times 10^{-6} \text{ gm moles/cm}^3$$

f = Correcting factor, a function of molar fraction of inert in bulk gas stream, $C_{2b}/N = y_{N_2}$. For $y_{N_2} = 0.934$, f = 1.026.

Thus,

$$i_L = \frac{(2)\ (96500)\ \left(\frac{0.623}{10}\right)}{(.0254)} (4.4 \times 10^{-6})\ (1.026)\ \frac{\text{amps}}{\text{cm}^2}$$

$$= 2.14 \text{ amps/cm}^2 \text{ or } 2140 \text{ ma/cm}^2$$

If the fuel cell is operated at 100 ma/cm^2, the resulting concentration polarization, η, would be:

$$\eta = \frac{RT}{nF} \ln \frac{i}{i_L - i}$$

$$= \frac{(8.3)\ (373)}{(2)\ (96500)} \ln \frac{2140}{2140-100}, \text{ volts} \times 10^3\ \frac{\text{mv}}{\text{v}}$$

$$= 0.8 \text{ mv}$$

APPENDIX 4

FUEL CELL-REACTANT WEIGHT TRADE-OFF STUDIES

Preliminary fuel cell-reactant weight trade-off studies were conducted to select the type and number of Allis-Chalmers modules required for the selected missions. Two approaches are possible. The first consists of establishing the voltage-current density characteristics of the Allis-Chalmers cells for each module type. Fuel cell operating points can be selected and appropriate cell sizes calculated for the desired module voltage and gross power output. Module weights are then estimated by assuming that the specific weight characteristics of the fuel cell will remain constant for each system type. This approach would probably result in minimum system weight, but it involves a redesign and construction of new cell stacks with different areas and numbers of cells. This approach was dropped because of the associated increase in development costs.

The second approach consisted of using the Allis-Chalmers modules as-is, with the performance data presented by Platner (12). Here, the number and type of modules per system can be varied within limits. The resulting cell operating voltage will influence the reactant storage requirements. Estimated reactant storage and tankage weights were added to the module weight to obtain a rough approximation of the system weight. Modules were selected to minimize this preliminary system weight projection.

Initial estimates of reactant storage requirements were calculated from:

$$\text{Hydrazine Storage Weight, } W_H = \frac{\dot{M}_{H_2}\ (60)\ \theta_m\ (MW_{feed})\ (1 + \delta\theta_s)\ (1 + \frac{1}{\alpha})}{\Psi_H\ \gamma_H\ Z_H\ (454)\ W_f\ C}, \text{lbs}$$

where: $\dot{M}_{H_2}$ = Hydrogen flow rate required to fuel cell, moles/min

60 = Minutes/hr

θ_m = Mission on-load time, hrs

MW_{feed} = Hydrazine molecular wt. = 32 gms/gm mole

$(1 + \delta\theta_s)$ = Storage stability factor with θ_s = dead storage, time = 3 years, and δ = decomposition rate = $\frac{0.01}{3}$. Entire factor = 1.01

$(1 + \frac{1}{\alpha})$ = (Weight tankage and fuel)/wt. fuel stored = 1.2

Ψ_H = Hydrogen utilization factor = 1.0

γ_H = Hydrogen yield factor = 0.948 (assuming 0.98 for conversion efficiency and 0.967 for diffuser recovery factor)

Z_H = 2 moles H_2/mole N_2H_4

454 = gms/lb

W_f = Weight fraction N_2H_4 in feed = 1.0.

ζ = Tankage expulsion efficiency = 0.95.

Substitution of these factors gives:

$$W_H = 2.846\ \dot{M}_{H_2}\ \theta_m,\ \text{lbs}$$

Similarly, the value for hydrogen peroxide is:

$$W_P = \frac{\left(0.5\ \dot{M}_{H_2}\right)(60)\ (\theta_m)\left(MW_{feed}\right)\left(1 + \delta\theta_s\right)\left(1 + \frac{1}{\alpha}\right)}{\Psi_0\ \gamma_0\ Z_0\ (454)\ W_f\ \zeta}\ \text{lbs}$$

where: $0.5\dot{M}_{H_2}$ = Oxygen flow rate, moles/min

$(MW)_{feed}$ = 34 gms/gm mole

$1 + \delta\theta_s$ = 1.01 (assumed)

$1 + \frac{1}{\alpha}$ = 1.2 (assumed)

Ψ_0 = 1.0

γ_0 = 1.0

Z_0 = 0.5 mole O_2/mole H_2O_2

W_f = 0.98 (98 wt. % H_2O_2)

ζ = 0.95

Therefore: $W_P = 5.850\ \dot{M}_{H_2}\ \theta_m$, lbs

Summing:

Reactant Storage Weight, $W_S = W_H + W_P = 8.696\ \dot{M}_{H_2}\ \theta_m$

Values of $\dot{M}_{H_2}$ can be calculated from:

$$\dot{M}_{H_2}, \frac{\text{moles } H_2}{\text{min}} = \frac{(1 + \pi)P_N}{E_c}\ \frac{(60)}{(96500)\ (2)} = 3.42 \times 10^{-4}\ \frac{P_N}{E_c}$$

where: Π = Parasitic power factor = 0.1.

P_N = Net system power output, watts.

60 = Seconds/min.

E_c = Fuel cell voltage.

9650 = Coulombs/eq.

2 = Equivalents/mole.

Thus:

$$W_S = 8.696\ (3.42 \times 10^{-4})\ \frac{P_N}{E_c}\ \theta_m,\ \text{lbs}$$

Now, for every combination of power output, P_N, and mission on-load time, θ_m, the value of W_S depends on fuel cell voltage, E_c. The 50-60 day performance data for Allis-Chalmers modules were used to estimate E_c (12). These calculations are summarized in Table A-3. An asterisk denotes lowest system projected weight.

Table A-3

Preliminary Weight Trade-Off Analysis

Mission On-Load Time, θ_m, Hrs	Net Power Output, P_N, Watts	Module Type and Number(1)	Gross Module Power, Watts	Fuel Cell Voltage, E_c	Weight, lbs		System
					Fuel Cell	Reactants + Tankage	
100	200	R(1)	220	0.893	30	66.6	96.6*
		R(2)	110	0.936	60	63.6	123.6
100	500	R(2)	275	0.875	60	170	230*
		R(3)	183.3	0.907	90	163.9	253.9
		L(1)	550	1.003	150	148	298
100	1000	R(4)	275	0.873	120	340	460
		L(1)	1100	0.987	150	301	451*
100	5000	L(1)	5500	0.873	150	1700	1850*
		L(2)	2750	0.940	300	1580	1880
1000	200	R(1)	220	0.893	30	666	696*
		R(2)	110	0.936	60	636	696
		L(1)	220	1.013	150	587	737
1000	500	R(2)	275	0.875	60	1700	1760
		R(3)	183.3	0.907	90	1640	1730
		R(4)	137.4	0.928	120	1604	1724
		G(1)	550	0.980	169	1519	1688
		L(1)	550	1.003	150	1483	1633*
1000	1000	R(5)	220	0.893	150	3330	3480
		G(1)	1100	0.944	169	3120	3289
		L(1)	1100	0.987	150	3000	3150*
		L(2)	550	1.003	300	3266	3566
1000	5000	L(1)	5500	0.873	150	17040	17190
		L(2)	2750	0.940	300	15840	16140
		L(3)	1834	0.964	450	15440	15890
		L(4)	1375	0.977	600	15230	15830*

(1) Allis-Chalmers modules: R = Radiation Cooled
G = Gas-Liquid Cooled
L = Liquid Cooled

APPENDIX 5

REACTANT RADIOLYSIS YIELDS

Reactant radiolysis yields were estimated, assuming the presence of alpha-emitting plutonium 238 radioisotope heating elements. The radiation level at a distance of 6 inches from a 6 gm source of Pu^{238} is about 2.5 mr/hr (private communication from Mr. Harold Coleman, Marketing Manager, Nuclear Products Department, Monsanto Company, Dayton, Ohio). The radiolysis yield, $G_{N_2H_4}$, for hydrazine is about 5.2 molecules decomposed/100 ev absorbed (35). For a mission lasting 3 years, or 2.6×10^4 hours, the weight of decomposed hydrazine is trivial.

W, gm N_2H_4 decomposed =

$$\frac{32 \text{ gms}}{\text{gm mol}} \times \frac{1 \text{ gm mole}}{6.02 \times 10^{23} \text{ mol}} \times \frac{5.2 \text{ mol } N_2H_4}{\text{ev absorbed}} \times 6.24 \times 10^{13} \frac{\text{ev}}{\text{r}}$$

$$\times 2.5 \times 10^{-3} \frac{\text{r}}{\text{hr}} \times 2.64 \times 10^4 \text{ hrs} = 1.1 \times 10^{-6} \text{ gms}$$

Similarly, the radiolysis yield for hydrogen peroxide, $G_{H_2O_2}$, is only 13.4 (92), even if complete efficiency is assumed. Again, the decomposed peroxide weight is very small.

APPENDIX 6

POTASSIUM HYDROXIDE-MODERATED HYDRAZINE REACTOR

Preliminary in-house data indicated that hydrazine might decompose selectively to hydrogen and nitrogen at low temperature in the presence of potassium hydroxide moderator. Therefore, this approach was evaluated briefly, using the apparatus shown in Figure A-5. Neat hydrazine feed was injected into a recirculating 35 wt. % potassium hydroxide solution and passed through a 9 mm I.D. Vycor reactor containing 15 gms of Esso 104 catalyst.

Figure A-5

POTASSIUM HYDROXIDE - MODERATED SYSTEM

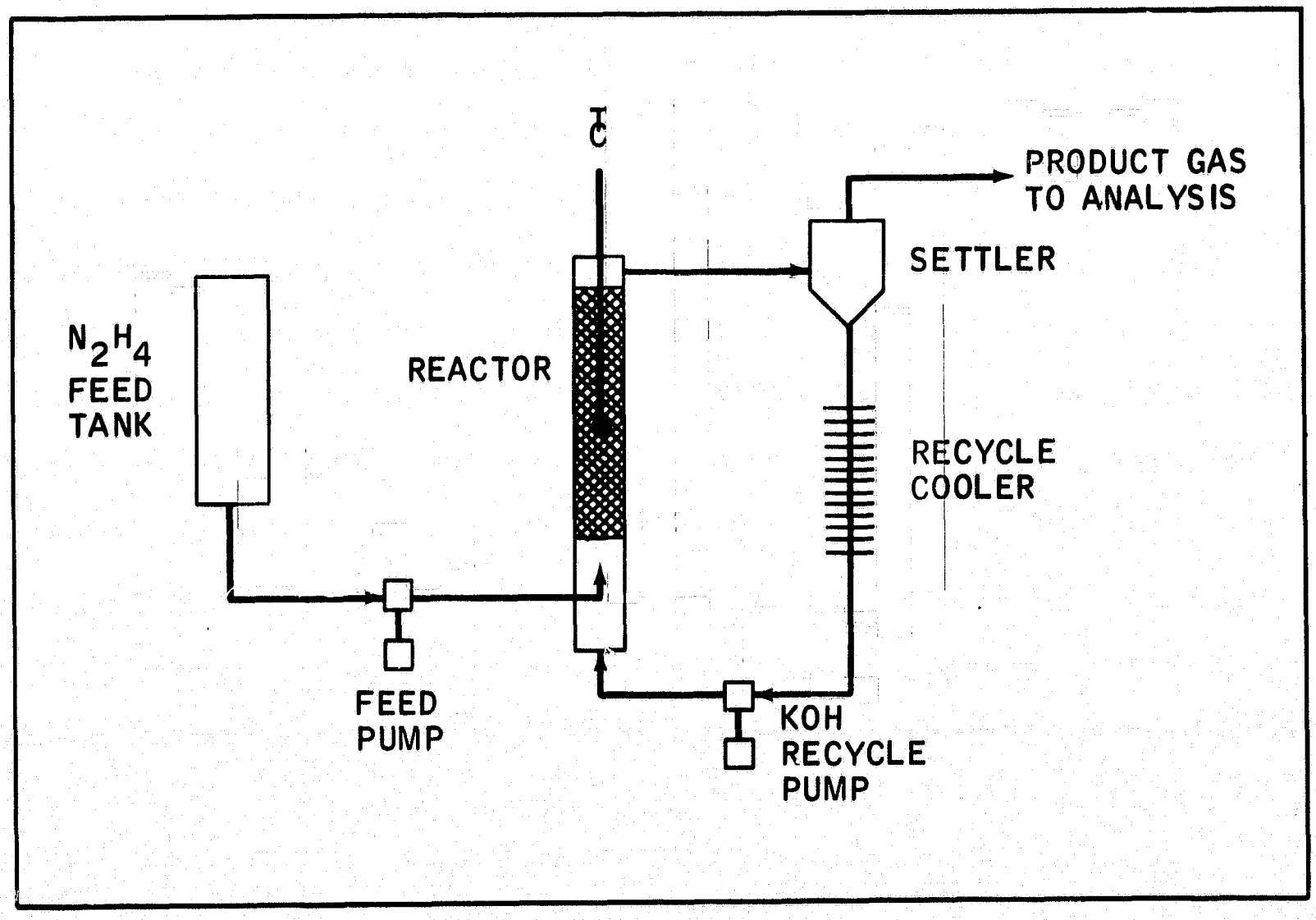

Although the data in Table A-4 show that initial selectivity was good, continued operation resulted in much poorer selectivity. Evidently, the release of ammonia product was suppressed initially as the circulating solution became saturated with dissolved ammonia. Although data are lacking for caustic solutions, the solubility of ammonia in water is quite high. Furthermore, the desorption rate of ammonia may be slow.

Closer inspection of the data shows that the apparent decomposition mechanism shifted to the following overall stoichiometry:

$$N_2H_4 \longrightarrow NH_3 + 1/2\ N_2 + 1/2\ H_2$$

Thus, equimolal amounts of nitrogen and hydrogen are obtained in the product. Clearly, this low temperature approach will not give the required high hydrogen yields.

Table A-4

Hydrazine Decomposition with
Potassium Hydroxide Moderator

Run No.	N_2H_4 Feed Rate, cc/min	KOH Recycle Rate, cc/min(1)	Reactor Temp., °C(2)	Gas Product Make, cc/min @ STP	Gas Analysis, Vol. %		
					NH_3	N_2	H_2
132-1	1	100	30	68	1.4	47.4	51.2
132-2	1	25	99	1025	69.4	15.0	15.6

(1) 35 wt. % KOH, liquid holdup volume = 140 cc.

(2) 15 gms Esso 104 catalyst charge. A 1M N_2H_4 in 35 wt. % KOH solution was used to evaluate catalyst activity. Some gas evolution was noted at -40°C and moderate gas evolution was obtained at +25°C with the following catalysts: Esso 104, Shell 405, Raney cobalt. The test solution was clear at -50°C.

APPENDIX 7

HYDRAZINE DECOMPOSITION REACTOR ASSEMBLY

The hydrazine decomposition runs were carried out using the assembly shown in Figure A-6. A graduated delivery funnel was used as feed tank. Initial runs were made with a Buehler diaphragm pump controlled by a Flex-o-pulse timer. This resulted in unstable reactor performance, caused by discrete feed pulsing. Later runs were conducted with an argon pressurant driving gas to provide smooth feed flow. A small, tantalum float rotameter was used to measure flow rate. The reactor consisted of Vycor tubes with diameters ranging from 6 to 25mm I.D. and varying length. Temperatures were measured with two thermocouples, placed at either end of the catalyst bed. Initially, a wide tube feed line was used, together with an inert, packed zone prior to the catalyst bed. This construction resulted in burn-back, as the decomposition flame front receded into the feed tube. This was corrected by switching to capillary feed lines and removing the inert packing zone by extending the active catalyst bed directly to the feed line entrance A tantalum screen was used to contain the catalyst charge.

The hot off-gases were cooled and passed through a helium-filled sample bomb prior to metering. Primol D oil, pre-saturated with ammonia, was used as working fluid in the wet test meter. Sample analysis was conducted in a gas chromatographic train, using polyethylene-imine on Poropak Q packing to separate ammonia and nitrogen. Helium was used as carrier gas. An independent GC analysis, using molecular sieve packing, was made for hydrogen. The GC units were calibrated immediately before use.

The catalyst charge consisted of uniform loadings of Esso 104 catalyst or composite loadings of Esso 104 and/or Shell 405 hydrazine catalyst, together with Girdler G-47 or Haldor-Topsoe KM-1R ammonia decomposition catalysts, as noted in Appendix 8. When required, ammonia catalyst activiation was carried out in-situ, using the procedures described in Appendix 9.

The entire assembly, from feed tank to reactor effluent line was mounted within a large cold box, pre-chilled before attempting low-temperature start-up from -40°C to +5°C. Initial cold runs were made with a cooling bath jacket adjacent to the reactor walls. Heat abstraction rates were very high, resulting in complete reaction quenching, and no auto-ignition.

Figure A-6

LABORATORY HYDRAZINE DECOMPOSITION UNIT

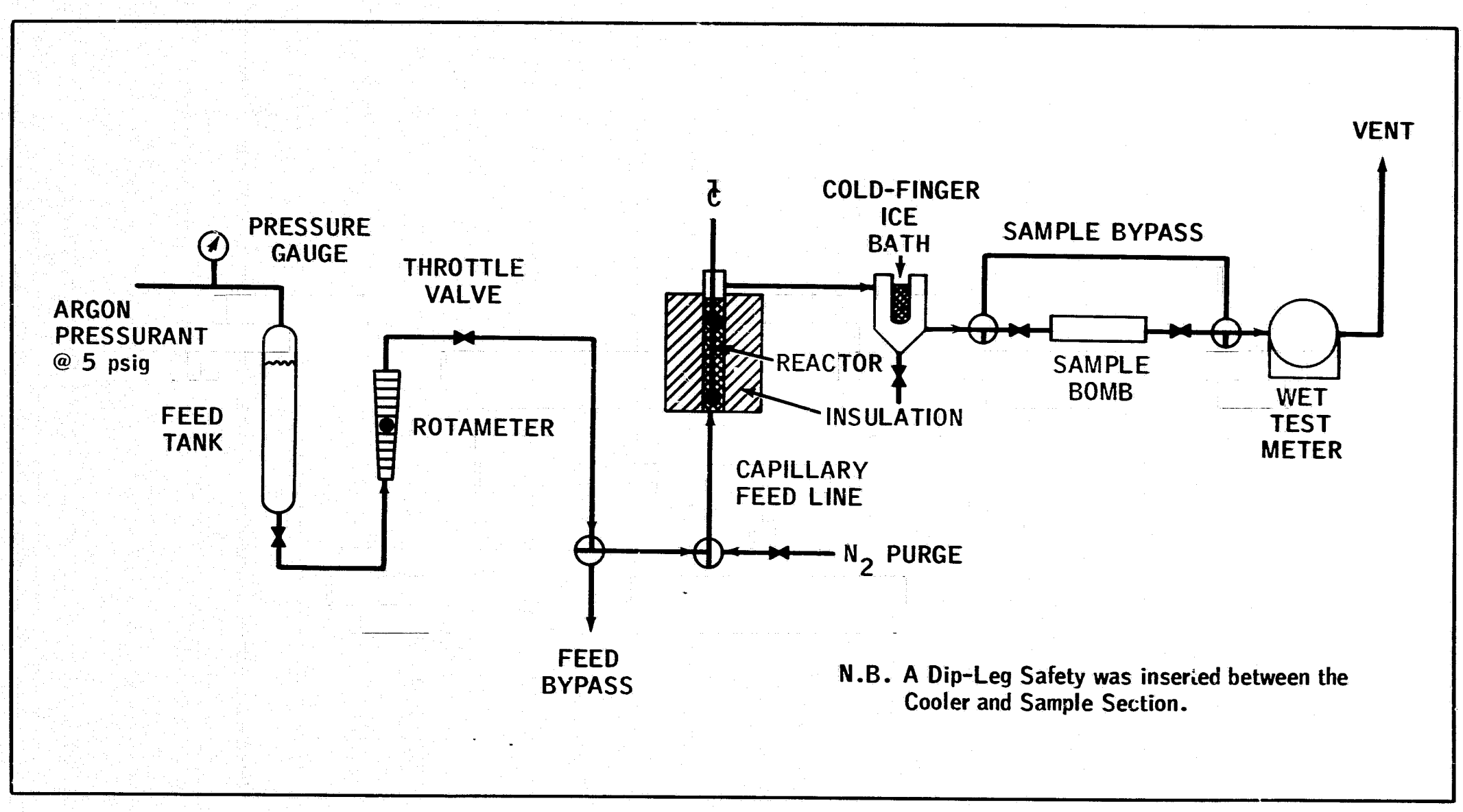

APPENDIX 8

HYDRAZINE DECOMPOSITION DATA

Run No. 409-	Ambient Temp., °C	Feed Composition	N_2H_4 Space Veloc., WHSV(1)	Reactor Temp., °C(2)		Gas Yield, l/min @ STP	Product Gas Comp., Vol. %			NH_3 Decomp., X
				Inlet	Outlet		NH_3	H_2	N_2	
85-1	25	N_2H_4	2.4	704	68	0.84	46.9	28.4	24.7	0.29
2			3.4	788	154	1.00	50.4	25.0	24.6	0.25
3			4.2	810	216	1.46	35.8	36.4	27.8	0.40
4			5.6	827	321	2.09	40.8	34.2	25.0	0.36
5			8.4	843	432	2.35	23.8	48.7	27.5	0.58
6			11.2	860	482	1.99	20.6	53.2	26.2	0.63
7			16.9	821	540	1.66	16.4	54.9	28.7	0.69
88-1	25	N_2H_4	2.4	777	67	0.76	47.8	25.7	26.5	0.26
2			3.4	816	122	1.19	34.5	38.3	27.2	0.42
3			4.2	821	174	1.54	25.9	40.5	33.6	0.51
4			5.6	860	288	2.32	23.9	43.1	33.0	0.55
5			8.4	793	371	3.61	24.8	40.2	35.0	0.52
6			11.2	827	443	4.80	19.3	46.4	34.8	0.62
7			16.9	821	521	7.16	14.2	50.9	34.9	0.70
91-1	25	N_2H_4	4.5	677	221	0.84	45.6	22.4	32.0	0.25
2			6.3	760	327	1.20	31.7	39.0	29.3	0.39
3			7.9	749	468	1.53	36.8	35.0	28.2	0.39
4			10.5(3)	777	521	2.29	31.2	41.6	27.2	0.47
5			7.0	732	354	1.52	36.5	35.9	27.6	0.40
6			9.0	749	466	1.55	36.7	34.7	28.6	0.39
7			5.2	704	318	0.99	49.2	26.8	24.0	0.27
96-1	25	N_2H_4	4.5	732	266	0.98	36.5	34.9	28.6	0.39
2			6.3	766	332	1.44	30.8	36.6	32.6	0.44
3			7.9	780	366	1.94	22.4	45.1	32.5	0.57
4			10.5	793	471	2.54	24.0	44.0	32.0	0.55
5			7.0	804	360	1.42	32.8	38.0	29.2	0.44
6			9.2	816	438	1.95	29.0	42.0	29.0	0.49
99-1	25	N_2H_4	4.9	260	154	0.83	56.8	17.2	26.0	0.17
2			6.9	260	265	1.19	52.7	22.3	25.0	0.22
3			8.6	N.A.	329	1.50	50.3	24.7	24.8	0.25
4			11.5	N.A.	382	2.23	36.6	35.0	28.4	0.39
5			17.2	N.A.	488	3.66	27.9	41.8	30.3	0.50
6			34.4(3)	N.A.	588	6.49	19.8	47.7	32.5	0.62
7			9.6	N.A.	282	1.59	37.8	35.2	27.0	0.38
115-1	25	N_2H_4	1.3	620	25	0.67	61.7	16.4	21.9	0.14
2	25	N_2H_4	7.8	107	350	6.66	12.2	57.2	30.6	0.76
116-1	25	N_2H_4	8.4	108	418	7.70	7.3	62.1	30.5	0.85
2	25	N_2H_4	2.4	660	220	1.77	29.4	44.3	26.3	0.48
119-1	-40(4)	$N_2H_4 \cdot H_2O$	N.A.	-40	-40	None	--	--	--	--
127-1	-40	$N_2H_4 \cdot H_2O$	N.A.	286(5)	78	1.17	62.0	14.0	24.0	0.14
2	-40	$N_2H_4 \cdot H_2O$	N.A.	204	232	1.33	64.0	12.0	24.0	0.12
129-1	5	N_2H_4	3.9	688	46	3.27	7.1	59.4	33.5	0.85
130-1	5	N_2H_4	4.5	704	204	3.85	8.0	59.4	32.6	0.83

(1) WHSV = gms N_2H_4/gm Cat-hr, based on <u>total</u> catalyst loading. Details of reactor catalyst charge are listed in Table A-5.
(2) As recorded at end of run. Considerable variation observed during run.
(3) Breakthrough observed.
(4) Obtained with cold fluid jacket adjacent to reactor wall. Subsequent cold start runs made in prechilled refrigerator.
(5) Temperature history during start-up listed in Table A-6.

APPENDIX 8 (CONT'D)

HYDRAZINE DECOMPOSITION DATA

Table A-5

Reactor Details

Run No. 409-	Reactor I.D., mm	Catalyst Charge(1)			Remarks(3,4)
		Type(2)	Weight, gms	Length, mm	
69	9	Esso 104	18.0	140	
70	4	Esso 104	7.5	N.A.	
73	25	Esso 104	40.0	35	Backburn
74,77	9	Esso 104	15.9	140	
79	9	Esso 104	8.0	72.5	
84	13	Esso 104	31.4	140	Backburn
85	9	Esso 104	15.1	140	Commenced formal runs.
88	9	Esso 104	15.1	140	
91, 96	9	Esso 104	8.1	75	
99	6	Esso 104	7.4	140	
103	4	Esso 104	3.0(?)	140	10-20 mesh Cat; high ΔP.
115, 116 and 119	9	Shell 405(a)	0.76	10	
		Esso 104(b)	15.0	140	
		Girdler G-47(b)	10.31		8-9 mesh.
		Girdler G-47(c)	4.06	N.A.	8-9 mesh; high ΔP.
127, 129 and 130	9	Shell 405(a)	5.0	N.A.	30 mesh.
		Shell 405(b)	5.0	N.A.	30 mesh.
		H.T. KM-1R(b)	5.0	N.A.	8-9 mesh.
		H.T. KM-1R(c)	11.7	N.A.	8-9 mesh.

(1) For combination reactors: (a) = inlet bed, (b) = center bed, and (c) = outlet bed. Catalyst particle size was 1/8" pill, except as noted.

(2) Apparent bulk densities:

Esso 104	ca. 1.80 gm/cc	Girdler G-47	1.22 gm/cc
Shell 405	1.44 gm/cc	Haldor Topsoe KM-1R	1.72 gm/cc

(3) Runs 69-84 were preliminary shakedown runs using uninsulated reactors. The GC analytical train was not operative.

(4) Pulse feed used for Runs 69-103. Argon pressurant feed system used for Runs 115-130.

APPENDIX 8 (CONT'D)

HYDRAZINE DECOMPOSITION DATA

Table A-6

Start-up Characteristics of Run 127-1

Time After Start-up, min	Reactor Temp., °C	
	Inlet	Outlet
0	-40	-40
1	204	--
2	232	-4
4	266	--
4.5	271	71
5	271	--
6	277	77
7	277	78
15	282	78
22	286	78

APPENDIX 9

AMMONIA DECOMPOSITION REACTOR ASSEMBLY

Ammonia decomposition runs were conducted in the assembly shown in Figure A-7. A 9 mm I.D. Vycor reactor was used, mounted in a temperature-controlled electric furnace. Within the reactor, the active catalyst bed was preceded by an inert bead preheating zone. Space limitations permitted the insertion of only one thermocouple, which was located within the ammonia decomposition catalyst bed.

As-received catalysts were charged and activated (reduced) *in situ* using high flow rates of pure hydrogen to reduce the partial pressure of water over the catalyst. Following activation, feed gases of varying composition were metered into the reactor. The assembly construction downstream from the reactor and the analytical procedures used are identical with those described in Appendix 7.

Figure A-7
LABORATORY AMMONIA DECOMPOSITION UNIT

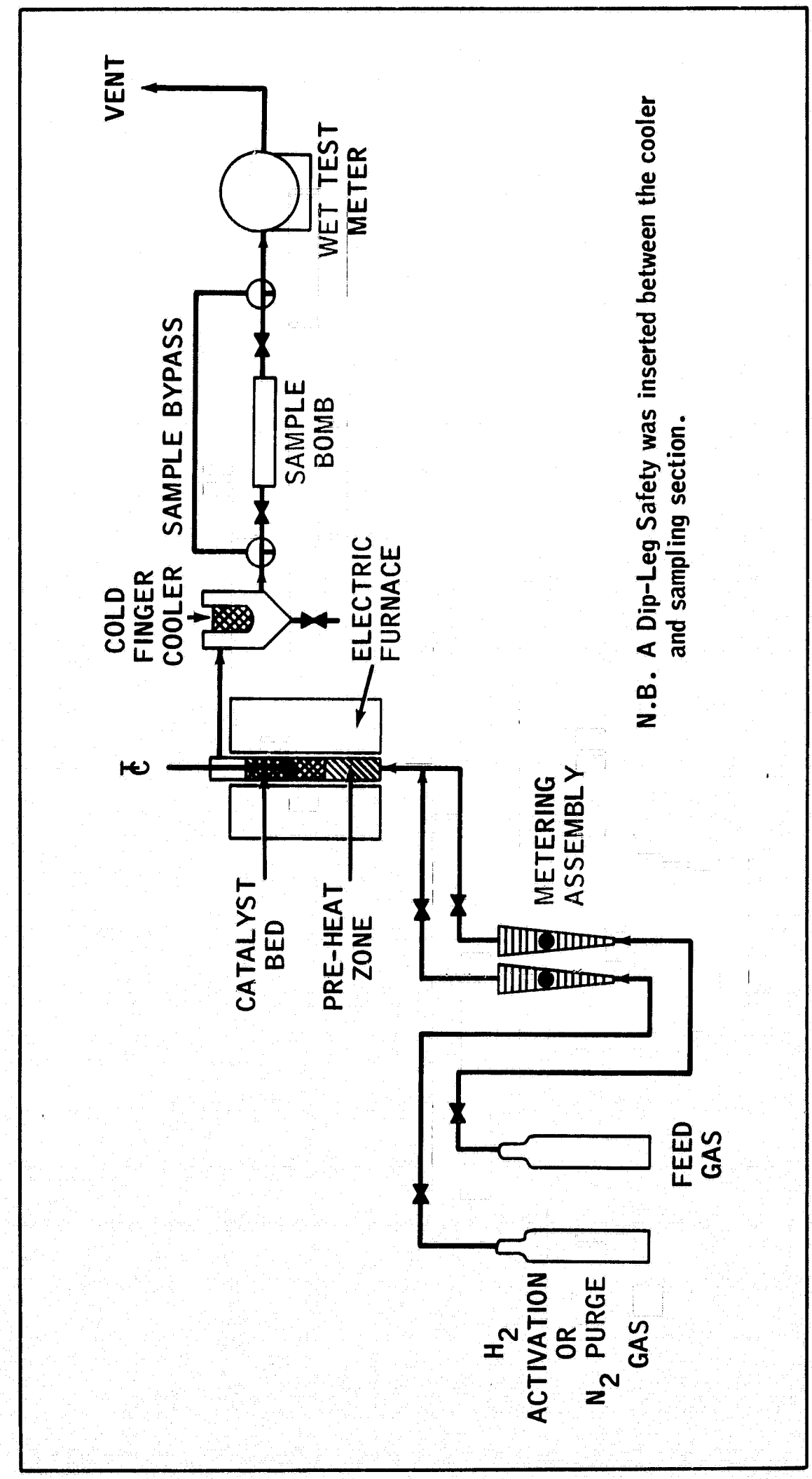

APPENDIX A-10

AMMONIA DECOMPOSITION DATA AND ANALYSIS

Run No. 409-	Feed Rate, cc/min @ STP(1)	Reactor Temp., °C(2)		Product Gas Composition, Vol. %			Fractional NH_3 Conversion, x	Reactor Contacting Parameter, V_r/F_{A_o}(3)	Rate Constant, k x 10^4
		Inlet	Outlet	NH_3	H_2	N_2			
106-7	2440	633	718	14.8	48.9	36.3	0.38	3-7	18.7
8	1200	620	670	18.8	51.6	29.6	0.24	622	4.9
9	3700	560	695	21.8	48.5	29.7	0.14	202	8.8
10	860	590	660	11.0	50.5	38.5	0.53	868	11.3
107-11	4238	485	670	22.7	45.7	31.6	0.12	176	8.4
12	4238	700	800	(1.4)	N.A.	(11.5)	0.93	176	456
13	3700	700	800	0.0	60.2	39.8	1.00	202	> 860
108-1	3910	693	815	0.0	62.2	37.8	1.00	113	> 532
2	2470	675	793	0.86	67.7	31.4	0.96	179	118
3	1050	688	810	0.0	67.3	32.7	1.00	420	> 142
112-1	3910	621	704	11.4	56.4	32.2	0.67	113	62

(1) Feed gas for Runs 106-107: 26.7% NH_3, 44.7% H_2, 28.6% N_2. Feed gas for Runs 108-111: 45.2% NH_3, 26.1% H_2, 28.7% N_2.

(2) Girdler G-47 catalyst, 8.9 cc charge in 9 mm I.D., Vycor reactor; catalyst bed length = 140 mm.

(3) V_r/F_{A_o} = cc catalyst-min/mole NH_3 input.

APPENDIX 10 (CONT'D.)

AMMONIA DECOMPOSITION DATA AND ANALYSIS

The ammonia decomposition data were analyzed using the conventional Temkin-Pyzhev equation:

$$NH_3 \text{ Decomposition Rate, } r = - \frac{d\left(P_{NH_3}\right)}{d\theta} = k \frac{\left(P_{NH_3}\right)^a}{\left(P_{H_2}\right)^b} \qquad (1)$$

where: k = Rate constant

P_{NH_3}, P_{H_2} = Partial pressure of ammonia and hydrogen, atm.

θ = Time

a, b = Experimental coefficients (theoretical values also available)

This rate expression was incorporated into an integral reactor design equation:

$$- \frac{d\left(P_{NH_3}\right)}{d\theta} = \frac{dx}{d\left(V_R/F_{A_o}\right)} = - \frac{k\left(P_{NH_3}\right)^a}{\left(P_{H_2}\right)^b} \qquad (2)$$

where V_R = Catalyst bed volume, cc

F_{A_o} = Inlet NH_3 feed rate, moles NH_3/min

x = Fractional NH_3 conversion

After rearranging and integrating, this equation becomes:

$$\int_0^X \frac{\left(P_{H_2}\right)^b}{\left(P_{NH_3}\right)^a} dx = \frac{k\, V_r}{F_{A_o}}$$

Solution is accomplished graphically, after converting the partial pressure expressions to equivalent values in terms of x.

APPENDIX 10 (CONT'D.)

AMMONIA DECOMPOSITION DATA AND ANALYSIS

At any time:

$$P_{NH_3} = Y_{NH_3}\,\pi_T$$

$$P_{H_2} = Y_{H_2}\,\pi_T \qquad (4)$$

$$Y_{N_2} = 1 - Y_{NH_3} - Y_{H_2}$$

where: Y = composition, mole fraction

π_T = total pressure, atm

By material balance:

$$NH_3 \longrightarrow 0.5\ N_2 + 1.5\ H_2$$

Moles at Start:	$(NH_3)_o$	$(N_x)_o$	$(H_2)_o$
During Reaction:	$(NH_3)_o\,(1-x)$	$(N_2)_o + 0.5x$	$(H_2)_o + 1.5\,x$

where: x = Fractional ammonia conversion

$(\ )_o$ = Moles gas in feed

Therefore,

$$Y_{NH_3} = \frac{(NH_3)_o\,(1-x)}{(NH_3)_o\,(1-x) + (N_2)_o + 0.5x + (H_2)_o + 1.5\,x} \qquad (5)$$

Similar expressions can be derived for Y_{H_2} and Y_{N_2}.

Substitution of (5) into (4) and then into (3) yields:

$$\int_0^X \frac{\left[\dfrac{\left(Y_{H_2}\right)_o + 1.5x\left(Y_{NH_3}\right)_o}{1 + x\left(Y_{NH_3}\right)_o}\right]_a^b}{\left[\dfrac{(1-x)\left(Y_{NH_3}\right)_o}{1 + x\left(Y_{NH_3}\right)_o}\right]_a^b} dx = \frac{k\,V_r}{F_{A_o}} \qquad (6)$$

where $(Y_i)_o$ = Feed gas composition

X = Overall ammonia conversion

Values of a and b, available from the literature for various catalysts, are shown below (44, 54).

Catalyst	a	b
Unpromoted Iron (G-47)	0.9	1.50
Doubly Promoted Iron	0.72	0.35

Values of k were calculated for the Girdler G-47 catalyst data using Equation (6). These are tabulated in this Appendix. For the reactor design cases, values of k were first calculated from literature data on doubly-promoted catalysts. Then Equation (6) was used to predict V_r, the catalyst bed volume. The "feed" composition for these calculations was assumed equivalent to the hydrazine decomposition reactor effluent, at a design value of fractional ammonia conversion, x = 0.7. For this condition, the following ammonia decomposition inlet feed gas composition is obtained.

Component	Mole Fraction, $(Y_i)_o$
NH_3	0.154
N_2	0.308
H_2	0.538

Graphically computed values of the left-hand side of Equation (6), using the design inlet feed composition, are presented below for the two catalyst cases.

	Value of Integral	
	a = 0.9	a = 0.72
X	b = 1.50	b = 0.35
0.00	0.00	0.00
0.2	0.50	0.69
0.4	1.20	1.54
0.6	2.26	2.70
0.8	4.23	4.51
0.9	6.16	6.04
0.95	8.00	7.32
0.97	9.25	8.10
0.99	12.10	9.69

APPENDIX 11

REACTANT FLOW RATE CALCULATION

Reactant flow rate requirements were calculated using the following equations:

$$\text{Hydrazine Flow Rate, } \dot{W}_{N_2H_4} = \dot{M}_{H_2} \times \frac{1}{\Psi_H} \times \frac{1}{\gamma_H} \times \frac{1 \text{ mol } N_2H_4}{2 \text{ mol } H_2} \times \frac{32 \text{ gms } N_2H_4}{\text{mol } N_2H_4}, \frac{\text{gms}}{\text{min}}$$

where: $\dot{M}_{H_2}$ = Hydrogen consumption in fuel cell, gm moles H_2/min

Ψ_H = Hydrogen utilization factor = 1.0

γ_H = Hydrogen generator yield, fraction of theory

$= \gamma_{reactor}\ \gamma_{diffuser} = (0.98)\ (0.967) = 0.948$

and,

$$\dot{M}_{H_2}, \frac{\text{gm ml } H_2}{\text{min}} = \frac{(1 + \pi)\ P_N \text{ watts}}{E_c \text{ volts}} \times \frac{1 \text{ volt amp}}{\text{watt}} \times \frac{1 \text{ coulomb}}{\text{amp sec}} \times \frac{60 \text{ sec}}{\text{min}} \times \frac{1 \text{ eq}}{96500 \text{ coul.}} \times \frac{1 \text{ gm mol } H_2}{2 \text{ eq}}$$

or

$$\dot{M}_{H_2} = 3.42 \times 10^{-4}\ \frac{P_N}{E_c}$$

where: π = Parasitic power factors = 0.1

P_N = Net power output, watts

E_c = Fuel cell design voltage (See Appendix 4.)

The Allis-Chalmers modules were assumed to operate with infrequent purging, so that hydrogen utilization, $\Psi_H = 1$. Also, the coulombic efficiency was assumed to be unity, with no unwanted side reactions. The design reactor yield factor, $\gamma_{reactor}$, was selected as 0.98 to permit reasonable sizing of the ammonia decomposition catalyst requirements. The design diffuser yield factor, $\gamma_{diffuser}$, was calculated as 0.967, based on the analysis in Appendix 16. The overall parasitic power factor, π, was assumed to be 0.1, more than twice that required for the fuel cell operation. Platner states that π = 0.01-0.015 for the Allis-Chalmers radiation and liquid-cooled modules (12).

The corresponding expression for hydrogen peroxide solution flow rate is:

$$\text{Hydrogen Peroxide Flow Rate, } \dot{W}_{H_2O_2}, \text{gm/min} = \dot{M}_{O_2} \times \frac{1}{\Psi_0} \times \frac{1}{\gamma_0} \times \frac{1 \text{ mol } H_2O_2}{0.5 \text{ mol } O_2} \times \frac{1 \text{ gm sol.}}{W_f \text{ gm } H_2O_2}$$

where: $\dot{M}_{O_2}$ = Oxygen consumption in fuel cell = $0.5\ (M_{H_2})\ \frac{\text{gm mol } O_2}{\text{min}}$

Ψ_0 = Oxygen utilization factor = 1.0

γ_0 = Oxygen generator yield, fraction of theory = 1.0

W_f = 0.98, assuming 98 wt. % H_2O_2 feed

The calculated reactant flow rates are tabulated below.

Mission On-Load Time, θ_m, Hrs	Net Power Output, P_N, Watts	Fuel Cell System Voltage(1)	Reactant Flow Rates, Gms/Min	
			Hydrazine, $W_{N_2H_4}$	98% Hydrazine Peroxide, $W_{H_2O_2}$
100	200	0.893	1.29	2.65
	500	0.875	3.30	6.75
	1000	0.987	5.85	11.98
	5000	0.873	33.1	67.5
1000	200	0.936	1.23	2.53
	500	1.003	2.88	5.90
	1000	0.987	5.85	11.98
	5000	0.977	29.6	60.5

(1) Based on 50-60 day performance values. (See Appendix 4.)

APPENDIX 12

REACTANT STORAGE REQUIREMENTS

Reactant storage requirements were estimated using the following general expression:

$$W_{Reactant,\ lbs} = \dot{W}\ \frac{gms}{min} \times 60\ \frac{min}{hr} \times \theta m,\ hrs \times \frac{1}{\rho} \times (1 + \delta\ \theta_s) \times \frac{1\ lb}{454\ gms}$$

where: $\dot{W}$ = Reactant design flow rate, $\frac{gms}{min}$ (See Appendix 11.)

θ_m = Mission on-load time, hrs

ρ = Tankage expulsion efficiency

δ = Storage stability factor

θ_s = Dead-storage time, yrs

Bladder-expulsion and capillary-action tanks were considered. The expulsion efficiency, ρ, of bladder tanks was taken as 0.98 (93). The value for capillary tanks was assumed, arbitrarily, to be somewhat less, 0.95. A conservative storage stability factor, δ = 0.062, was used, equivalent to 2% decomposition/yr. This exceeds the values noted in the text in Figures 11 and 22 for hydrazine and hydrogen peroxide, but agrees with previous design experience (93). The reactant storage requirements are tabulated below.

Mission On-Load Time, θ_m, Hrs	Net Power Output, P_N, Watts	Reactant Storage, Lbs			
		Bladder Tankage		Capillary-Action Tankage	
		Hydrazine	98% Hydrogen Peroxide	Hydrazine	98% Hydrogen Peroxide
100	200	18.4	37.9	19.0	39.1
	500	47.2	96.5	48.8	99.5
	1000	83.6	171	86.5	177
	5000	473	965	489	998
1000	200	176	362	182	374
	500	412	843	425	872
	1000	837	1713	865	1771
	5000	4233	8652	4377	8941

APPENDIX 13

TANKAGE WEIGHT ESTIMATES

This appendix describes the procedures used to estimate tankage weights. Spherical tank shape was assumed throughout.

Reactant Tankage Weights

Reactant tank weights were estimated using the following procedures. For bladder-expulsion tanks:

1. Reactant volume, $V_R = \dfrac{(1 + u)\ W_R}{\sigma_R\ (62.4)}$, ft^3

where: u = Ullage factors to accommodate thermal expansion

W_R = Reactant storage weight (See Appendix 12.)

σ_R = Reactant specific gravity at 25°C initial fill temperature; $\sigma_{N_2H_4} = 1.004$, $\sigma_{98\%\ H_2O_2} = 1.432$.

2. Bladder inner radius, $r_{i_B} = \left(\dfrac{V_R}{4.189}\right)^{1/3}$, ft

3. Average bladder radius, $\bar{r}_B = r_{i_B} + \dfrac{t_B}{2}$

where: t_B = Bladder thickness, assumed = 0.00083 ft (0.010 inch)

4. Bladder material volume, $V_B = 4\pi\ \bar{r}_B^{\,2}\ t$, ft^3

5. Bladder weight, $W_B = \rho_B\ V_B$, lbs

where: ρ_B = Bladder density, 137.3 lbs/ft^3 for Teflon (98% H_2O_2) or 56.2 lbs/ft^3 for butyl rubber (N_2H_4).

6. Tank inner radius, $r_{i_T} = r_{i_B} + t_B + 0.02083$, ft

where: 0.02083 = Circumferential clearance space for bladder retaining screens (0.25 inches)

7. Average tank radius, $\bar{r}_T = r_{i_T} + \frac{t_T}{2}$, ft

where: t_T = tank thickness, assumed = 0.00416 ft (0.050 inches)

8. Tank wall volume, $V_T = 4\pi \bar{r}_T^2 t_T$, ft^3

9. Tank wall weight, $W_T = \rho_T V_T$, lbs

where: ρ_T = Tank material density, 169.3 lbs/ft^3 for 1060 Al (98% H_2O_2) or 276.5 lbs/ft^3 for 6Al-4V titanium (N_2H_4)

10. Total weight, $W = W_B + W_T$, lbs

Weights were not estimated for the metallic internals of the bladder tanks.

A similar procedure was used for estimating the weight of capillary-action tanks, using the symbols defined above:

1. $V_R = \frac{W_R}{f \sigma_R (62.4)}$, ft^3

where: f = Fill factor or fraction of tank initially filled, assumed = 0.98 (allowance for thermal expansion)

2. $r_{i_T} = \left(\frac{V_R}{4.189}\right)^{1/3}$, ft

3. $\bar{r}_T = r_{i_T} + \frac{t_T}{2}$, ft

where: t_T = Tank thickness, assumed = 0.00416 ft (0.050 inches)

4. $V_T = 4\pi \bar{r}_T^2 t_T$, ft^3

5. $W_T = \rho_T V_T$, lbs

6. Total weight, $W = (1 + i) W_T$

where: i = Internals weight factor for capillary array = 0.05, assumed

Typical tankage weights are listed below. The capillary action tanks were selected on the basis of slightly lower weight and ease of venting. Weights for all missions were obtained from a graph of log (tank weight) versus log (reactant weight). A complete listing of capillary-action tank weight is given in Phase 5, Table 6.

Mission On-Load Time, θ_m, Hrs	Net Power Output, P_N, Watts	Weight Summary, Lbs							
		Bladder Tanks				Capillary Tanks			
		N_2H_4		98% H_2O_2		N_2H_4		98% H_2O_2	
		Reactant	Tank	Reactant	Tank	Reactant	Tank	Reactant	Tank
100	200	18.4	2.9	37.9	2.5	19.0	2.7	39.1	2.1
100	5000	473	23.8	965	20.5	489	23.3	998	18.1
1000	5000	4233	100.9	8652	87.2	4377	100.6	8941	78.1

The effect of reactant thermal expansion at 40°C was checked. The capillary action tanks were sufficiently oversized to accommodate the expansion from 25°C, even if constant tank volume is assumed. Allowable internal pressures were calculated for the largest tanks using a 25°C working stress of 128,000 psi for titanium and 18,000 psi for aluminum, with wall thickness = 0.05 inches (68, 79). Permissible pressures are 415 psi for the hydrazine tank and about 52 psi for the 98 wt.% hydrogen peroxide. These are within acceptable centerline design limits.

Product Accumulation Tanks

The hydrogen and oxygen product accumulation tanks were sized to deliver fuel cell feed for the design start-up period of 15 minutes. The perfect gas equation was used:

$$V_{AT} = \frac{nRT}{P}, \text{ ft}^3$$

where: V_{AT} = Accumulation tank volume, ft^3

n = Lb moles gas stored = $\frac{\dot{M}\ (15)}{454}$, where $\dot{M}$ = gm moles gas required/min (See Appendix 11.)

R = Gas constant, 10.71 psi ft^3/ lb mole, °R

T = Fill temperature = 610°R (150°F)

P = Fill pressure = 30 psia for H_2, 150 psi for O_2

Tank weights were estimated from:

$$W_{AT} = 4\pi\left(\frac{t_T}{12}\right)\bar{r}_T^{\,2}\rho_T, \text{ lbs}$$

where: W_{AT} = Tank weight, lbs

t_T = Tank thickness = 0.05 inches

$\bar{r}_T$ = Average tank radius = $\left(\frac{V_{AT}}{4.189}\right)^{1/3} + \frac{1}{2}\left(\frac{t_T}{12}\right)$, ft

ρ_T = Wall material density = 500.4 lbs/ft^3 for stainless steel

Tank weights were calculated for contained volumes ranging from 0.01 to 100 ft^3 and plotted on log-log graph paper to permit interpolation. The specific values of accumulator tank weight for each mission are listed in Phase 5, Table 6.

Nitrogen Pressurant Tank

The nitrogen pressurant tank was sized to provide sufficient gas to expel the contents of the hydrazine feed tank:

$$V_{NT} = 1.1\ V_{N_2H_4}$$

where: V_{NT} = Volume of nitrogen tank contents, ft^3 (filled at 450 psia, 150°F)

$V_{N_2H_4}$ = Volume of hydrazine storage tank, ft^3 (assumed at 40 psia, 40°F)

$= 4.189\ r_{i_T}^{\,3}$

Thus:

$$N_N = \left(\frac{PV}{RT}\right)_{NT} = 1.1\left(\frac{PV}{RT}\right)_{NTE}$$

where: N_N = Moles nitrogen pressurant required

NT = Nitrogen pressurant tank

NTE = Nitrogen pressurant tank expanded to fill hydrazine storage tank

Insertion of the appropriate temperatures and pressures yields:

$$V_{NT} = 0.119\ V_{N_2H_4}$$

The capillary tankage case was chosen to estimate $V_{N_2H_4}$. Again, spherical stainless steel tanks, with 0.05 inch wall thickness, were used to contain the pressurant. Tank weights were calculated for a number of missions and a graph of log (pressurant tank weight) versus log (hydrazine reactant storage weight) was used to estimate interpolated values for the remaining missions. Final estimates of pressurant tank weights are listed in Phase 5, Table 6.

Miscellaneous Tankage and System
Hardware and Control Circuitry

Only rough estimates were made for the tankage connections, pressure regulators, flow lines, vent valves, etc. It was assumed that the 200 watt system would require 10 lbs of miscellaneous hardware and about 2 lbs of control circuitry. Corresponding values for the 5000 watt system were 20 and 3 lbs, respectively. Straight-line interpolations were used for intermediate power levels.

APPENDIX 14

INTEGRAL REACTOR DESIGN

An integrated reactor design, similar to those illustrated in Phase 3, Figures 18 and 19, was used for the gas generator subsystems. This appendix discusses the procedures used to estimate the catalyst weight requirements and the reactor weights.

Catalyst Weight Requirements

Experimental data showed that complete hydrazine decomposition could be accomplished with Esso 104 or Shell 405 catalyst at a space velocity of 15 gms N_2H_4/hr gm cat or 0.25 gms N_2H_4/min gm cat. Thus, the weight of hydrazine decomposition catalyst can be calculated directly from the appropriate system feed rate.

The weight of ammonia decomposition catalyst was calculated assuming a fractional ammonia conversion of X = 0.98. The ammonia unit feed composition and design procedure were discussed in Appendix 10. The final design assumed that an active decomposition catalyst, similar to that of Takezawa (54) would be used. As noted earlier, catalyst weight requirements critically depend on the average bed temperature. It was assumed that the bed temperature could be maintained at 500°C. Atmospheric pressure rate data were the only data available for these calculations, even though the proposed reactor operating pressure is 500 psi. The decomposition reaction may be inhibited or accelerated at high pressure, depending on the values of the exponents "a" and "b" in the Temkin-Pyzchev rate equation discussed in Appendix 10. Additional data are needed to define this effect firmly.

The hydrogen peroxide decomposition catalyst requirements were defined using a design flow rate of 1 gm (neat) H_2O_2/min gm cat. The catalyst requirements for all subsystems were low, as shown below. No debit was taken for potential catalyst deactivation during use.

Simplified trade-off studies were made to determine the minimum reactor wall weight as a function of cylindrical tube diameter and length. The Lamé equation was used to determine the required wall thickness:

$$t_R = \frac{PD}{2SE}$$

where: t_R = wall thickness, in.

P = working pressure = 500 psi

D = reactor inner diameter, in.

S = allowable stress at 2000°F = 1800 psi for cast ACI-type HK stainless steel (68). Density = 0.286 lbs/in.^{3}

E = longitudinal weld efficiency factor = 1.0

External insulation requirements were calculated to limit heat losses from the reactor. The heat load was assumed equal to the enthalpy difference of the outboard peroxide decomposition products between the adiabatic reaction temperature, 1749°F, and the design product outlet temperature, 1500°F. Mean specific heat values of 0.572 and 0.265 BTU/lb °F were used for water vapor and oxygen, respectively. The heat flux was equal to the load divided by the outer shell area. A Min K insulation was selected with an effective thermal conductivity of 0.25 $\frac{\text{BTU-inch}}{\text{hr ft}^2\ °\text{F}}$ and density of 20 lbs/ft^3 (80). Insulation thickness was calculated for the cylindrical geometry reactors (84) using:

$$\frac{Q}{L} = \frac{2\pi k \Delta T}{\ln\left(\frac{r_1}{r_2}\right)}, \frac{\text{BTU}}{\text{hr ft}}$$

where: Q/L = heat flux per unit cylinder length, BTU/hr ft

k = thermal conductivity

ΔT = temperature difference = 1749-40° = 1709°F

r_1, r_2 = inner and outer insulation radius

Minimum On-Load Time, θ_m, Hrs	Net Power Output, P_N, Watts	Decomposition Catalyst Requirements, gms				
		Hydrazine[1]	Ammonia @[2] Indicated Temp., °C			98 Wt.% Hydrogen Peroxide[3]
			500	600	700	
100	200	5.2	30	5	--	2.6
	500	13.2	78	13	--	6.6
	1000	23.4	138	22	--	11.7
	5000	132.4	780	126	--	66.3
1000	200	4.9	29	5	1	2.5
	500	11.5	68	11	3	5.8
	1000	23.4	138	22	5	11.7
	5000	118	698	117	27	59.3

(1) Esso 104 or Shell 405 catalyst.

(2) Haldor Topsoe KM-IR catalyst with activity and kinetics assumed equal to Takezawa catalyst (54).

(3) I-6A catalyst.

Reactor Weight Estimates

Reactor weight estimates were made assuming a concentric placement of catalyst beds, as shown for the integral reactor in Phase 3, Figure 18. An outboard envelope contained the peroxide decomposition catalyst. The required catalyst volumes are listed below:

Reactor Size	Catalyst Volumes, cc[1]		
	N_2H_4	NH_3	98% H_2O_2
Smallest (100 hrs @ 200 watts)[2]	3.6	17.4	1.7
Largest (100 hrs @ 5000 watts)[3]	92	453	42.2

(1) Catalyst densities, g/cc: N_2H_4 = 1.44, NH_3 = 1.72, H_2O_2 = 1.57

(2) Total catalyst weight = 37.8 gms or 0.083 lbs.

(3) Total catalyst weight = 978.3 gms or 2.16 lbs.

Component	Reactor Component Weight, Lbs	
	Smallest (100 hrs @ 200 Watts)	Largest (100 hr @ 5000 Watts)
Total Catalyst Charge	0.08	2.16
Reactor Wall	1.45	5.55
Insulation	1.72	0.32
Sub Total	3.25	8.03
Fittings and Contingency @ 20%	0.65	1.6
Final Total	3.9	9.6

Reactor weights for intermediate sizes were estimated by interpolation, using a graph of log (Reactor Weight) versus log (Hydrazine Flow Rate). Final weights are listed in Phase 5, Table 6.

APPENDIX 15

FEED PUMP SELECTION

A detailed search for appropriate feed pumps was not conducted. However, a number of pumps look attractive. These include:

- Conelec, Inc. electrojector pump having a discharge pressure of 350 psig. The pump consumes 20 watts parasitic power (12-14 v DC). Weight was not specified.
- Ryvon International Co. micropump, having discharge pressures as high as 1500 psig for flows up to 10-60 liters/hr.
- Volkswagen fuel injector pumps.
- Vickers subminiature vane pump cartridges, operable at 50-1500 psig discharge with flows ranging from 0.1 - 0.3 gpm. These pumps have operated for 1000 hrs and are only 0.75 in. in diameter.

It was assumed that an adequate pump would weigh about 2 lbs for 200-500 watt units, 3 lbs for 1000 watt unit and 4 lbs for the 5000 watt unit. The parasitic power estimates calculated from incompressible fluid pump work equations were trival. These calculations were made using a volumetric efficiency = 0.9 and mechanical efficiency = 0.67 for the pumps. The conservative assumed parasitic power factor, $\pi = 0.1$, should provide adequate design flexibility.

APPENDIX 16

PALLADIUM DIFFUSER DESIGN

The simplified method of Hunter (81) was used to size the palladium diffuser units. The required recovery rate of pure hydrogen product was calculated from:

$$\text{Required Hydrogen Flow, } \dot{W}_{H_2} = \dot{M}_{H_2} \frac{\text{gm moles}}{\text{min}} \times \frac{60 \text{ min}}{\text{hr}} \times \frac{1 \text{ lb mole}}{454 \text{ gm mole}} \times \frac{359 \text{ SCF}}{\text{lb mole}}, \text{ SCF}$$

where: $\dot{M}_{H_2}$ = Fuel Cell Hydrogen Flow Requirement, $\frac{\text{gm moles } H_2}{\text{min}}$ (See Appendix 11.)

Design conditions for the diffuser were:

Inlet Stream: Temperature = 800°F
Total pressure = 480 psia
Hydrogen content = 0.666 (mole fraction)
Hydrogen partial pressure = (0.666) (480) = 319 psia

Pure Hydrogen Product: Pressure = 30 psia
Hydrogen Content = 1.0 (mole fraction)
Hydrogen partial pressure = 30 psia

Bleed Purge Product: Pressure = 480 psia
Hydrogen content = 0.065 (minimum to provide a positive partial pressure driving force across Pd membrane)

With these conditions, the hydrogen recovery factor, $\gamma_{diffuser} = \frac{1}{(1+\alpha)(0.666)} = 0.966$, where $(1+\alpha)$ = molar feed rate to unit. From a diffuser nitrogen material balance, $\alpha = 0.553$. Referring to Hunter, the diffuser design factors for a 0.063 inch diameter Pd tube with 0.003 inch wall are $F_1 = 0.380$ and $F_2 = 0.96$. The calculated specific transport rate was multiplied by $\left(\frac{3}{10}\right)^2$ to compensate for the proposed increase in tube wall thickness needed to ensure operability with an absolute working pressure differential of 450 psi across the membrane. A transport value of 0.199 SCFH/ft tubing was obtained.

The diffuser consists of diffuser tubing and outer shell, as illustrated in Figure A-8. A series of nested tube coils was assumed with diameters ranging from 1 inch to 2 inches, in 0.25 inch increments. Coil lengths were estimated from:

$$\text{Coil lenght, } L_c, \text{ Ft} = \frac{(\text{Tube length, ft})(D_{tube})}{\pi D_{coil}}$$

Figure A-8

PALLADIUM DIFFUSER ASSEMBLY

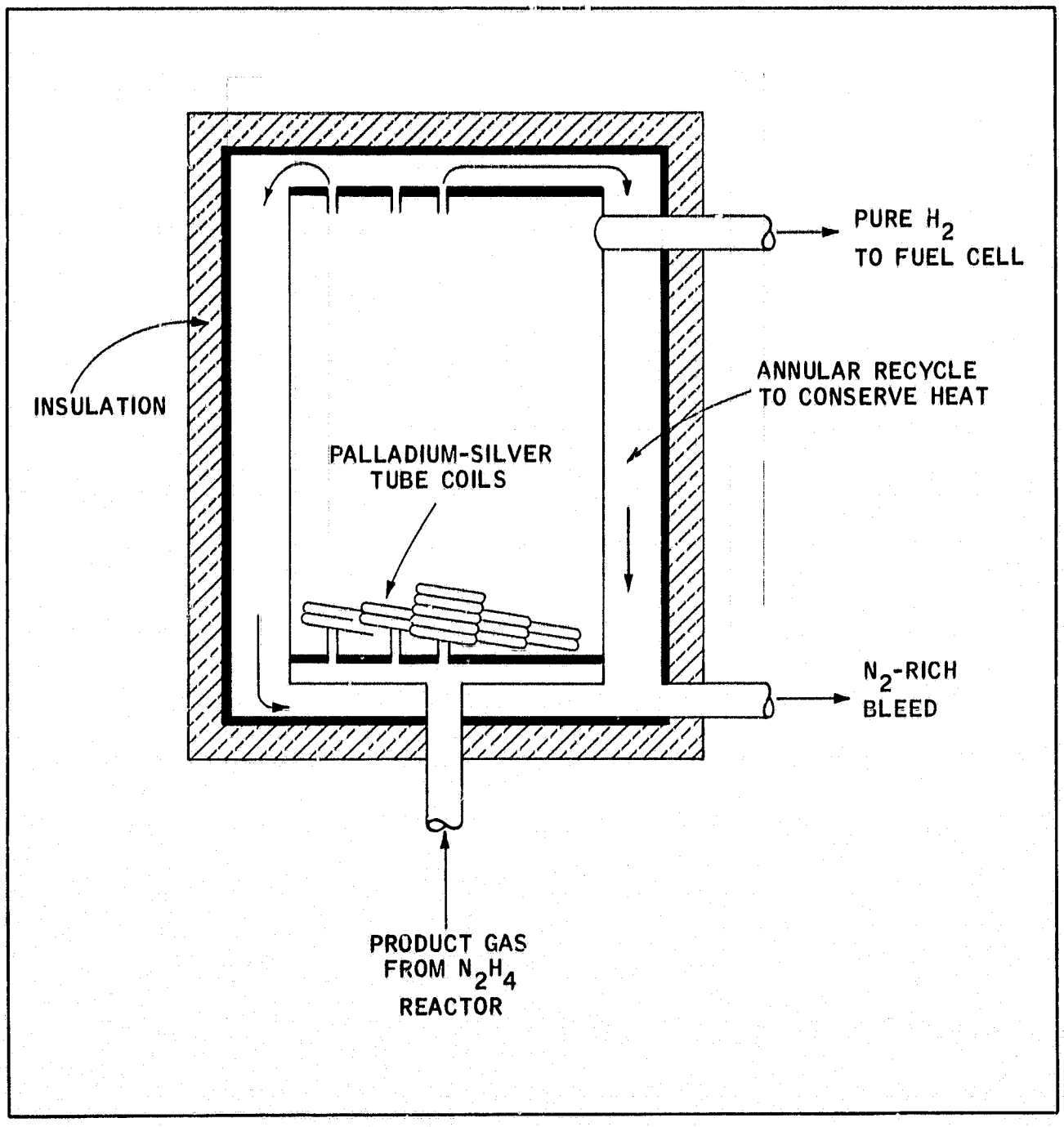

The outer shell casing was assumed to be a 0.05 inch thick stainless steel cylinder. An annular clearance space was provided to permit heat conservation by flowing hot bleed gas around an inner shell assembly. A stress calculation showed that the outer shell could withstand the 450 psi differential at 800°F.

The diffuser tube length and component weight details are summarized below. Final estimates of total diffuser weight are given in Phase 5, Table 6.

Mission On-Load Time, θ_m, Hrs	Net Power Output, P_N, Watts	Pd Tubing Length, ft	Component Weight, Lbs		
			Pd Tubing	Casing	Insulation + Hardware(1)
100	200	18.3	0.16	1.0	0.2
	500	46.7	0.40	1.0	0.2
	1000	82.8	0.72	1.2	0.2
	5000	468	4.05	3.7	0.4
1000	200	17.4	0.15	1.0	0.2
	500	40.7	0.35	1.0	0.2
	1000	82.8	0.72	1.2	0.2
	5000	418	3.62	3.7	0.4

(1) Taken as $0.2\ W_{casing}$.

Estimated diffuser start-up time was calculated for a typical case by equating the sensible heat changes of the diffuser hardware and the hot bleed gas stream:

$$\Delta\theta = \frac{(M\ C_p\ \Delta T)_{diffuser}}{(M\ C_p\ \Delta T)_{Product\ Gas}}\ , \text{min}$$

where: $\Delta\theta$ = Start-up time, minutes

M_D = Diffuser weight = 1.1 (tube weight) = 0.1505 lbs

C_{p_D} = Specific heat = $0.063\ \frac{BTU}{lb\ °F}$ for Pd

ΔT_D = Diffuser temperature rise = 800-40 = 760°F

M_{PG} = Product (nitrogen) gas flow =

$$\frac{(1.29)\ \frac{gms\ N_2H_4}{min}\ \ (28)\ \frac{gm\ N_2}{gm\ mol\ N_2}}{(454)\ \frac{gms}{lb}\ (32)\ \frac{gms\ N_2H_4}{gm\ mol\ N_2H_4}\ (1)\ \frac{gm\ mol\ N_2H_4}{gm\ mol\ N_2}}$$

$$= 0.00284\ \text{lbs}\ N_2/\text{min}$$

$C_{p_{PG}}$ = Specific heat = $0.265\ \frac{BTU}{lb\ °F}$ for N_2

T_{PG} = Product gas temperature difference = 932-100 = 832°F, assuming product gas leaves ammonia bed at 932°F (500°C) and leaves annular flow section of diffuser at 100°F.

Thus:

$$\Delta\theta = \frac{(0.1505)\ (.063)\ (760)}{(.00248)\ (.265)\ (832)} = 13.3 \text{ minutes}$$

APPENDIX 17

HEAT EXCHANGE DESIGNS

Simplified design procedures were used to size the gas generator system product coolers.

Fuel Cell Coolant Radiators

The generalized data presented by Cohn (5) were used to size the fuel cell coolant radiators required by the liquid-cooled Allis-Chalmers modules. For deep space missions, these modules will require a cooling surface of about 12 ft^2/kw, weighing about 1.5 lbs/ft^2. This approach was considered adequate, although data are available on the specific heat rejection characteristics of the Allis-Chalmers modules (12).

The radiation-cooled modules do not require additional coolant radiators. However, the final system capsule design must permit heat radiation to space during fuel cell operation. The louvered capsule walls discussed in Phase 5 may be a suitable approach. Specific radiator weights are listed in Phase 5, Table 6.

Product Space Radiators

Gaseous reaction products are cooled in space radiators prior to storage in appropriate accumulation tanks. Again, a simplified approach was taken to estimate radiator area and weight. The radiator duty was estimated using a heat balance on the product stream. The radiator area required to dissipate this heat load was calculated using a thermal radiation heat balance for the radiator surface.

For the pure hydrogen stream:

$$Q_{H_2} = \dot{W}_{H_2} \bar{C}_p \left(T_{diffuser} - T_{accumulator} \right), \frac{BTU}{hr}$$

where Q_{H_2} = Heat duty to cool hydrogen, $\frac{BTU}{hr}$

$\dot{W}_{H_2}$ = Hydrogen product flow rate, ranges from 0.0213 lbs/hr to 0.546 lbs/hr, depending on mission power level

$\bar{C}_p$ = Average specific heat between 150°F and 800°F = 3.46 BTU/lb °F

$T_{diffuser}$ = Effluent diffuser temperature = 800°F

$T_{accumulator}$ = Product storage temperature = 150°F.

The duty, Q_{H_2}, ranges from 47.9 to 1227 BTU/hr. The specific heat transfer characteristics within the product tube were not considered. The radiator area was calculated using:

$$\frac{Q_{H_2}}{A_{rad}} = \sigma \epsilon_t \left[\frac{\bar{T}_R + 460}{100} \right]^4 - \alpha_s \left[\frac{K_s}{(AU)^2} \right], \frac{BTU}{hr\ ft^2}$$

where: A_{rad} = Radiator area (exposed to space), ft^2

σ = Boltzman constant (experimental) = 0.173 BTU/hr ft^2 $°R^4$

ϵ_t, α_s = Thermal emissivity and solar absorptivity of radiating surface. Values of ϵ_t = 0.92 and α_s = 0.18 were assumed based on Apollo-proven use of zinc oxide and potassium silicate (Z 93) surfaces (101).

$\bar{T}_R$ = Average radiator temperature = 475°F

K_s = Solar flux constant = $\frac{2 \text{ gm cal}}{\text{min cm}^2}$ or 442.4 $\frac{BTU}{hr\ ft^2}$ for normal incident solar rays at AU = 1 (117)

AU = Distance from sum, astronomical units = 5 for assumed Jupiter mission (maximum value for grand tour to Neptune would be AU = 9).

Radiator weights were calculated assuming 1.5 lbs/ft^2 and these were related to hydrazine flow rates, $\dot{W}_{N_2H_4}$, using a linear graph of W_{rad} versus $\dot{W}_{N_2H_4}$. A similar procedure was used to size the nitrogen product cooler. Here, $\bar{C}_p$ = 0.258 BTU/lb °F. Final values are tabulated below.

Mission On-Load Time, θ_m, Hrs	Net Power Output, P_N, Watts	Hydrazine Feed Rate, $\dot{W}_{N_2H_4}$, Gms/Min	Product Space Radiators			
			Hydrogen		Nitrogen	
			Area, Ft^2	Wt., Lbs	Area, Ft^2	Wt., Lbs
100	200	1.29	0.04	0.06	0.02	0.03
	500	3.3	0.10	0.15	0.05	0.08
	1000	5.85	0.18	0.27	0.09	0.14
	5000	33.1	1.01	1.52	0.53	0.79
1000	200	1.23	0.04	0.06	0.02	0.03
	500	2.88	0.09	0.13	0.05	0.08
	1000	5.85	0.18	0.27	0.09	0.14
	5000	29.6	0.91	1.36	0.53	0.79

Water Condenser

The hydrogen peroxide decomposition products were assumed available at 1500°F and 500 psia. The product flow rate range is:

	Flow Rate, Lb/Hr	
	Water	Oxygen
Smallest Unit (200 W)	0.189	0.161
Largest Unit (5000 W)	4.81	4.12

These products must be cooled to 150°F to provide an oxygen product with about 99.3% purity (water vapor considered as diluent). The heat duty involved was estimated using the steam tables (68) and an oxygen heat balance, with $\bar{C}_p$ = 0.247 BTU/lb °F.

The heat loads are summarized below:

Net Power Output, Watts	Heat Duty, BTU/Hr		
	Water	Oxygen	Total
200	316	53.7	370
5000	8048	1374	9422

It was assumed that the water condenser/radiator would be located within the capsule at an ambient temperature of 40°F. Thus,

$$\frac{Q_{cond}}{A_{rad}} = (0.173)\ (0.9)\ \left[\left(\frac{825 + 460}{100}\right)^4 - \left(\frac{40 + 460}{100}\right)^4\right] \text{, BTU/hr ft}^2$$

Where ϵ_t = 0.9 and the average condenser wall temperature is 825°F. Simple stainless steel tubes were used as radiators, although external pin-fins may help (93).

Net Power Output, Watts	Radiator Size		
	Area, Ft^2	Length, Ft(1)	Weight
200	0.089	1.36	0.092
5000	2.27	23.1	2.27

(1) For 200 watt unit: 1/4" O.D., BWG 22 stainless steel tube.
For 5000 watt unit: 3/8" O.D., BWG 18 stainless steel tube.

Weights for other power outputs were estimated by linear interpolation and are listed in Phase 5, Table 6.

Water Separator

An induced-vortex, cyclone device will be used to separate condensed water from the oxygen product. The design and fabrication of this unit were discussed by AIResearch (18). A unit weighing 5 lbs was required for separating reactant bubbles from a high flow rate, circulating electrolyte system. For the present application, it was assumed that a similar device would weigh between 1 and 3 lbs.

System Power Output, Watts	Estimated Separator Weight, Lbs
200	1
500	1.5
1000	2
5000	3

APPENDIX 18

HYDROGEN PEROXIDE REACTOR ASSEMBLY

Hydrogen peroxide decompositon studies were carried out in the assembly shown in Figure A-9. The feed delivery section consisted of a pressurized graduated dropping funnel, rotameter assembly, Teflon valves and Teflon capillary tubing. Rigorous passivation procedures were used, as recommended by Schumb (91). Degreasing and nitric acid treatment followed by contacting with concentrated hydrogen peroxide effectively eliminated premature decomposition of the feed solutions within the delivery section.

Again, 9mm ID Vycor reactors were used, with the peroxide decomposition catalyst contained between aluminum screens. A stainless steel reactor was also used. The hot off-gases were pre-cooled before entering a condenser/recovery unit, where product water was removed. The oxygen flow, essentially at room temperature, was then measured in a wet-test meter, using oxygen-saturated water as working fluid.

Cold-start runs were performed with the feed delivery and reactor sections pre-cooled in a refrigerated cold box. Occasionally, frost formation prevented accurate reading of the feed tank and rotameter float levels.

Figure A-9

LABORATORY HYDROGEN PEROXIDE DECOMPOSITION UNIT

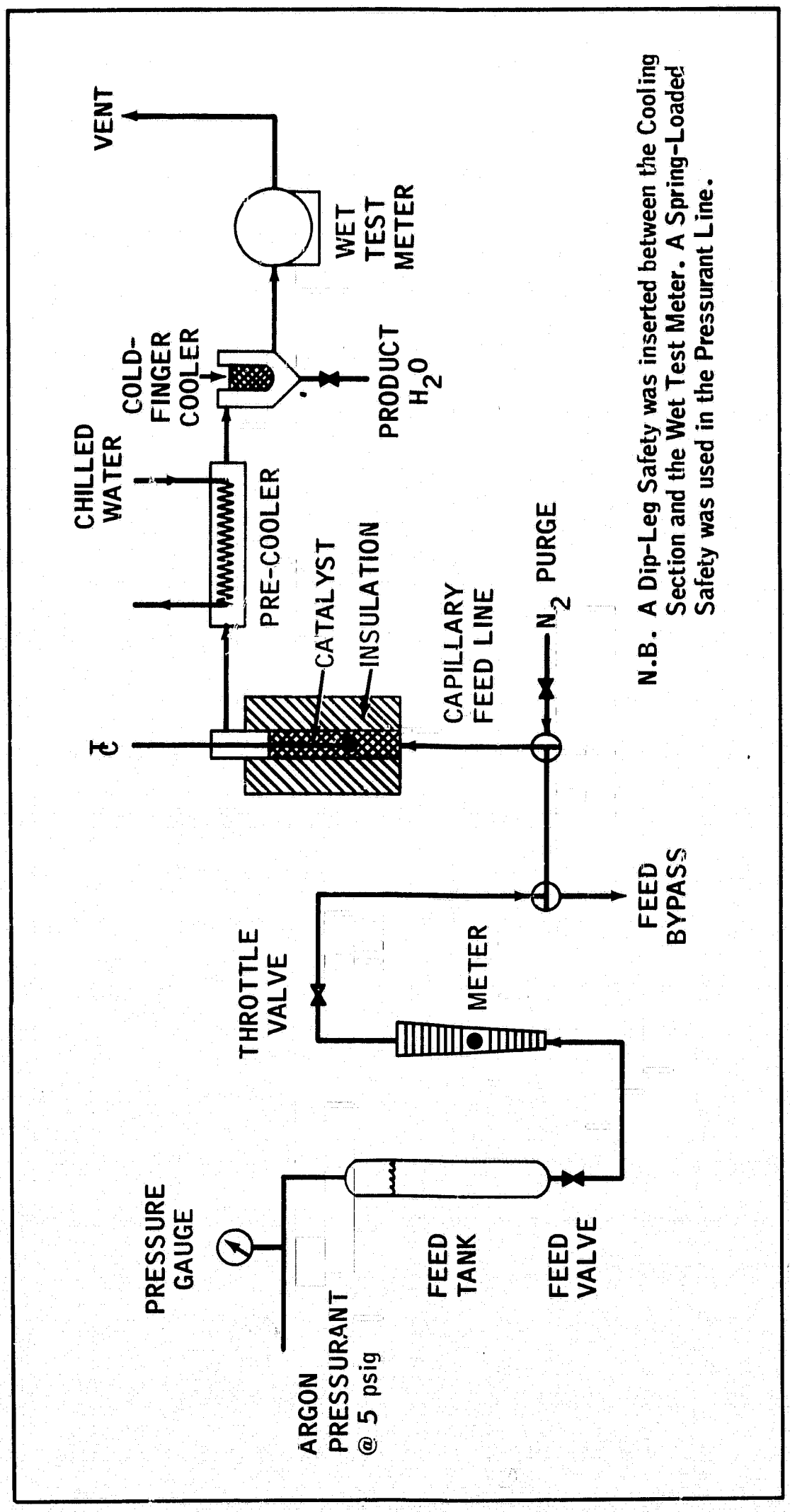

APPENDIX 19

HYDROGEN PEROXIDE DECOMPOSITION DATA

Run No. 409-	Ambient Temp., °C	Feed Composition, Wt. % H_2O_2	Catalyst(1,4) Type	Catalyst(1,4) Wt., Gms	H_2O_2 Space Velocity, WHSV(2)	Reactor Temp., °C	Oxygen Yield Gms O_2/Gm H_2O_2(3)	Remarks
136-1	5	90	I-6A(I)	15.0	3	91	0.49	
136-2	5	90	I-6A(I)	15.0	15	650	0.47	
137-1	-40	70	Ag_2O	15.0	10	94	0.48	
137-2	-40	70	Ag_2O	15.0	27	97	0.47	
139-1	-40	70	I-6A(II)	7.38	N.A.	-40	0.00	No ignition.
141-1	25	90	I-6A(II)	7.38	15	92-213	0.52	
142-1	25	90	I-6A(I)	12.07	22	295-380	0.42	
142-2	25	90			54	613-648	0.44	
144-1	25	98			36	486-505	0.40	
144-2	25	98			59	642-720	0.48	
144-3	25	98			130	732-775	0.32	

(1) Confidential catalyst I-6A developed by FMC; (I) = single fire, (II) = double fire preparation. All catalysts used as 1/8" pills, except Run 139, where 8-10 mesh particles were used. Apparent bulk density = 1.57 gm/cc. Additional activity data in Table A-7.

(2) WHSV = gms H_2O_2/gm cat-hr, based on H_2O_2 content of feed, not total feed. Low temperature data are approximate because frost formation prevented accurate feed rate measurement.

(3) Theoretical value = 0.47.

(4) 9 mm I.D. Vycor reactor used for all runs, except 139 and 141, where stainless steel tube was substituted.

APPENDIX 19 (CONT'D)

HYDROGEN PEROXIDE DECOMPOSITION DATA

Table A-7

Activity of Hydrogen Peroxide Decomposition Catalysts

Catalyst	Test Solution, Wt. % H_2O_2	Temp., °C(1)	Activity
Silver Screen	30	25	Slight.
	30	-25	Nil.
	90	5	Very active after 10 seconds, violent after 35 seconds.
	98	5	Violent initially.
Silver Oxide	30	25	Very active.
	30	-25	Active.
Esso 104	30	25	Moderate.
	30	-25	Slight.
I-6A (Single fire)(2)	30	25	Active.
	30	-25	Slight.
	90	5	Mild gas evolution initially, violent after 40 seconds.
	90	5	Mild initially, violent after 85 seconds (used catalyst).
	98	5	Violent initially.
	98	5	Mild initially, violent after 38 seconds (used catalyst).
I-6A (Double fire)(2)	90	5	Very slight initially, continues at mild rate.
	98	5	Very mild initially, continues at mild rate.

(1) Both test solution and catalyst pellet at test temperature, initially. Pellet dropped into 2-5 cc of solution.

(2) Confidential FMC catalyst composition.

APPENDIX 20

THERMAL CONTROL STUDIES

A thermal control system is required to ensure that the gas generator and fuel cell systems are maintained within acceptable temperature limits. A minimum temperature of +40°F (4°C) was selected, fixed by the freeze point of neat hydrazine. The maximum permissible temperature, for prolonged exposure, would be about 100°F (38°C), fixed by the autodecomposition of the stored reactants. An adequate system was not devised, but time limitations prevented a comprehensive review of the problem.

Equilibrium Surface Temperatures in Space

The nature of the control problem was illustrated briefly by calculating the equilibrium surface temperature of an insulated flat plate exposed to solar flux of varying intensity. A thermal balance shows that:

$$\sigma \epsilon_t \left[\frac{T_s + 460}{100} \right]^4 = \frac{\alpha_s K_s}{(AU)^2}$$

or

$$T_s = 100 \left[\frac{\alpha_s}{\sigma \epsilon_t} \quad \frac{K_s}{(AU)^2} \right]^{1/4} - 460, \ ^\circ F$$

where: T_s = Surface temperature, °F

α_s = Solar absorptivity

ϵ_t = Thermal emissivity

K_s = Solar flux = 442.4 $\frac{BTU}{hr\ ft^2}$ at A.U. = 1 (117)

A.U. = Distance from sun, astronomical units ($A.U._{earth} = 1$)

σ = Boltzman constant (experimental) = 0.173 BTU/hr ft^2 $^\circ R^4$

Values of T_s were calculated for a range of $\frac{\alpha_s}{\epsilon_t}$. The results are presented in Phase 5, Figure 25.

Radioisotope Heaters

A grossly simplified, quasi-analytical approach was used to evaluate the use of radioisotope heating elements as a means of passive thermal control. Ten grams of plutonium 238 heat elements were assumed to be distributed within the power plant capsule sheath. The sheath wall interior was assumed to be lined with a space-age cryogenic insulation. Nylon screen with 0.00025 in. Al coated polyester radiation shields was selected as typical. The effective thermal conductivity of this material was taken as 1×10^{-4} $\frac{BTU\text{-}inch}{hr\ ft^2\ ^\circ F}$ (80).

A heat flux balance shows that:

$$\sigma \epsilon_t \left[\frac{T_s + 460}{100} \right]^4 = \frac{\alpha_s K_s}{(A.U.)^2} + \frac{k}{t_I} (T_s - T_i)$$

and

$$\frac{k}{t} (T_W - T_I) = \frac{Q_{RI}}{A_c}$$

where: k = Insulation thermal conductivity = 1×10^{-4} $\frac{\text{BTU inch}}{\text{hr ft}^2 \text{ °F}}$

t_I = Insulation thickness, inches

T_s = Sheath wall temperature, °F (assumed constant on both surfaces, facing space and adjacent to outer surface of insulation)

T_i = Capsule interior temperature, °F (assumed equal to inner insulation surface temperature)

Q_{RI} = Heat released by Pu^{238} isotope = 1.229 $\frac{\text{BTU}}{\text{hr gm}}$ (10 gms used)

A_c = Total area of capsule sheath, ft^2 (calculated for in-line component packaging, assumes all of area is exposed to solar flux)

Values of A_c are tabulated below.

Mission On-Load Time, θ_m, Hrs	Net Power Output, P_N, Watts	Capsule Sheath		Insulation	
		Area, A_c, Ft^2	Weight, Lbs(1)	Thickness, Inches	Weight, Lbs(2)
100	200	24.3	17.1	0.05	0.51
	500	42.9	30.2	0.09	1.6
	1000	76.5	45.3	0.16	5.1
	5000	159.3	69	0.33	21.9
1000	200	78.6	55.4	0.16	5.2
	500	121.4	81.4	0.25	12.7
	1000	178.6	117	0.38	28.3
	5000	467.7	287	1.00	195

(1) Assumed to be 0.05 inch, 1060 Al weighing 0.098 lbs/in^3. Thus, sheath weight = 0.706 $(A_C - A_R)$, lbs, where A_R = space radiator area (weights assigned previously).

(2) Assumes density = $\frac{5 \text{ lbs}}{ft^3}$

Thermal balances were computed at AU = 9 to determine the insulation thickness required to maintain the capsule interior at +40°F. Values of $\alpha_s = \epsilon_t = 0.25$ were used to estimate the outer sheath temperature. The calculations were repeated at AU = 1 and 5 and the results are shown in Phase 5, Figure 26.

Unclassified
Security Classification

DOCUMENT CONTROL DATA - R & D

(Security classification of title, body of abstract and indexing annotation must be entered when the overall report is classified)

1. ORIGINATING ACTIVITY *(Corporate author)*

Esso Research and Engineering Company
Government Research Laboratory
Linden, New Jersey

2a. REPORT SECURITY CLASSIFICATION

Unclassified

2b. GROUP

3. REPORT TITLE

Study of Multiple Electrochemical Power Source

4. DESCRIPTIVE NOTES *(Type of report and inclusive dates)*

Final Technical Report, 11 June, 1968 to 15 December, 1968

5. AUTHOR(S) *(First name, middle initial, last name)*

George Ciprios

6. REPORT DATE	7a. TOTAL NO. OF PAGES	7b. NO. OF REFS
January, 1969	114	118

8a. CONTRACT OR GRANT NO.	9a. ORIGINATOR'S REPORT NUMBER(S)
NAS 7-673	GR-1-MPS-69
b. PROJECT NO.	
c.	9b. OTHER REPORT NO(S) *(Any other numbers that may be assigned this report)*
d.	

10. DISTRIBUTION STATEMENT

11. SUPPLEMENTARY NOTES	12. Sponsoring Activity
	National Aeronautics and Space Administration Washington, D. C.

13. ABSTRACT

A study was conducted to define the feasibility of a fuel cell multiple-reserve electrochemical power source for projected space missions. Neat hydrazine and 98 wt. % hydrogen peroxide are used as storable reactants. Appropriate high temperature reactors, containing propellent decomposition catalysts, are used to generate hydrogen and oxygen feed gases for the fuel cell.

Allis-Chalmers fuel cell modules were selected for the center-line design on the basis of low specific weight and demonstrated boot-strap start-up capability. Catalysts with adequate activity are available to permit instantaneous reactor start-up with either reactant at +5°C, the design dead-storage temperature. Only small amounts of catalyst were needed for complete reactant decomposition but added amounts of ammonia decomposition catalyst are required to increase hydrogen yield. A palladium diffuser is used to recover ultrapure hydrogen, permitting efficient fuel cell operation. Overall system thermal control in near-sun and deep-space environments is a critical problem requiring further study.

Integrated power plant specific weights ranged from 122 to 292 WH/lb for mission on-load times of 100 or 1000 hrs and power levels of 200 to 5000 watts. Projected fuel cell/gas generator system costs were low, making this an attractive space power approach.

DD FORM 1 NOV 68 1473 REPLACES DD FORM 1473, 1 JAN 64, WHICH IS OBSOLETE FOR ARMY USE.

Unclassified
Security Classification

14. KEY WORDS	LINK A		LINK B		LINK C	
	ROLE	WT	ROLE	WT	ROLE	WT
Multiple Reserve Battery						
Battery						
Fuel Cell, Hydrogen-Oxygen						
Space Power						
Hydrazine						
Hydrazine Decomposition						
Ammonia						
Ammonia Decomposition						
Hydrogen Peroxide						
Hydrogen Peroxide Decomposition						
Hydrogen Generator						
Oxygen Generator						